2009

Seismic design of drilled shafts in clay

Aaron Trask Shelman
Iowa State University

Seismic design of drilled shafts in clay

by

Aaron Trask Shelman

A thesis submitted to the graduate faculty
in partial fulfillment of the requirements for the degree of
MASTER OF SCIENCE

Major: Civil Engineering (Structural Engineering)

Program of Study Committee:
Sri Sritharan, Major Professor
Igor Beresnev
Fouad Fanous

Iowa State University

Ames, Iowa

2009

TABLE OF CONTENTS

LIST OF TABLES

LIST OF FIGURES

NOMENCLATURE

Abbreviations

AASHTO = American Association of State and Highway Transportation Officials
ALR = P/f′cAg = axial load ratio
ASTM = American Society for Testing and Materials
ATC = Applied Technology Council
CIDH = cast-in-drilled-hole
CPT = cone penetration test
PTC = Parametric Technology Corporation
SFSI = soil-foundation-structure-interaction
UHPC = ultra high performance concrete
USCS = Unified Soil Classification System
USGS = United States Geological Service
VSAT = Versatile Section Analysis Tool
e.g. = exempli gratia (roughly translated as “for example”)
i.e. = id est (roughly translated as “that is”)
ult = ultimate limit state
yld = first yield limit state

Symbols

C_1 = coefficient dependent on end fixity condition (Priestley et al., 2007)
C_3 = coefficient for changing moment pattern (Priestley et al., 2007)
D = column or pile shaft diameter
D′ = effective core diameter for a circular concrete shaft
D^* = reference pile diameter used in Priestley et al. (1996)
E_p = pile modulus of elasticity
E_s = soil modulus of elasticity
EI = flexural stiffness of foundation (Reese et al., 1975)
EI_{eff} = effective flexural stiffness
H = height of column above ground
H_{cp} = height to contraflexure point from top of column
H_{IG} = height to in-ground hinge from top of column
I_e = effective moment of inertia for pile cross-section
I_w = weak axis moment of inertia for foundation shaft
K = soil subgrade modulus in units of force per length cubed
K_{sp} = stiffness of soil-pile system when subjected to lateral loading
K_c = stiffness of a cantilever when subjected to lateral loading
L = overall length of column-pile shaft
L_a = above ground column height
L_a^* = normalized depth to maximum moment
L_{cant} = equivalent cantilever height from column top to effective fixity location
L_f = depth to effective fixity from ground surface
L_f = length of foundation
L_m = depth to maximum moment location from ground surface

L_m^* = normalized depth to maximum moment location
L_{col} = height of column above ground surface
L_{ma} = depth to point of maximum moment from top of column
L_{mb} = depth below maximum moment to first point of zero moment
L_{m0} = depth to first point of zero moment from top of column
L_{sp} = length of strain penetration
L_p = analytical plastic hinge length
L_{pa} = analytical length of plastic hinge above the maximum moment location
L_{pb} = analytical length of plastic hinge below the maximum moment location
$L_{p,actual}$ = actual length of plastic hinge
$L_{p,IG}$ = analytical plastic hinge length due to in-ground hinging (Priestley et al., 2007)
M = moment
M_{max}^* = normalized flexural strength of foundation shaft
M'_y = first yielding moment capacity of shaft cross-section corresponding with ϕ'_y
M_y = yield moment capacity of shaft cross-section corresponding with ϕ_y
M_u = ultimate moment capacity of shaft cross-section corresponding with ϕ_u
N_k = bearing capacity factor
P = axial load applied to column-pile shaft
R_c = characteristic length of column-pile shaft = $\sqrt[4]{EI_{eff}/k_h}$
V = lateral force applied at top of column-pile shaft
V_s = soil shear force
V_{sy} = soil shear force at the yield condition
V_{su} = soil shear force at the ultimate condition
V_t = corrected lateral load at the top of the column
V_{t1} = uncorrected lateral load at the top of the column
V_y = yield lateral load at top of column
V_u = ultimate lateral load at top of column
V_u^* = normalized lateral strength of soil-pile system
b = width of foundation in Reese et al. (1975)
b = exponent in p-y curve development using Reese et al. (1975) suggestions
c = neutral axis depth in concrete shaft for a given curvature
c_u = maximum unconfined compressive strength of soil
d_b = diameter of reinforcing bar
d_{bl} = diameter of longitudinal reinforcing bar
f'_c = specified ultimate concrete compressive stress
f′ce = expected ultimate concrete compressive stress
f'_t = concrete tensile stress
f_y = specification yield steel stress of reinforcing bars
f_{ye} = expected yield steel stress of reinforcing bars
f_u = ultimate steel stress of reinforcing bars
g = acceleration due to gravity
h_s = height of soil between the maximum and zero moment locations
k = coefficient in L_p equation for a fixed head condition (Priestley et al., 2007)

k = initial p-y modulus used in LPILE analyses in units of force per length cubed
k_h = constant modulus of subgrade reaction in units of force per length squared
p = soil subgrade reaction per unit length of pile
p_u = ultimate soil subgrade reaction per unit length of pile
s_u = maximum unconfined compressive strength of soil
w/c = water to cement ratio
x = depth from ground surface to location of soil spring in Reese et al. (1975)
x = distance from bottom of pile to a point along length of column-pile shaft
y = displacement of soil/pile according to Reese et al. (1975)
y_{50} = displacement of soil/pile at one-half the ultimate soil subgrade reaction
z = depth below ground surface
Δ = displacement of system at top of column
Δ_D = design displacement of system at top of column
Δ_e = elastic displacement of system at top of column
Δ_{ea} = corrected elastic displacement of system at top of column from cantilever action above the maximum moment location
Δ_{ea} = uncorrected elastic displacement of system at top of column from cantilever action above the maximum moment location
Δ_{eb} = elastic displacement of system at top of column from elastic rotation below the maximum moment location
Δ_g = displacement of column-pile shaft at ground level
Δ_{La} = above ground cantilever displacement
Δ_p = plastic displacement of system at top of column
Δ_{pu} = plastic displacement of system at top of column for the ultimate limit state
$\Delta_{p,IG}$ = plastic displacement of system at top of column due to in-ground hinging
Δ_{sp} = displacement of soil-pile system
Δ_t = translation of foundation shaft at the maximum moment location
Δ_{trans} = displacement of the system at the maximum moment location
Δ_{ty} = translation at the maximum moment location for the yield limit state
Δ_t = translation at the maximum moment location for the ultimate limit state
Δ_y = yield displacement of system at top of column
$\Delta_{y,F}$ = yield displacement of system at top of column due to fixed head condition
$\Delta_{y,IG}$ = yield displacement of system at top of column due to in-ground hinging
Δ_u = ultimate displacement of system at top of column
α_{ma} = coefficient for computing the maximum moment location
α_{m0} = coefficient for computing the first zero moment location
β_{ma} = coefficient for computing the maximum moment location
β_{m0} = coefficient for computing the first zero moment location
χ_{ma} = coefficient for computing the maximum moment location
ε = soil strain from laboratory testing (Reese et al., 1975)
ε_c = concrete strain
ε_{co} = concrete cracking strain
ε_{cu} = ultimate strain of concrete

$\varepsilon_{dc,c}$ = damage control strain for concrete
$\varepsilon_{dc,s}$ = damage control strain for steel reinforcing bars
ε_{su} = ultimate strain of steel
ε_{50} = soil strain at fifty percent of maximum principal stress
ϕ = curvature of shaft cross-section
ϕ_e = elastic curvature of shaft cross-section
ϕ_{ls} = limit state curvature of shaft cross-section
$\phi_{ls,c}$ = damage control limit state curvature of shaft cross-section for concrete failure
$\phi_{ls,s}$ = damage control limit state curvature of shaft cross-section for steel failure
ϕ'_y = first yielding curvature of shaft cross-section
ϕ_y = idealized elasto-plastic yield curvature of cross-section used in Chai (2002)
ϕ_y = yield curvature of shaft cross-section
ϕ_p = plastic curvature of shaft cross-section
ϕ_u = ultimate curvature of shaft cross-section
γ = effective unit weight of soil
γ_m = effective moist unit weight of soil
η = coefficient to modify the ultimate soil shear force to a yield condition
λ_p = normalized analytical plastic hinge length
μ_Δ = displacement ductility of system
μ_ϕ = curvature ductility of foundation shaft
θ_{eb} = elastic rotation from effects below the maximum moment location
θ_{eby} = elastic rotation from effects below the maximum moment location at yield
θ_{ebu} = elastic rotation from effects below the maximum moment location at ultimate
θ_g = rotation of column-pile shaft at ground level
θ_p = plastic rotation of column-pile shaft
θ_{pa} = plastic rotation above point of maximum moment
θ_{pb} = plastic rotation below point of maximum moment
θ_y = yield rotation of column-pile shaft at the maximum moment location
θ_u = ultimate rotation of column-pile shaft at the maximum moment location
ρ_l = longitudinal reinforcement ratio
ρ_s = horizontal (spiral) reinforcement ratio
ξ_a = coefficient for locating the above ground height
ξ_f = coefficient for locating the equivalent depth to fixity
ψ = soft soil modification factor in translation computations
~ = approximately

Units

cm = centimeter (1 cm = 0.01 m)
ft = feet
in. = inch
kN = kilonewton (1 kN = 1000 N)
kip = 1000 pound-force
kPa = kilopascal (1 kPa = 1000 Pa)

ksi	= kip per square inch (1 ksi = 1000 psi)
ksf	= kip per square foot (1 ksf = 1000 psf)
lb	= pound-force
m	= meter
mm	= millimeter (1 mm = 0.001 m)
MN	= meganewton (1 MN = 1E+06 N)
MPa	= megapascal (1 MPa = 1E+06 Pa)
Pa	= pascal (1 Pa = 1 N/m^2)
psi	= pound-force per square inch
psf	= pound-force per square foot
°C	= degrees Centigrade
°F	= degrees Fahrenheit

ACKNOWLEDGEMENTS

The research presented within this report was completed due to the continued support from the Alaska University Transportation Center, the Alaska Department of Transportation and Public Facilities and the Department of Civil, Construction and Environmental Engineering at Iowa State University in Ames, Iowa.

The author would like to thank Dr. Sritharan for the opportunity to work on the project. His continued support towards the success of the project was greatly appreciated, especially during the times when it seemed like the project was at a standstill.

The author would also like to thank his family and friends for their unrelentless support throughout the research process. The author was lucky enough to have such a wonderful group of people around him to provide love and understanding.

ABSTRACT

In the field of bridge engineering, columns supported on cast-in-drilled-hole (CIDH) shafts are common due to the elimination of a column-foundation connection, simplicity of construction and reduced construction costs. Due to these benefits, this combination of column and foundation is frequently used in high seismic regions. The modeling of lateral load behavior of the column-shaft system, however, is a complex matter due to the effects of soil-foundation-structure-interaction (SFSI). The research presented within this project identifies numerous challenges associated with the current state of practice of accounting for SFSI in cohesive soils and develops a new method that accounts for SFSI in cohesive soils.

The project undertook an extensive literature review as well as an examination of codes and guidelines to identify the challenges within current practice. This process found that although many models exist to simplify the use of the Winkler soil spring concept, none of the simplified models are able to capture both the elastic and inelastic lateral load response of an integrated column/foundation system. The challenges arose for the following reasons:

1. some models are only applicable in the elastic range;
2. models recommended for use in cohesive soils and cohesionless soils were only verified against experimental data obtained in cohesionless soils;
3. the nonlinearity of materials (i.e., soil, concrete and steel reinforcement) were not accounted for in the development of the models; and
4. plastic action within the different methods is generally lower than what actually will be found using a detailed analysis method such as that based on fully implementing the Winkler spring concept.

In addition to the aforementioned shortcomings, the existing methods ignore the effects of seasonal freezing in their development; even though it significantly alters the lateral load response of CIDH shafts. However, it was found that this approach is not appropriate as two-thirds of the bridges in the United States are affected by seasonal freezing. This problem is only further exacerbated by the fact that half of the bridges in high seismic regions are also affected by seasonal freezing. After identifying these issues, a new method was developed that more accurately predicts the lateral load response of columns supported on CIDH shafts in cohesive soils.

The new approach presented within this report uses a set of three springs to determine a bilinear force-displacement response of the column/foundation system using minimal input parameters about the structure and surrounding soil. The model was developed as a cantilever supported on a flexible base located at the expected maximum moment location. First, a rotational spring and a translational spring were placed at the maximum moment location to capture the behavior of the foundation shaft at and below the location. The final translational spring was located halfway between the maximum moment location and the ground surface to capture the resistance of the soil above the maximum moment location. By basing the system on the maximum moment location, the point at which the most damage will occur is defined. The global response of the system as well as the local response of the CIDH shaft over the entire lateral loading range is also captured.

Comparing the alternative method to results from experimental testing performed at Iowa State University and LPILE analyses of several different systems, the new model was found to well simulate the response of the column/foundation system in cohesive soils. The developed method was able to predict the secant stiffness to the first yield location within 10%. Yield and ultimate limit states were within 10% of the detailed analyses performed in LPILE (Reese et al., 2004) and correlated well with the full-scale experimental testing performed by Suleiman et al. (2006). The overall comparisons included multiple displacement and rotation factors as well as local curvatures developed near the maximum moment location. These aforementioned local comparisons of the CIDH shaft, along with a global comparison of the entire system, were performed to minimize any errors that occurred during the model development.

CHAPTER 1: INTRODUCTION

1.1 Historical Background

A bridge, by definition, is a time, place, or means of connection or transition (Merriam-Webster 2008). In ancient times, this may have been as easy as a log that had fallen across a river or as complicated as a Roman arch bridge. As the years have passed, the design of bridges has become more complicated due to the desire to provide functionality along with an artistic appearance such as the pedestrian bridges located in Des Moines, Iowa. With the ever changing demands on designers, significant advancements of knowledge within structural behavior and construction materials have been made in order to further advance the innovation in bridge design.

Figure 1-1: Arched pedestrian bridge over I-235 in Des Moines, Iowa (Iowa DOT, 2009)

1.2 Seismic Engineering Practices

Structural engineering is an expanding field based on knowledge ascertained over the decades. In the specialized field of seismic engineering, the design of structures has been constantly evolving as knowledge about earthquakes and their effects on structural response progresses. The earliest records of earthquakes go back as far as 1831 BC, in the Shandong province of China (USGS 2009). China, however, is not the only location in the world to have recorded early earthquakes. In the United States, European settlers experienced

earthquakes as early as 1663 AD (USGS 2009). From this point in time, earthquakes within the United States have been steadily recorded.

One of the more significant sets of earthquakes in the history of the United States is the New Madrid Series of 1811 – 1812. This series contained three earthquakes with a magnitude of at least 8 and had devastating effects on structures in the central United States due to the efficiency of the geological features to propagate seismic energy (USGS 2009). As time progressed, more information was gained about dynamics and structural behavior, demonstrated, in particular when a full earthquake ground acceleration record was collected during the 1940 El Centro earthquake. This information allowed structures to be designed to target ground acceleration using a force-based approach that would relate back to the ground accelerations measured during 1940. However, it was not until the 1980's when engineers began to realize that a force-based approach combined with an allowable stress method would not be a sound approach for the seismic design of structures (Priestley et al. 2007). The problem with a force-based approach without emphasizing adequate displacement capacities became prevalent with damage caused by the 1971 San Fernando earthquake, the 1989 Loma Prieta earthquake and the 1994 Northridge earthquake to name a few (see Figure 1-2). Today, an approach that relies on the final performance of structures is slowly taking over. This method ensures that an appropriate design is created such that the desired performance of the structure is met over the lifespan of the structure.

Figure 1-2: Earthquake damage: San Fernando (left); Loma Prieta (top right); Northridge (bottom right) [photos accessed through USGS website (2009)]

1.2.1 Seismic Loading

Since the first full record of ground accelerations were first captured during the 1940 El Centro Earthquake, the understanding of seismic loading has been constantly evolving. The evolution in seismic loading has generally come from two different sources. The first source of evolution is the improvement of technology over the years. The improvement of technology has led to more data collections with enhanced accuracy in capturing seismic events across the entire world. The increased amount of data collected has led to maps and time history data files that are able to provide more localized accelerations based on previously recorded events as well as the geology of the areas. The second major point of evolution is the continuously learned knowledge of structural behavior and its effects on the design process. A key component of this evolution is the understanding of material behavior and how the nonlinearity in the material properties can be used to ensure a structure that performs as desired. By using the nonlinearity of material properties, structures are now being designed to form a hinge point and essentially deform in a ductile manner while losing minimal capacity. This evolution of design also led to a better understanding of hysteretic damping and how it may be used to dissipate the seismic energy applied to a structure.

Although a great deal of evolution has occurred with data collection and understanding of structural behavior, the analysis methods used for determining the final seismic loading have been relatively unchanged. The analysis methods are generally classified into two areas, a full dynamic analysis and a simplified analysis. The full dynamic analysis will use a previously recorded or artificially generated earthquake time history in a numerical integration method that will generate the full response of the structure, forces and displacements, due to the energy imparted by an earthquake ground motion. The simplified method uses an approximation based on the period of the structure to establish a design base shear force that is then distributed to the different levels of the structure based on the modal shapes of the structure. These distributed shear values are then used to determine the design forces for individual members of the structure. No matter what method is chosen for determining the seismic loading of the structure, the response of the structure is necessary to understand in order to ensure an adequate response during a seismic event.

1.2.2 Capacity Design Philosophy

In high seismic regions of the United States, such as California, Alaska and South Carolina, structures are now designed to ensure an adequate response to seismic loading. In order to maintain a satisfactory performance, structures are designed in accordance with standards as specified by the owning agency. The standards within the high seismic regions generally follow a design philosophy that uses capacity design principles (Priestley et al., 1996). These principles as stated by Priestley et al. (1996) are summarized as follows:

- the structure is allowed to respond inelastically through flexural yielding and formation of plastic hinges under design-level earthquakes;
- plastic hinge locations are pre-determined and detailed to ensure that ductile response can occur; and
- undesirable mechanisms (e.g., shear failure) are prevented through the provision of a suitable strength margin.

The capacity design principles are not currently widely used around the United States (Priestley et al., 2007) even though the principles can be used within a force-based design. The future of earthquake engineering, however, is steadily progressing toward the principles of capacity design as the performance based method of design takes over. This is the case as the lifespan of a structure will only be met if designed such that it will not fail in all possible scenarios including seismic events. Designs will be further improved, as well, since the capacity design principles will ensure other modes of lateral loading shall not collapse the structure.

1.2.3 Temperature Concerns

The capacity design principles, as stated above, heavily rely on allowing flexural yielding and preventing undesirable effects in the structure; however, little research has been performed into the effects of seasonal cold temperatures on ductile behavior of structures when subjected to a seismic event. This is a major deficiency in the field of earthquake engineering as some of the largest earthquakes (e.g., 1811-1812 New Madrid Series and the 1964 Great Alaska Earthquake) actually occurred during winter months that cause ground freezing in the earthquake affected regions of the United States. It has been shown in an exploratory research program by Sritharan et al. (2007) that the seasonally frozen effects can

cause brittle failure structures unless their effects are accounted for in seismic design. The effects of cold temperature are further exacerbated by the unknown effects caused to the moment-curvature response of a critical member section, an important element in determining flexural yielding. The significance of these two issues are made even more critical as they are in direct violation of the capacity design principles. These principles state that the designer should allow flexural yielding while preventing an undesirable failure mode such as a brittle failure. In the exploratory research that examined the performance of continuous columns supported on drilled shaft foundations, Suleiman et al. (2006) drew the following conclusions regarding the lateral load response of a full-scale test in wintry conditions with respect to summer conditions:

- Effective elastic stiffness increased by 170%;
- Lateral load resistance increased by 44%;
- The maximum moment location shifted upwards by 0.84 m (33 in.);
- The plastic region length reduced by 64% in the foundation shaft; and
- The gap opening at the base of the column reduced by 60%.

These results can be seen below where the cyclic testing data is presented graphically (see Figure 1-3). The results demonstrate the drastic difference between seasonal wintry conditions and summer conditions where one can see a significant difference in the lateral force at a comparable displacement between the two experiments. Due to the large variation in the lateral response of the system, any new development in the design process of an integrated column-foundation shaft should give consideration to this issue.

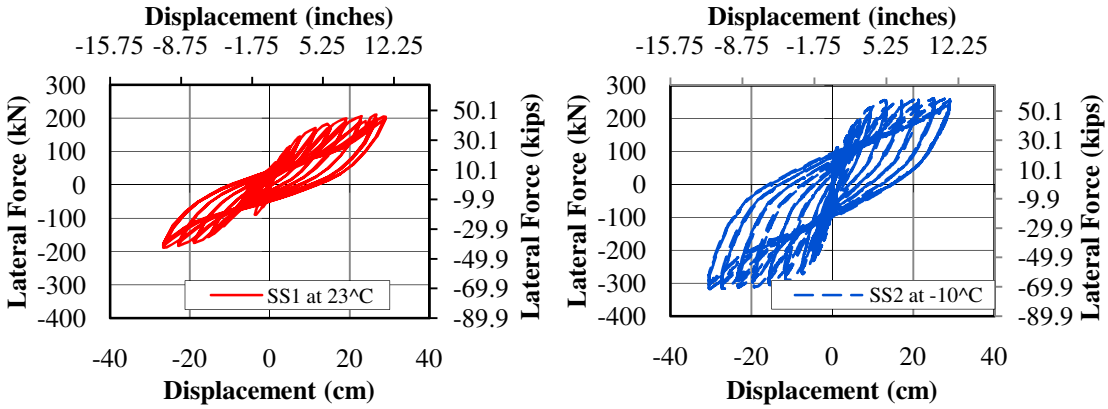

(a) SS1 at 23 °C (b) SS2 at -10 °C

Figure 1-3: Cyclic load testing results [Suleiman et al., 2006]

1.3 Types of Foundations

Over the years bridge superstructures have undergone many changes in seismic regions for both artistic and structural reasons. However, bridge substructures have essentially remained unchanged and can be classified into two main groups, those utilizing shallow foundations and those utilizing deep foundations. Shallow foundations are foundations located on competent soils that are able to support the structure directly through bearing for vertical loads. Shallow foundations require a large enough base to prevent overturning and sliding in order to handle horizontal loading. When the soil is not competent enough to support the structure or a shallow foundation is not cost effective, deep foundation systems are used.

1.3.1 Shallow Foundations

Shallow foundations are typically referred to as spread footings and consist of a rectangular pad of concrete that bears directly on the soil as depicted in Figure 1-4. This method of foundation construction generally requires less excavation and no specialized equipment, making this a cost-effective foundation when the soils permit. Although a spread footing is easy to construct and can lessen building costs, the cross-section of the spread footing may be inefficient because the footing has to be extremely large to prevent a failure due to bearing capacity, overturning or sliding. Inefficiency also appears within the spread footing because of how seismic loads are handled. When dealing with seismic loads, the typical method of design for a shallow foundation is to allow inelastic action to occur within the bridge column for ease of inspection, repair and design. By allowing the inelastic action to occur in the column, conversely, extensive amounts of reinforcement are generally required to keep the response of the footing elastic due to large shear demands at the interface between the column and base in both the vertical and horizontal directions. Therefore, this type is not commonly used in seismic bridge design practice. Another disadvantage to the spread footing is that the footing must be placed on a competent soil that will not cause significant settlement. Spread footings cannot be used in most bridge locations due to site constraints and the availability of competent soils to support the structure.

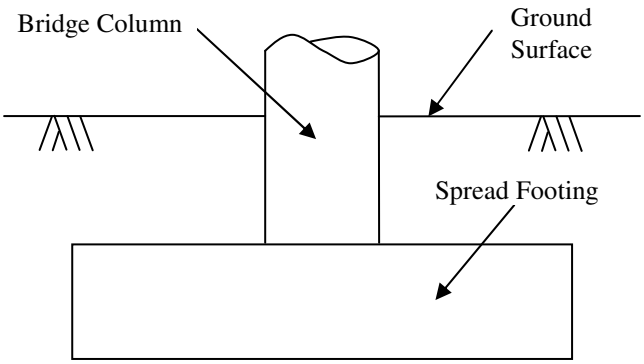

Figure 1-4: Typical configuration of a spread footing

1.3.2 Deep Foundations

When spread footings are not a suitable substructure support, deep foundations are used. Deep foundations use piles to transmit vertical and horizontal loads to the soil through the development of skin as well as tip resistance and passive lateral earth pressure, respectively. Pile systems come in many different forms and materials, as depicted in Figure 1-5, with specific advantages and disadvantages to each. For example, pile supported spread footings are generally assumed to maintain elastic behavior below the ground surface unlike a continuous column-foundation shaft, known as drilled or cast-in-drilled-hole (CIDH) shafts, which are typically designed to form inelastic action below the ground surface. Differences between types of piles also occur within the placing methods (i.e., driven versus cast-in-place). Unlike driven piles, cast-in-place concrete piles are able to develop an extremely high axial load as the piles are designed for the ultimate condition. The steel non-displacement driven pile disturbs less soil area during placement, thus allowing for a better characterization of soil properties and a more economical design. In general both driven and cast-in-place piles are very advantageous in areas where:

- environmental concerns prohibit excavation;
- weak soils cause excessive settlement;
- spread footings are not cost effective; and
- bridge locations, where deemed appropriate.

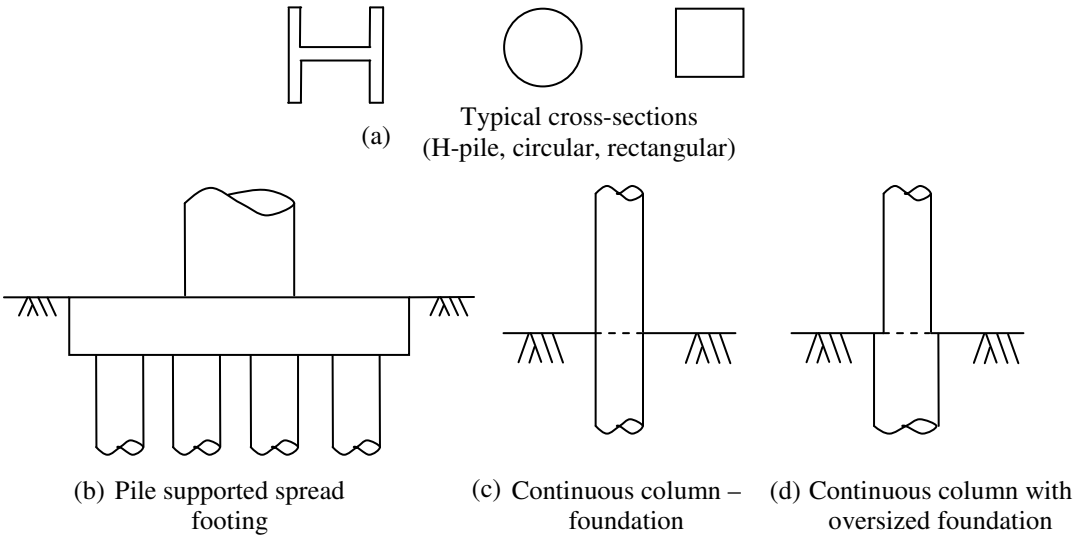

Figure 1-5: Different deep foundation systems

Currently, columns that extend into the ground as cast-in-drilled-hole (CIDH) shafts, as depicted in Figure 1-6, are a common column and foundation system due to the simplicity of construction, elimination of a column to foundation connection and reduced construction costs. The aforementioned benefits are continuing to make the continuous column foundation system more desirable to engineers in the bridge design community. Since the nature of the research performed during this project focuses on columns supported by drilled shafts, this foundation type will be the focus for the remainder of the report.

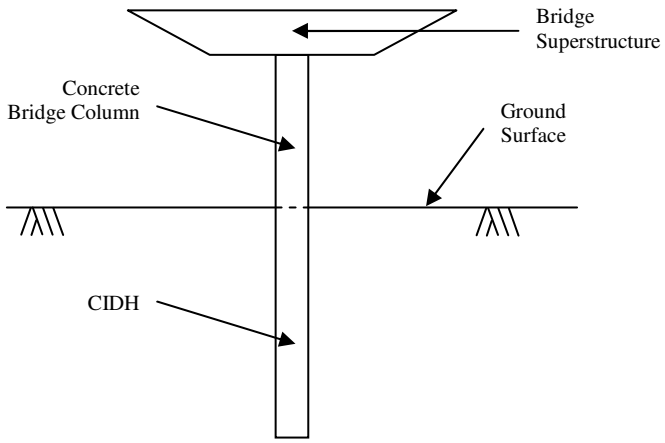

Figure 1-6: Typical bridge bent with a continuous column to cast-in-drilled-hole (CIDH) shaft from longitudinal axis

1.4 Soil-Foundation-Structure-Interaction

When performing seismic design, lateral loading is a critical portion of the design process and must be examined correctly. During the design process of integrated column-foundation systems, such as the one depicted in Figure 1-6, the effects of soil-foundation-structure-interaction (SFSI) further complicate the lateral loading analysis and thus the design methodology. SFSI complicates the process for multiple reasons, but all hinges on one issue: how to correctly model the effects of the soil onto the structural design. A dependable approach to capture these effects is by a complicated numerical analysis method that models the soils using nonlinear springs and determines the force-displacement response of piles subjected to lateral loading in soil as well as the overall structural response.

In addition to the complexity of the analysis, soil properties involved in SFSI, especially those near the ground surface, greatly influence the response of a CIDH shaft and the column that it is supporting. Soil located near the ground surface has the greatest influence on the response of the system, as this is where the soil is providing the largest amount of resistance to lateral movement. The amount of resistance provided within this critical region is the largest area of variability due to the depositional nature of soil, the type of soil present, the stiffness of the soil and the environmental surroundings (e.g., temperature). In addition to providing resistance to lateral movement, soil stiffness along the foundation depth dictates the global and local displacements of the system, the local curvature demand and much more.

Although soil is inherently variable with location and depth, the influence of SFSI on the design of continuous column-foundation systems subjected to lateral loading has been researched by numerous people [e.g., Reese et al. (1975), Priestley et al. (1996), Priestley et al. (2007), Budek et al. (2000), and Chai (2002)]. In the studies, researchers were typically looking for a way to better define the response of these system when subjected to lateral loading. For example Reese et al. (1975) improved on the definition of soil springs in cohesive soils whereas Chai (2002) expanded the definition of the flexural strength and ductility of an extended pile shaft. No matter what research was undertaken, the end goal was to obtain an accurate representation of the expected lateral response of the column, foundation and surrounding soil. A typical column-pile shaft with its expected displacement, expected moment profile and critical locations is presented in Figure 1-7. The critical

locations identified are the maximum moment location, the surrounding area needs the most confinement in seismic design, and the typical fixity point, current models assume that the foundation shaft is fully fixed against all deformation at this point.

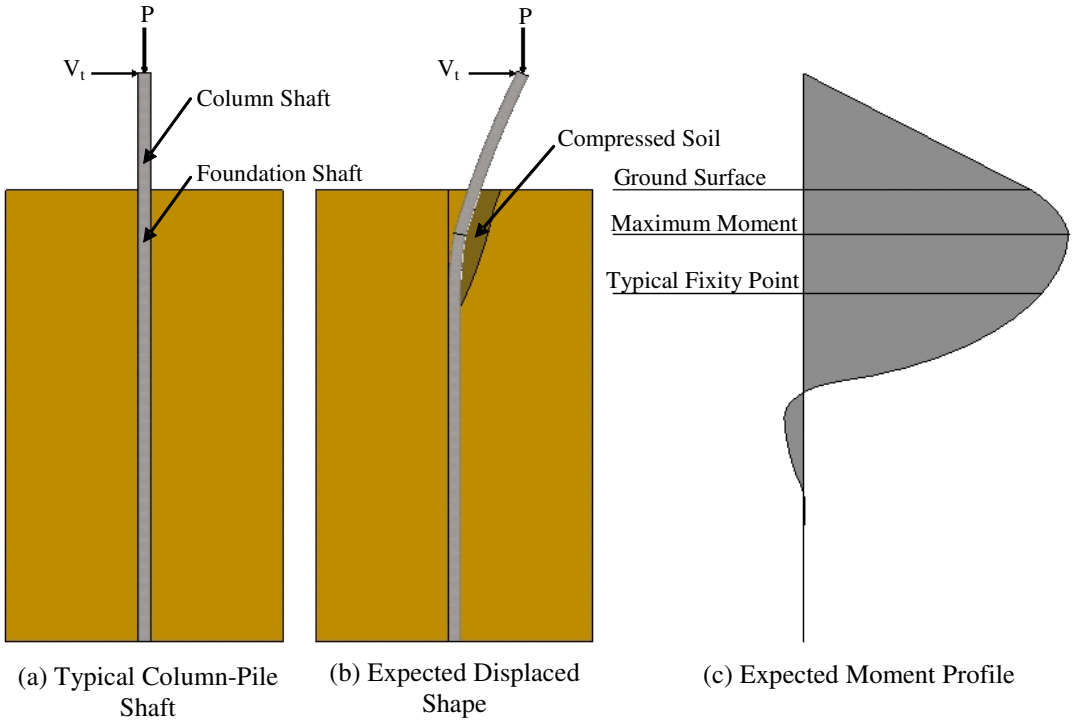

Figure 1-7: Typical response of a column supported on a CIDH shaft

1.4.1 State of Practice

Today's practice suggests simple and complex methods to account for the effects of SFSI. Although the complex methods are generally able to capture the realistic lateral load response, they take a considerable amount of time to complete and require a great deal of information about the structure and soil surrounding the foundation shaft. In this approach, it is especially important to accurately represent the soil as this will dictate the response on the local and global levels. To reduce the amount of information and time required to account for SFSI, simplified methods [e.g., Chai (2002), Priestley et al. (2007), etc.] are suggested for use in current guidelines and specifications (AASHTO, 2007 and 2009). These simplified methods generally establish an equivalent fixed base cantilever loaded laterally at the column tip without the presence of soil between the fixity location and ground surface. Even though this approach to modeling the overall system allows for simple calculations that can be

performed in significantly less time than a more complex approach, these simplified methods are not capturing the realistic response depicted in Figure 1-7.

The first reason as to why a realistic response is not captured occurs due to the fact that the base is assumed to be completely fixed against deformation. The fully fixed base implies that the maximum moment location occurs at this point and that no forces or displacements will occur below this point along the length of the foundation shaft. These implications, however, are not an accurate representation of the system as forces and displacements are expected to occur at and below this location and must be accounted for correctly (see Figure 1-7 and Figure 1-8).

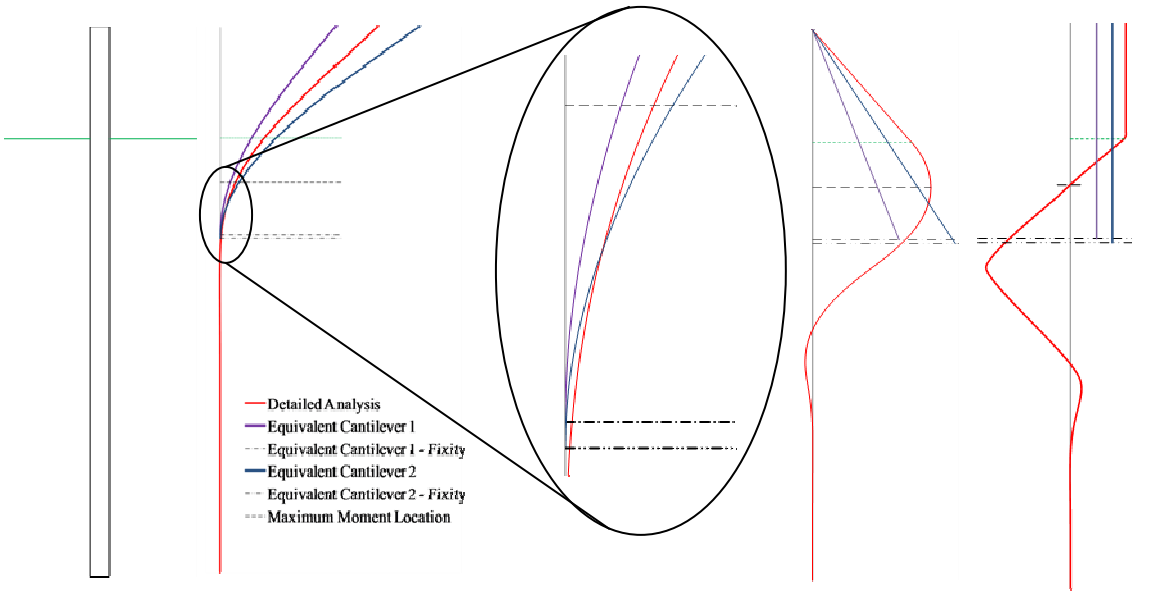

(a) Integrated Shaft (b) Deflection Profile (c) Moment Profile (d) Shear Profile

Figure 1-8: Comparison of equivalent cantilevers with expected response

Besides the challenges associated with capturing the displacement and forces along the length of the column and foundation shafts correctly (see Figure 1-8), a number of other challenges arise in the development and use of models in existence today. The first one stems from the way in which the different models were developed and verified for use in a cohesive soil. The major issue that arises within the verification area is that although models were developed for both cohesive and cohesionless soils, they were only verified against cohesionless soil experiments. Verifications are performed in this manner due to the ability of a researcher to better control the high variability of soil material properties. Even though

the different methods were verified in this manner, they were still suggested for use in cohesive soils although they do not capture the lateral response of integrated systems tested in clay soils (see Chapter 3). In addition, verifications were performed in a column of uniform soil which is not a realistic assumption in actual field conditions.

A second challenge associated with the models appears in the defining of the lateral response of a CIDH shaft. The model presented by Chai (2002) suggests that a perfectly plastic response between the yield and ultimate limit states will provide a good estimation of lateral response. This, however, is not accurate as can be seen in Figure 1-3 where an increase between the yield and ultimate limit states occurs. The increase comes from the combined effects of material nonlinearity in soil, concrete and steel when the column is pushed past the first yield state. In the method suggested by Priestley et al. (2007), the lateral shear forces applied at the top of the column are not easily determined since a significant amount of information is needed about damping and the design level earthquake. The last point made within this area is that some of the methods (e.g., AASHTO 2009) are only applicable when all of the materials are behaving within an elastic manner.

A third concern associated with the development of the models is that none of the researchers gave consideration to the effects of seasonal freezing in the development of the different models. Although ignored in the development, it is clear that wintry conditions significantly alter the effects of SFSI. The effects were previously mentioned with the quick overview of the research performed by Suleiman et al. (2006) and Sritharan et al. (2007) at Iowa State University. These challenges as well as others are expanded on in the report that follows in the literature review provided in Chapter 2 and the examination of common methods used in practice provided in Chapter 3.

1.4.2 Alternative Approach

When performing a design or analysis in engineering a free-body diagram (FBD) is typically used to represent a system and simplify the force and displacement calculations based on known constraints in the system. Using this approach, a FBD was constructed for a column supported on a CIDH shaft (see Figure 1-9a). In this diagram, the effective height of the system, L_{ma}, was taken to be the distance from the column tip to the maximum moment location. This point was chosen for the following reasons:

1. the maximum moment will occur here and this point must be defined for analysis and design purposes,
2. the most confinement will be placed in the area immediately surrounding this point to allow plastic action to form once the foundation shaft exceeds the yielding capacity, and
3. the point is the simplest location to cut the system without having to define multiple locations to account for plastic action and soil stiffeness.

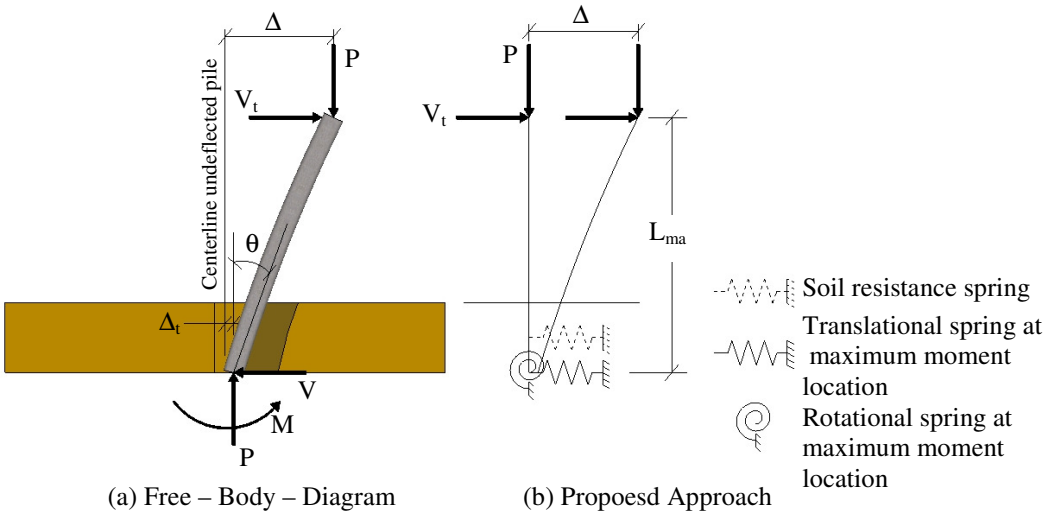

Figure 1-9: Alternative approach to accounting for SFSI

By constructing a FBD for this system, one can see that a flexible foundation system and the inclusion of a soil spring as shown in Figure 1-9b is more applicable to account for the effects of SFSI. In this approach, the rotational spring located at the maximum moment location would account for the elastic rotations occurring below this point as well as all of the plastic rotations, above and below this point, within the system. The translational spring as part of the flexible foundation accounts for the fact that the column-pile shaft system does not experience zero lateral displacement at the maximum moment location. By including this spring the displacement that forms due to the curvature of the pile below the maximum moment is included in addition to the possibility of a variable shear force along the shaft. The second translational spring, accounts for the resistance of the soil to lateral movement above the maximum moment location thus providing a more realistic representation. Although one soil spring is depicted, this could be replaced by multiple springs to better

define soil properties in this critical region more accurately. Through the inclusion of springs into the proposed model, the effects of soil stiffness are included into their definitions. In the springs at the flexible foundation, for example, the rotation and the lateral displacement will decrease when compared with an equivalent system pushed to the same force at the column tip in a softer soil. In addition, the soil spring would create a larger resistance to lateral movement thus causing the global displacement to decrease.

1.5 Scope of Research

In the current state of practice of designing bridges subjected to lateral loading in clay soils, a significant number of deficiencies were noted in current research performed by the author (see Chapters 2 and 3) at Iowa State University (ISU). The literature review within the current study has found that deficiencies in practice are located in the range of applicable soils, the model verifications, the handling of seasonal temperature effects and the lateral response over the full elastic and inelastic range. Based on the deficiencies noted within today's practices, the current project was undertaken with the overall scope being the development of a simplified model suitable for determining the lateral load response of deep bridge pier foundations in clay that is also able to account for seasonal temperature effects. In order to develop the simplified model, the project focuses on the following objectives:

1. A detailed examination of the current SFSI practice through a literature review;
2. A verification of existing models presented in current codes and the literature review;
3. The development of a simplified equation based model to capture the local and global responses of a continuous column-foundation system in clay with the inclusion of seasonal temperature effects; and
4. To formulate design and analysis recommendations suitable for continuous column-foundation systems in clay while ensuring the ability to handle seasonal temperatures.

1.6 Report Layout

The remainder of the report discusses in detail the procedures of the aforementioned project. The discussion began with the introduction to the project in this chapter by providing background information and the scope of the research undertaken in this study. The second chapter presents a detailed literature review into the current state of practice for

the design and analysis of drilled shafts subjected to lateral loading in clay soils. Using the information provided within Chapter 2, the third chapter provides a comparison of the different methods through an example column-foundation system. The fourth chapter of the report presents a new simplified methodology for the seismic design of drilled shafts in clay soils along with its verification. The fifth and final chapter of this report provides the conclusions and recommendations determined upon completion of the project.

CHAPTER 2: LITERATURE REVIEW

2.1 Introduction

In the seismic design and analysis of columns supported on CIDH shafts, SFSI is a component that must be included in any modeling techniques. Over the years, researchers are constantly improving the methods of accounting for SFSI through experimental and analytical studies, Table 2-1. The goal of each study normally falls within two categories, improvement or simplification of the soil spring concept (described in Section 2.2.1) used in today's practice.

Table 2-1: Studies on lateral loading of drilled shafts

Researcher	Year	Type of Study	Study Overview
Reese and Welch	1975	Experimental	Development of soil subgrade reaction-displacement curves (p-y curves) in clay soils for use in the Winkler soil spring concept
Crowther	1990	Experimental	Modification of curves by Reese and Welch for use in frozen clay soils
Priestley et al.	1996	Analytical	Determination of inelastic rotation and ductility of a column/foundation shaft in cohesionless soils
Budek et al.	2000	Analytical	Parametric study on the inelastic seismic response of reinforced concrete bridge column/pile shafts in non-cohesive soils to simplify Winkler model. Verified against experimental and in-situ testing.
Chai	2002	Analytical	Analytical model for the flexural strength and ductility of drilled shafts subjected to lateral loads in cohesive and non-cohesive soils
Chai and Hutchinson	2002	Experimental	Experimental testing on full scale drilled shafts in cohesionless soils. Used to verify the analytical model proposed by Chai (2002)
Suleiman et al.	2006	Experimental	Experimental testing on full scale integrated column/foundation systems in cohesive soil to examine the effects of seasonal freezing on the lateral response.
Suarez and Kowalsky	2007	Analytical	Parametric study on cohesive and non-cohesive soils for the displacement-based seismic design of drilled shafts. Verified against experimentation by Chai and Hutchinson (2002)
Sritharan et al.	2007	Analytical	Parametric study to examine the effects of seasonal freezing in clay soils.

Although multiple studies have been performed, a lack of accurate simplified lateral loading models in cohesive soils exists, even though these are typical soils around deep foundations. Concerns with today's methods are due to the way in which cohesive soil models were verified, their inability to capture seasonal freezing effects, omission of nonlinear material properties after yielding, and the inability to capture the global and local lateral response of CIDH shafts over the elastic and inelastic regions expected at design-level and greater seismic events. The verifications, for example, have been performed using experimentation in cohesionless soils due to the ability of the researcher to better control material properties, although the models are still recommended for cohesive soils. Besides the verification concern, the seasonal freezing is a major issue as continuous bridge column/foundation shafts may experience cold temperatures as low as -40 °C (-40 °F) and still need to perform as stipulated by the capacity design principles during a seismic event. Based on the nature of this project and challenges associated with current methods of accounting for SFSI, this chapter will examine today's state of design, analysis and overall behavior of continuous column-foundation systems in clay soils subjected to seismic loads during all seasons of the year.

2.2 Analytical Investigation

During the examination of the current state of practice, an investigation into the multiple methods available for determining design displacements and the lateral response of bridge columns that are supported by CIDH shafts was performed. The investigation found that these methods range from simple to complex in both the amount of information needed and the number of steps needed to execute the methods. The remainder of this analytical investigation section will examine in detail some of the more common methods [e.g., Reese et al. (1975), Crowther (1990), Priestley et al. (1996), Applied Technology Council (ATC, 1996), Budek et al. (2000), Chai (2002), Priestley et al. (2007) and American Association of State and Highway Transportation Officials (AASHTO, 2007 and 2009)] used for determining the lateral response of continuous column/foundation systems.

2.2.1 Reese and Welch (1975)

The Winkler foundation method is a very common detailed method in foundation engineering that uses a series of soil springs placed along the shaft length, as depicted in Figure 2-1, to determine the lateral response of drilled shafts. This method breaks down the column/foundation shaft into a series of equal length beam-column elements. Each element is then characterized by specifying the moment resistance and corresponding flexural stiffness, E_cI_{eff}, where E_c is the concrete modulus of elasticity and I_{eff} is the effective moment of inertia of the section. The resistance of the soil surrounding the foundation shaft is then modeled as a series of nonlinear compression-only springs located at the mid-height of each beam-column element. The springs are characterized by a p-y curve in which p defines a soil subgrade reaction (force/length) for a given displacement, y, of the soil. After defining these parameters along with the loading conditions, a finite difference method is typically followed to complete the numerical calculations. The finite difference method uses a numerical iteration process to handle the nonlinear material properties and ensure that equilibrium is obtained between the lateral soil springs, foundation element displacements and foundation element forces. A key component within this method is to accurately define the resistance of the soil surrounding the foundation shaft through the use of p-y curves. Although soil is highly variable in nature, many researchers have attempted to quantify the lateral resistance of different soils. In clay soils, an accepted method to represent the lateral behavior of soil was provided by Reese and Welch (1975).

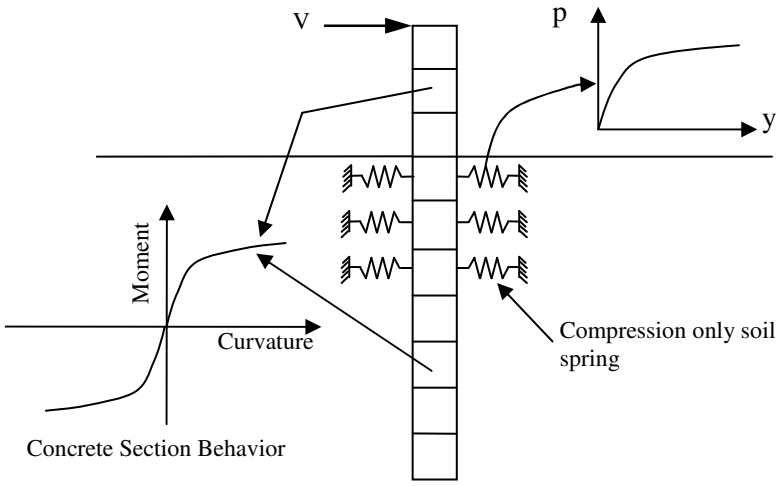

Figure 2-1: Winkler foundation model

In 1975, Reese and Welch performed experimental testing on full scale drilled shafts in a stiff to very stiff red clay (Beaumont clay). The goal of the project was to determine a soil modulus value that could be used in the well known differential equation, Equation 2-1, which relates the soil and structure for use in the Winkler foundation system when a deep foundation is loaded laterally. The differential equation is developed based off of structural equilibrium in the beam-column element shown in Figure 2-2 where M is the applied moment and V_v is the horizontal shear force.

$$EI\frac{d^4y}{dx^4} + P\frac{d^2y}{dx^2} - p = 0;\ p = -E_s y \tag{2-1}$$

where, EI = flexural stiffness of foundation;
y = lateral deflection of beam-column element and soil;
x = length along foundation;
P = axial load on column/foundation shaft
E_s = soil modulus; and
p = soil subgrade reaction.

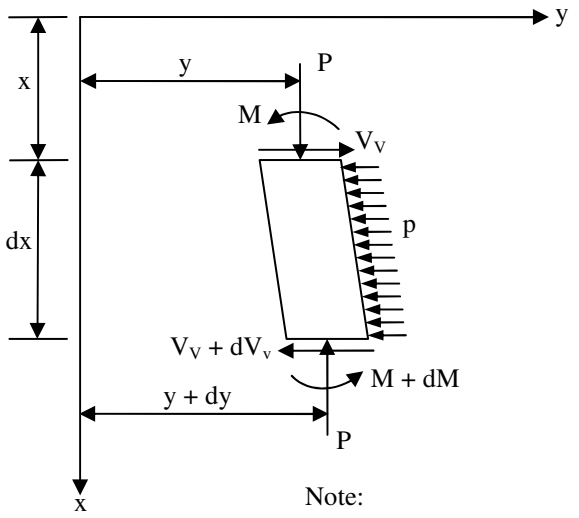

Figure 2-2: Beam-column element used in differential equation derivation

In order to obtain a relationship for the soil modulus, the experimental testing was performed ensuring that the moment profile along the length of the shaft could be determined. Using the computed moment value, a lateral deflection of the soil and

foundation shaft could be determined with a soil reaction at differing depths using standard beam theory from mechanics and numerical iteration processes. After completing the analysis of the data, Reese and Welch (1975) found that a power series with the soil reaction, p, normalized with respect to the ultimate soil reaction, p_u, and the soil deflection, y, normalized against the deflection at one-half the ultimate soil reaction, y_{50}, would provide a good representation of the horizontal soil resistance. Using this relationship, the following procedures were suggested to determine the short-term static p-y curves in clay soils:

1. Obtain the best estimate of variation of undrained shear strength, c_u or s_u, effective unit weight, γ, and strain corresponding to one-half the maximum principal stress difference, ε_{50}, along the length of shaft. If ε_{50} is unavailable, use a value of 0.005 or 0.010 with the larger value being more conservative.
2. Compute the ultimate soil resistance per unit length using the smaller of Equations 2-2 and 2-3.

$$p_u = \left(3 + \frac{\gamma x}{c_u} + 0.5\frac{x}{b}\right) c_u b \tag{2-2}$$

where, x = depth from ground surface to point of spring
b = width or diameter of foundation

$$p_u = 9 c_u b \tag{2-3}$$

3. Compute the deflection at one-half the ultimate soil subgrade reaction using Equation 2-4

$$y_{50} = 2.5 b \varepsilon_{50} \tag{2-4}$$

4. Compute the points describing the p-y curve using Equation 2-5. (Note: $p = p_u$ for all values of y beyond $y = 16y_{50}$).

$$\frac{p}{p_u} = 0.5\left(\frac{y}{y_{50}}\right)^{1/4} \tag{2-5}$$

A second method was also presented in conjunction with the above procedure if laboratory testing was performed on soil samples taken from the site. The idea being that the p-y curve can be derived on the basis that it will follow the same shape as the soil stress-strain curve. Using this concept, the p-y curve could be constructed using the relationship

shown in Equation 2-6 to find the lateral deflection of the soil where the exponent b is taken to be one-quarter and Equation 2-5 to find the corresponding soil subgrade reaction.

$$\left(\frac{y}{y_{50}}\right)^{b} = \left(\frac{\varepsilon}{\varepsilon_{50}}\right)^{1/2} \tag{2-6}$$

2.2.2 Crowther (1990)

A key part in constructing the p-y curves for soils is to ensure that an appropriate exponent is used on the deflection criteria in the model produced by Reese and Welch (1975). Crowther (1990) examined the prediction of lateral displacements in frozen layered soils. The investigation included the use of data obtained from testing performed by Weaver and Morgenstern (1981) as well as Sayles and Haines (1974). During the study, Crowther demonstrated that by modifying the exponent, b, to a value of 0.33, a satisfactory performance could be obtained in frozen clays. This modification shall be important to this project as the new methodology must be able to handle seasonally cold temperatures.

2.2.3 Priestley et al. (1996)

Priestley et al. (1996) suggested that the plastic hinge length and depth of plastic hinge follow a hyperbolic trend related to a normalized value based on the flexural stiffness, EI_{eff}, of the foundation shaft and a soil subgrade modulus, K. The graphs, Figure 2-3, presented in this reference were an initial portion of the work that would be later published by Budek et al. (2000). Although the trends were initially suggested for soils in general, the research published later states that the trends were developed and verified only for cohesionless soils. The aforementioned graphs, therefore, are inappropriate for use in the modeling of a cohesive soil. In addition to being invalid for clay soils, no methodology was presented on how to use these graphs in the design of continuous column/foundation systems. The only suggestion provided for handling a bridge column that extends into the ground as a CIDH shaft is to perform an elastic analysis and shift the location of the maximum moment towards the ground surface. The upwards shift was stated to be 30% of the total depth predicted by an elastic analysis.

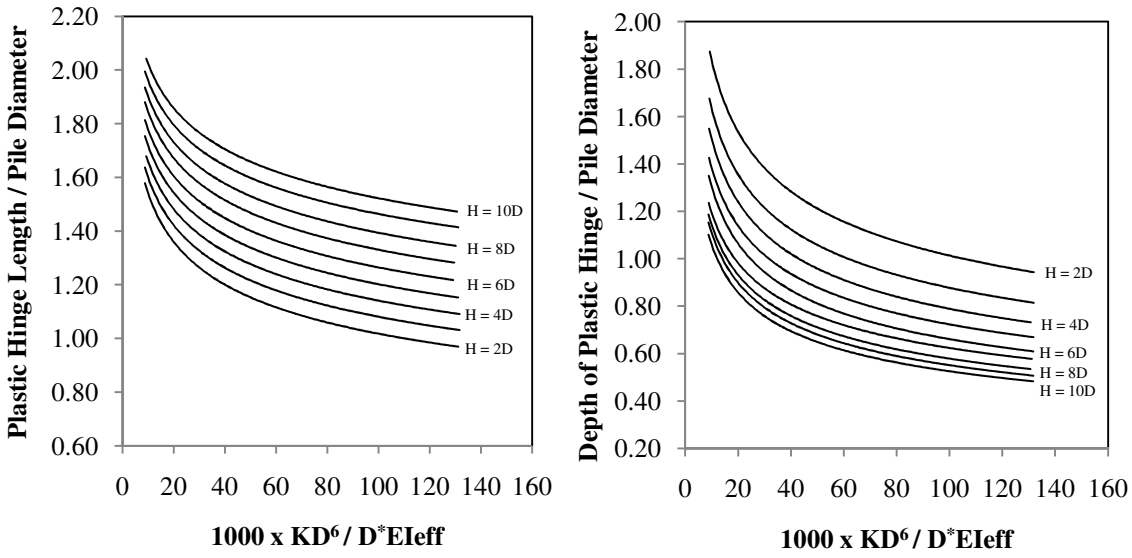

Figure 2-3: (a) Plastic hinge length; (b) depth to plastic hinge location [Reproduced from Budek et al., 2000]

2.2.4 Chai (2002)

Chai proposed a model to determine the lateral response of extended pile shafts while accounting for the effects of soil. The model relies on the use of two points, fixity and maximum moment, along the length of the system in order to determine the systems flexural strength and ductility. A visual representation of the model and the two points defining the fixity and the maximum moment locations used to determine the lateral loading and displacements of the column/foundation system in a uniform layer of soil, cohesive or non-cohesive, are shown in Figure 2-4.

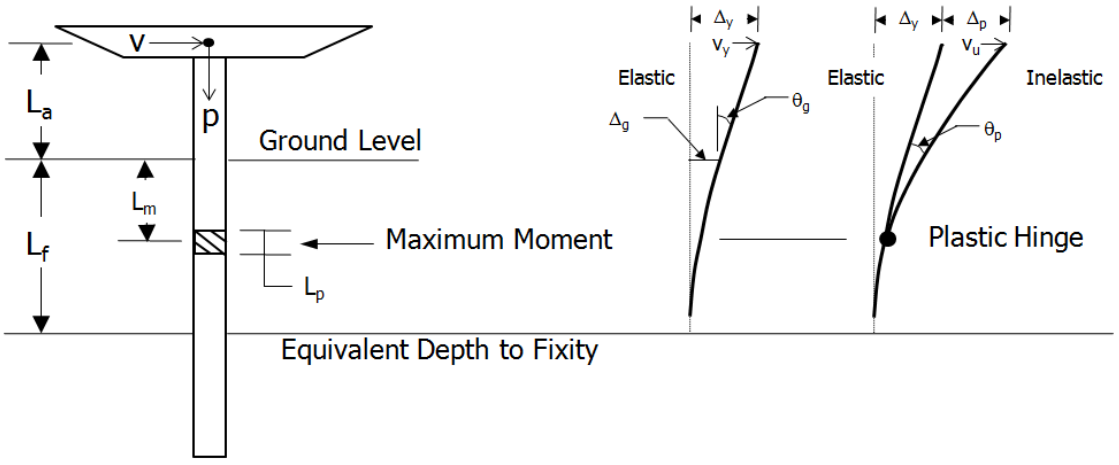

Figure 2-4: Equivalent fixed-base cantilever (reproduced from Chai 2002)

Chai started the development of the model by determining the point of fixity over the elastic and inelastic regions which would relate the stiffness of a soil-pile system, K_{sp}, to the stiffness of an equivalent fixed-base cantilever, K_c. The stiffness of the cantilever is defined as the shear force, V, applied at the top of the column divided by the lateral displacement at the top of the cantilever, Δ. The stiffness expression was further expanded into Equation 2-7 using principles of mechanics.

$$K_c \equiv \frac{V}{\Delta} = \frac{3EI_e}{(L_f+L_a)^3} \tag{2-7}$$

where, EI_e = effective flexural rigidity of the cantilever;
L_f = equivalent depth-to-fixity; and
L_a = above ground height of the column.

In order to relate the equivalent cantilever system to the soil-pile system in a cohesive soil which is the focus of this report, the closed form solution to ground movement (see Equations 2-8 and 2-9) of a long pile subjected to lateral loading produced by Poulos and Davis (1980) was used.

$$\Delta_g = displacement\ at\ ground\ level = \frac{V(L_a+\sqrt{2}R_c)}{k_h R_c^2} \tag{2-8}$$

where, $R_c = pile\ characteristic\ length = \sqrt[4]{\frac{EI_e}{k_h}}$; and
$k_h = constant\ modulus\ of\ subgrade\ reaction = 67s_u$

$$\theta_g = rotation\ of\ pile\ at\ ground\ level = \frac{V(\sqrt{2}L_a+R_c)}{k_h R_c^3} \tag{2-9}$$

The closed form solution was added to the above ground cantilever displacement, Δ_{La}, to develop Equation 2-10, which defines the total displacement of the soil-pile system, Δ_{sp}, within the elastic region.

$$\Delta_{sp} = \Delta_g + \theta_g L_a + \Delta_{L_a} \tag{2-10}$$

where, $\Delta_{L_a} = \frac{VL_a^3}{3E_c I_e}$; and
I_e = effective moment of inertia of the foundation shaft.

After obtaining the total displacement of the soil-pile system, the stiffness of the soil-pile system can be determined. At this point, K_c and K_{sp} are set equal to one another, thus locating the equivalent point of fixity. In order to efficiently equate the two stiffness terms,

the above ground height and depth to fixity were defined in terms of the characteristic length of the pile (i.e., $L_a = \xi_a R_c$ and $L_f = \xi_f R_c$ where ξ_a and ξ_f are coefficients for the above ground height and equivalent depth-to-fixity, respectively). The soil-pile system stiffness can be written as shown in Equation 2-11 with the coefficient for the equivalent depth-to-fixity being computed through Equation 2-12.

$$K_{sp} = \frac{3k_h R_c}{3\sqrt{2}+6\xi_a+3\sqrt{2}\xi_a^2+\xi_a^3} \tag{2-11}$$

$$\xi_f = \sqrt[3]{4.24 + 6\xi_a + 4.24\xi_a^2 + \xi_a^3} - \xi_a \tag{2-12}$$

Once the point of fixity is located, the maximum moment location is also needed in order to determine the ductility capacity of the system. Using a modified version of Broms (1964) soil pressure distribution acting on the pile (see Equation 2-13), shear and moment relationships are developed based off of static equilibrium of horizontal forces and bending moments. The shear and moment relationships are presented in Equation 2-14 and Equation 2-15, respectively.

$$p_u(z) = \begin{cases} \frac{1}{27} c_u \left[54 + 84\frac{z}{D} - 7\left(\frac{z}{D}\right)^2\right] \; for \; z \le 6D \\ 11.3 c_u \; for \; z > 6D \end{cases} \tag{2-13}$$

where, z = depth below the ground surface; and
D = pile diameter

$$V_u^* = 2L_m^* + \frac{14}{9}{L_m^*}^2 - \frac{7}{81}{L_m^*}^3 \quad for \; L_m^* \le 6 \tag{2-14}$$

where, $L_m^* = normalized \; depth \; to \; maximum \; moment = \frac{L_m}{D}$; and

$V_u^* = normalized \; lateral \; strength \; of \; soil - pile \; system = \frac{V_u}{c_u D^2}$;

$$M_{max}^* = 2L_a^* L_m^* + \left(1 + \frac{14}{9}L_a^*\right){L_m^*}^2 + \frac{7}{81}(12 - L_a^*){L_m^*}^3 - \frac{7}{108}{L_m^*}^4 \; for \; L_m^* \le 6 \tag{2-15}$$

where, $L_a^* = normalized \; aboveground \; height = \frac{L_a}{D}$; and

$M_{max}^* = normalized \; flexural \; strength \; of \; pile = \frac{M_{max}}{c_u D^3}$

The normalized depth to maximum moment and ultimate lateral strength of the system can now be determined using an idealized elasto-plastic moment-curvature response established for the cross-section of the foundation shaft. Chai (2002) then proposed that a

perfectly plastic response between the yield and ultimate conditions be assumed for the force-displacement response of the equivalent fixed-base cantilever. Using the aforementioned assumptions, the displacement ductility, μ_Δ, of the system and curvature ductility, μ_ϕ, of the foundation shaft are related, allowing the curvature demand for the foundation shaft to be determined based off of the desired displacement ductility of the system. In order to determine the yield displacement, Δ_y, for use in finding the ductility, two relationships for the ultimate lateral force, V_u, were equated and rearranged in order to find the lateral yield displacement. They are presented below as Equations 2-16 and 2-17.

$$V_u = \begin{cases} \frac{3EI_e}{\left(L_a^* + L_f^*\right)^3 D^3}\Delta_y \\ \frac{M_{max}}{M_{max}^* D} V_u^* \end{cases} \quad (2\text{-}16)$$

$$\Delta_y = \frac{\phi_y}{3}\frac{\left(L_a^* + L_f^*\right)^3 V_u^* D^2}{M_{max}^*} \quad (2\text{-}17)$$

where, ϕ_y = equivalent elasto-plastic yield curvature.

The plastic displacement, Δ_p, of the system is the final portion needed in order to determine the ultimate displacement, Δ_u, and therefore the displacement ductility of the system. The plastic action is found by assuming that all of the plastic rotation, θ_p, is concentrated at the maximum moment location and equal to the plastic curvature, ϕ_p, multiplied by the length of the plastic hinge, L_p. The plastic curvature is defined as a curvature, ϕ, beyond the yield point minus the idealized yield curvature. Chai then normalized the plastic displacement equation with respect to the column diameter leading to the final relationship depicted in Equation 2-18.

$$\Delta_p = \theta_p(L_a + L_m) = \lambda_p \phi_p (L_a^* + L_m^*) D^2 \quad (2\text{-}18)$$

where, $\theta_p = (\phi - \phi_y)L_p = \phi_p L_p$; and
λ_p = normalized plastic hinge length = L_p/D

Using the yield and plastic displacements, the displacement ductility of the system was related to the demand curvature ductility. The final relationship for the displacement ductility suggested by Chai is presented in Equation 2-19.

$$\mu_\Delta = 1 + 3\lambda_p(\mu_\phi - 1)\frac{(L_a^* + L_m^*)}{(L_a^* + L_f^*)^3}\frac{M_{max}^*}{V_u^*} \quad (2\text{-}19)$$

The normalized plastic hinge length in the model is a key component within the analysis as this plays a significant role in determining the ultimate displacement of the soil-pile system. As stated in Section 2.2.2, previous research found that the plastic hinge length varies with the lateral stiffness of the soil surrounding the foundation shaft; however, this was shown to be inaccurate in a companion paper to the analytical model presented by Chai (2002). The companion paper by Chai and Hutchinson (2002) found that the plastic hinge length was insensitive to the lateral stiffness of the soil through an experimental investigation. The experimental investigation was performed on full-scale column to drilled shaft systems in cohesionless soils of different densities. During the analysis of the data, the plastic hinge length was found to primarily depend on the aboveground height of the column. Using the results of the experimentation Chai suggests that a plastic hinge length varying from 1.0D at ground level to 1.6D at an aboveground column height of L_a = 6D. After this point the plastic hinge length is assumed to be constant for all other aboveground column heights. The suggested relationship for both cohesive and cohesionless soils is shown as a function of the normalized aboveground height in Equation 2-20 and graphically in Figure 2-5.

$$\lambda_p = \frac{L_p}{D} = \begin{cases} 1 + 0.1\frac{L_a}{D} & for\ \frac{L_a}{D} \le 6 \\ 1.6 & for\ \frac{L_a}{D} > 6 \end{cases} \quad (2\text{-}20)$$

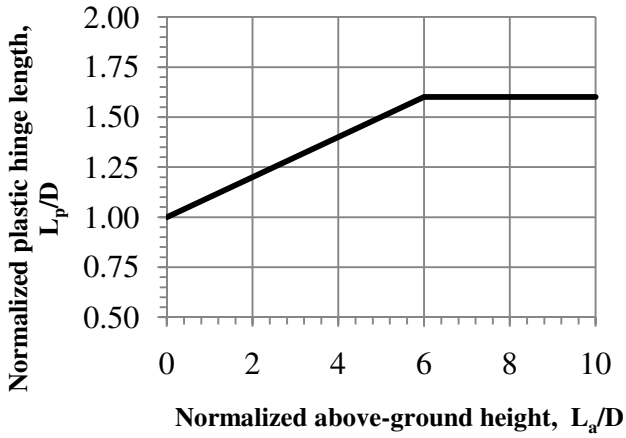

Figure 2-5: Assumed equivalent plastic hinge length of concrete piles (after Chai 2002)

Although Chai model was verified experimentally in Chai and Hutchinson (2002), some limitations are noted for this model and its verifications at first glance. The first limitation with the model is that the verification was performed only within a uniform layer of cohesionless soils, although recommended for both cohesive and non-cohesive soils. This would ensure that the model accurately represents a cohesionless soil, but it does not verify the validity of the cohesive soil model. The second challenge associated with the model is that a perfectly plastic response between the yield and ultimate conditions was assumed for the lateral response of the system. The perfectly plastic response is an inaccurate representation of actual conditions because it does not account for the strength gains accrued due to the combined effects of soil and material nonlinearity in the plastic region of lateral loading. The third limitation noted at first glance is that multiple locations, apparent fixity and maximum moment, are needed to define the global response of the system. By needing multiple points to define the system, the model cannot be easily input into a structural analysis program and used as part of the full analysis of the structure. If the model is input into structural analysis software, the maximum moment will form at the fixity location. This, however, is an inaccurate representation and why two points were used to define the overall response of the system. Further examination of this model is presented in Chapter 3 to identify other challenges associated with the use of this model.

2.2.5 Priestley et al. (2007)

In 2007, Priestley et al. published a textbook on displacement-based seismic design of structures. The book covers the multiple types of structures, steel to concrete and buildings to bridges, including the topic of bridge columns that extend into the ground as CIDH shafts. During the presentation of the aforementioned topic area, a model is introduced by Priestley et al. (2007) to determine the design displacement of a column/foundation system including the effects of SFSI, which is discussed in detail in the remainder of this section. A visual depiction of the terminology used within this method is presented within Figure 2-6 where $H_{cp} = 0$ when a pinned connection to the superstructure exists.

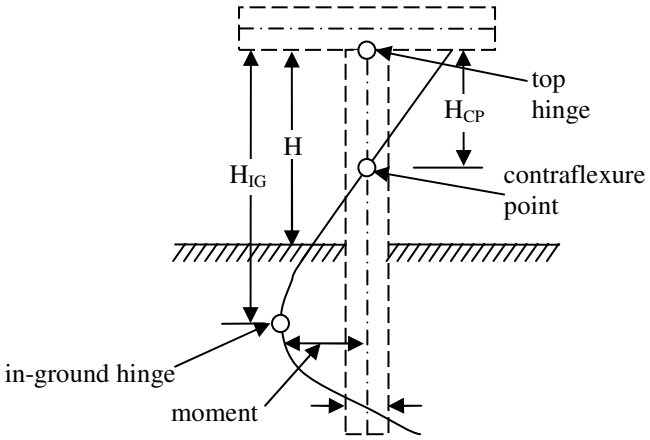

Figure 2-6: Moments in pile/column system (after Priestley et al., 2007)

The method introduced for handling soil-structure-interaction is a variation on the design displacement model suggested by the authors for use in a bridge column supported on a pier. For a pier supported bridge column, the design displacement is determined by adding the yield displacement to the plastic displacement. The yield displacement for a pier supported column is presented in Equation 2-21, where C_1 is a constant dependent on end-fixity; H is the effective height of the column and L_{sp} is a length used to account for the effects of strain penetration when appropriate.

$$\Delta_y = C_1 \phi_y \left(H + L_{sp}\right)^2 \tag{2-21}$$

Priestley et al. (2007) has suggested that the yield displacement is modified such that strain penetration is neglected and the effective column height is taken as the distance from the in-ground plastic hinge to the top of the column in a pinned connection to the superstructure, Equation 2-22.

$$\Delta_{y,IG} = C_1 \phi_y H_{IG}^2 \tag{2-22}$$

If a fixed connection is present at the level of the superstructure, the top hinge will dictate the design displacement and modifications must be made to Equation 2-21. These modifications include changing the coefficient for end fixity conditions to a fixed superstructure, replacing the effective height with the depth to the point of in-ground hinging, and using strain penetration effects. The new relationship is presented below as Equation 2-23.

$$\Delta_{y,F} = C_1 \phi_y \left(H_{IG} + L_{sp}\right)^2 \tag{2-23}$$

The modifications to the pier supported system were proposed based off of research done by Suarez and Kowalsky (2007). In the reference, the results of a parametric investigation into the effects of SFSI on drilled shafts were presented. For cohesive soils, two different undrained shear strengths, c_u = 20 kPa and 40 kPa (420 psf and 840 psf), were examined. An analysis of the data led to Equation 2-24 for locating the in-ground hinge as well as Equation 2-25 for modifying the coefficient that accounts for end-fixity conditions based off of the undrained shear strength parameter and head fixity.

$$\frac{H_{IG}}{D} = \begin{cases} 6.38 + 0.69\frac{H}{D} & for\ \ c_u = 20kPa\ (420\ psf) \\ 4.96 + 0.71\frac{H}{D} & for\ \ c_u = 40kPa\ (840\ psf) \end{cases} \tag{2-24}$$

$$C_1 = \begin{cases} 1.840 - 0.363ln\left(\frac{H}{D}\right) & for\ \ c_u = 20kPa\ (420\ psf) \\ 1.767 - 0.360ln\left(\frac{H}{D}\right) & for\ \ c_u = 40kPa\ (840\ psf) \\ 0.447 - 0.055ln\left(\frac{H}{D}\right) & for\ \ fixed\ head \end{cases} \tag{2-25}$$

After determining the modifications as presented above, the design displacements are computed for the column/foundation system using the following procedures:

1. Locate the in-ground plastic hinge using Equation 2-24;
2. Determine the yield and ultimate limit state curvatures of the foundation shaft, ϕ_y and ϕ_u, using equations presented in the text for the yield limit state and damage-control limit strains of concrete and steel to find the appropriate ultimate limit state curvature, ϕ_{ls};
3. Find the analytical plastic hinge length, L_p, based off the head fixity conditions. For a pinned condition, use the plastic hinge length presented in Section 2.2.3 as suggested by Chai (2002). For a fixed head condition, use Equation 2-26.

$$L_p = kH_{cp} + L_{sp} \geq 2L_{sp} \tag{2-26}$$

where, $k = 0.2\left(\frac{f_u}{f_y} - 1\right) \leq 0.08$;

$$L_{sp} = \begin{cases} 0.022 f_{ye} d_{bl} & for\ f_{ye}\ in\ MPa \\ 0.15 f_{ye} d_{bl} & for\ f_{ye}\ in\ ksi \end{cases};$$

f_u = ultimate stress of flexural reinforcement;

f_y = yield stress of flexural reinforcement;
f_{ye} = expected yield stress of CIDH shaft longitudinal reinforcement; and
d_{bl} = diameter of CIDH shaft longitudinal reinforcing bars.

4. Determine the end-fixity coefficient, C_1, using Equation 2-25;
5. Find the yield displacement using Equations 2-22 and 2-23 depending on head fixity conditions; and
6. Find the design displacement, Δ_D, using Equation 2-27 for the pinned head condition or Equation 2-28 for the fixed head condition.

$$\Delta_D = \Delta_{y,IG} + \left(\phi_{ls} - \phi_y\right) L_p H_{IG} \quad (2\text{-}27)$$

$$\Delta_D = \Delta_{y,F} + C_3\left(\phi_{ls} - \phi_y\right) L_p H_{IG} \quad (2\text{-}28)$$

where, C_3 = coefficient to account for changing moment pattern = 1.54

The method presented within this section appears to have limitations. The first limitation of this model for cohesive soils is that it is only applicable to soils in a limited range of undrained cohesive strengths, c_u = 20 kPa (420 psf) and 40 kPa (840 psf). The limited range is a concern as stiff cohesive soils could reach undrained shear strengths as high as 400 kPa (8350 psf). The next challenge associated with this method is that the verification of the model performed by Suarez and Kowalsky (2007) was only performed for cohesionless soils by using the experimental data produced by Chai and Hutchinson (2002). The third major limitation arises because the lateral shear demands are not produced by the model. The lack of this information means that a bilinear force-deflection curve cannot be produced.

2.2.6 American Association of State and Highway Transportation Officials (AASHTO)

In the United States of America, bridge design is generally dictated by the current specifications and interim revisions published by the American Association of State and Highway Transportation Officials (AASHTO). The code being used today was published in 2007 with interim revisions updated yearly to maintain changes while the next code is being developed. Within the AASHTO specifications (2007), two methods are deemed appropriate for ensuring that an adequate displacement capacity is provided for laterally loaded foundation shafts. Both methods require an extensive knowledge about the subsurface

surroundings as well as an iterative process that is not easy to perform using hand calculations.

The first of the two methods is to perform an analysis using the Winkler foundation method that was previously presented within Section 2.2.1. The second method suggested for use is the strain wedge model. This model uses an iterative process to relate the one-dimensional beam on an elastic foundation to that of an envisioned three-dimensional passive wedge of soil that will form on the front of a pile (see Figure 2-7) when pushed laterally (Ashour et al., 1998). Although both methods have been shown to accurately represent the behavior of laterally loaded CIDH shafts, the models require a great deal of knowledge about the pile and surrounding soil and take a significant number of iterations to complete especially within the inelastic displacement range.

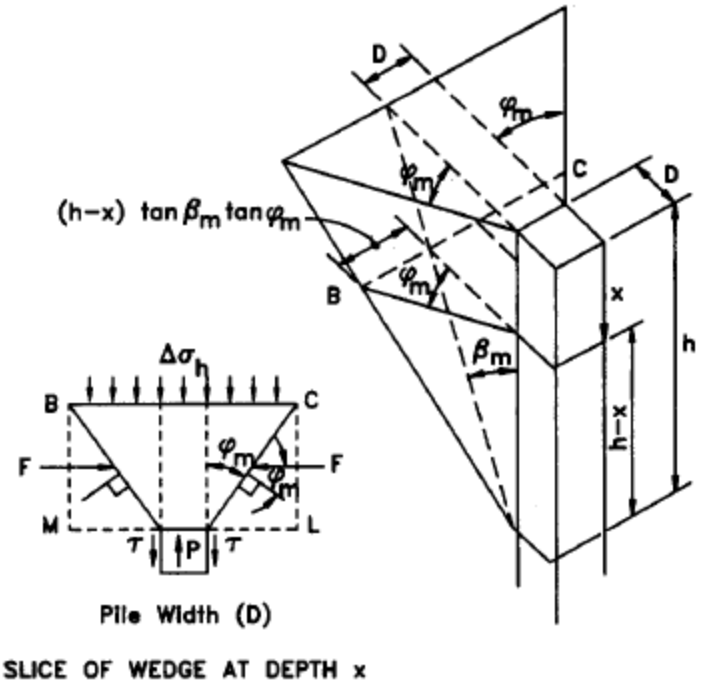

Figure 2-7: Basic strain wedge theory model in a uniform soil (Ashour et al., 1998)

In an attempt to update the specifications used for the LRFD seismic design of bridges, AASHTO recently published guidelines (AASHTO 2009) that may be used in conjunction with the previously discussed specifications. The new guidelines present multiple methods, from simple to complex, for determining the lateral response of pile foundations based on

site location, bridge design and site importance. Many of the models suggested in the main guidelines and commentary have already been discussed. Within the main commentary, the detailed method suggested for use is the Winkler foundation system that was presented in Section 2.2.1. The simple methods presented within the commentary were those proposed by Chai (2002) and Priestley et al. (2007), and they were previously discussed in Sections 2.2.4 and 2.2.5, respectively. Each of these methods was suggested for use in both cohesive and non-cohesive soils as specified by the authors.

The final method that was presented within the new guidelines is to determine the effective point-of-fixity for the soil-shaft system. This method is suggested within the main guidelines and uses an empirical equation to locate the effective point-of-fixity in which an equivalent cantilever system can be modeled without any surrounding soil and the base being fully constrained from deformation. The top of the equivalent cantilever system is modeled based on the constraints imposed by the bridge superstructure. In order to locate the equivalent point of fixity, Equation 2-29 was proposed for use in a uniform layer of cohesive soil. A secondary approach is suggested for a uniform layer of cohesionless soil, but is not presented here as the main focus of this project is on cohesive soil models. The empirical equation was found based on the research performed by Davisson and Robinson (1965).

$$L_f = 1.4\left(\frac{E_p I_w}{E_s}\right)^{0.25} \tag{2-29}$$

where, E_p = modulus of elasticity of pile (ksi);
E_s = soil modulus for clays = $0.465c_u$ (ksi);
I_w = weak axis moment of inertia for pile shaft (ft^4); and
c_u = undrained shear strength of clays (ksf).

The main limitation associated with this model is that the maximum moment will develop at the point of fixity. However, the maximum moment will generally not occur at the point of fixity but rather between this point and the ground surface. The location of the maximum moment is critical as this will determine the region at which the most damage will occur within the system and where the confinement reinforcement is required to maintain an adequate response of the concrete foundation shaft due to seismic loading. When compared with Chai (2002) and Priestley (2007) this method is much simpler to perform, but it is only

applicable in the elastic region of loading to be experienced by the column/foundation system.

2.3 Seasonal Freezing Investigation

As noted previously, some of the largest earthquakes recorded in the history of the United States and the world have taken place during winter months. Examples include the New Madrid earthquake sequence of 1811-1812, the Great Alaska earthquake of 1964 (M_L = 9.2), the Nisqually earthquake of 2001 (M_L = 6.9) in Washington, and several large magnitude Hokkaido earthquakes. Although the occurrence of major future earthquakes cannot be predicted, seasonal temperature variations across the United States are well known. In areas expected to seasonally freeze, the following temperature variations are expected:

- Alaska – 60 °C (110 °F) variation;
- Midwest – 30 °C (75 °F) variation;
- Eastern – 30 °C (75 °F) variation; and
- Western – 20 °C (50 °F)

Despite these drastic temperature changes, they are not accounted for in routine design although structural behavior and SFSI can be greatly influenced. Understanding the influences of cold temperature on structural behavior and SFSI are especially critical within the field of seismic engineering in order to prevent undesirable failure modes in the capacity design philosophy.

2.3.1 Effects of Seasonal Freezing

In order to understand the effects of seasonal freezing on deep bridge pier foundations, Sritharan et al. (2007) undertook an exploratory research program into the lateral response of integrated bridge column/foundation systems with a CIDH shaft subjected to seasonal freezing. The exploratory research program consisted of analytical and experimental components. Following completion of the experimental investigation (Suleiman et al., 2006) the analytical study was performed by Sritharan et al. (2007).

The experimental investigation was performed on three full-scale integrated bridge column-foundation systems located on the grounds of Iowa State University in Ames, Iowa. Using multiple cone penetration tests (CPTs), the soil present at the site was further classified

as low plasticity clay according to the Unified Soil Classification System (USCS). As part of the experimental investigation performed on this site, two of three specimens were identical and were constructed as continuous bridge columns that extended into the ground as drilled shaft foundations in order to directly compare the effects of seasonal freezing in a lateral loading situation. The third specimen, which will not be discussed within this report, consisted of a bridge column supported on an oversized drilled shaft foundation.

The two identical systems, SS1 and SS2, had 0.61 m (24 in.) diameter column shaft sections with column heights of 2.69 m (106 in.) and shaft lengths of 10.36 m (410 in.). The systems were reinforced longitudinally with a two percent longitudinal reinforcement ratio, ρ_l, along the entire column length as this represents an average steel ratio for columns in high seismic regions (Priestley et al., 1996) and Midwest bridge columns, which are generally not designed for seismic events. The aforementioned steel ratio was obtained by using twenty number six bars [d_b = 19 mm (0.75 in.), d_b = diameter of bar] as the longitudinal reinforcement. The transverse reinforcement ratio, ρ_s, was designed in accordance with codes for seismic regions and found to be eight tenths of a percent in the critical plastic hinge region. In order to obtain this transverse steel ratio, number three bar [d_b = 9.5 mm (0.375 in.)] in a spiral reinforcement pattern with a spacing of 63 mm (2.5 in.) was used along the entire column length and top two thirds of the foundation shaft. The remaining portion of the foundation shaft, a non-critical region, contained a number three bar spiral with spacing of 152 mm (6 in.). The cross-section details are presented graphically in Figure 2-8 below.

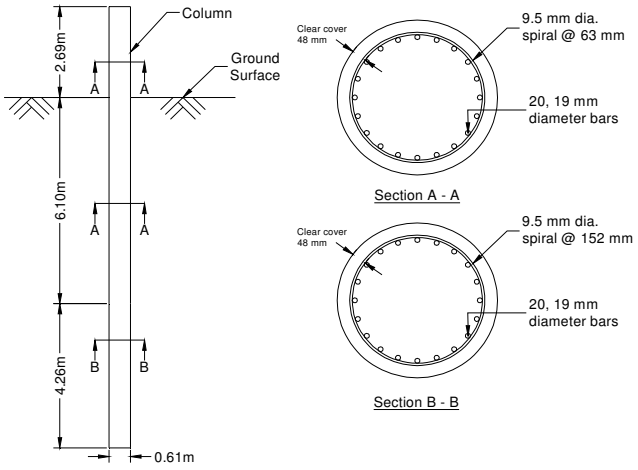

Figure 2-8: Cross-section details of column-shafts (after Sritharan et al., 2007)

As a part of this investigation, material testing was performed to identify changes caused by seasonal freezing. The material testing consisted of unconfined compressive strength tests for the concrete and cone penetration tests for the surrounding soil. The differences noted from the cone penetration testing were that the tip resistance differed markedly near the ground surface from an unfrozen state to a frozen state. In addition to the differences in tip resistance near the ground surface, a frozen soil layer of 0.75 m (~30 in.) was identified from temperature readings taken in the soil surrounding the foundation shafts. The unconfined compressive strength testing found that the concrete strength increased during the frozen state as opposed to the unfrozen state. To ensure that the correct deviation in material properties were determined, the aforementioned testing was performed at the same ambient temperatures as the testing of SS1 and SS2, 23 °C and -10 °C respectively.

The lateral loading of the columns consisted of repeated pushing and pulling against a reaction column in a quasi-static manner. One load cycle was used until the theoretical displacement for first yielding was reached. After this point, three loading cycles per target displacement were used. This method of loading was performed to effectively capture the effects of degradation that will occur after the initial loading to a specified target displacement. The testing continued in this manner until the limitations of the actuator were obtained, which was about 280 mm (11 in.) in the push direction and 290 mm (11.5 in.) in the pull direction. The final force-displacement response of the two systems is depicted in Figure 2-9 where the solid line is SS1 and the dashed line is SS2.

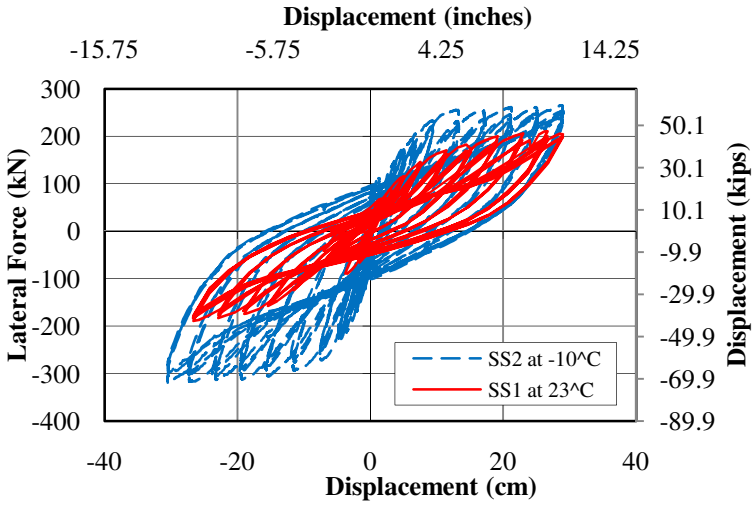

Figure 2-9: Measured force-displacement response (after Sritharan et al., 2007)

Based on the experimental data, a number of conclusions were drawn on the effects of seasonal freezing to the lateral loading of integrated column/foundation systems. The following conclusions were reported in Suleiman et al. (2006):

1. As expected, the continuous shaft increased the flexibility of the system due to the maximum moment forming below the ground surface.
2. With respect to SS1, SS2 experienced the following changes in the lateral load response:
    - Increased effective elastic stiffness by 170%;
    - Increased lateral load resistance by 44%;
    - Upward shift of the maximum moment by 0.84 m (~33 in.);
    - Reduced plastic region length by 64% in the foundation shaft; and
    - Reduced the gap opening at the base of the column by 60%.
3. Seasonal wintry conditions must be accounted for in the seismic design of continuous column to drilled shaft foundations because of the drastic changes seen in the lateral response of these systems.

The analytical investigation undertaken by Sritharan et al. (2007) examined the generalized effects of freezing temperatures and associated design implications on integrated column/foundation systems. LPILE (2004), which uses the finite difference method and the Winkler soil spring concept, was used to complete the analytical portion. To account for the effects of seasonally wintry conditions, material properties were modified as needed.

The response of the soil springs was of significant importance as this response will greatly dictate the lateral loading behavior of the column-shaft system. To modify the soil springs, unconfined compression stress-strain data was generated through laboratory experiments on glacial till specimens at -1 °C (30.2 °F), -7 °C (19.4 °F), -10 °C (14 °F)and -20 °C (-4 °F). Using this data, the p-y curves were generated using the procedure suggested by Reese and Welch (1975). The aforementioned method was modified based off of the work performed by Crowther (1990) with an exponent of 0.43 and experimental data to ensure that the model accurately captures the frozen soil response. For a direct comparison with the experimental testing, the soil profile produced by the cone penetration test (CPT) was used to generate the p-y curves. In order to do this, the unconfined compressive strength

of the soil was found using the recommendations of Robertson and Campanella (1983) with a bearing capacity factor, N_k, of fifteen. The final portions needed for the computer program, a soil subgrade modulus and strain at fifty percent of the soil strength, were found for the laboratory and CPT curves based on the recommendations of Reese et al. (2000).

The final modifications for the analysis were made to the concrete and steel properties. Concrete compressive strength properties were modified based on the research performed by Lee et al. (1988) in which it was found that the concrete strength and elastic modulus would increase by 22% and 10%, respectively, at -20 °C (-4 °F) when compared to the properties at 0 °C (32 °F). Steel properties for the wintry conditions were modified following the research performed by Filiatrault and Holleran (2001). This research found that the strength of steel would increase by 4.5% at -20 °C (-4 °F) when compared to the strength at 23 °C (73.4 °F). Using these modifications, the moment-curvature analyses were performed to accurately represent the flexural stiffness of the shaft as a function of temperature.

Using the above modifications, the analyses were run and compared to the experimental results as appropriate. These comparisons concluded that the modeling would accurately capture the effects of seasonally frozen conditions, thus allowing the remaining analyses at different temperatures to be legitimized. A number of conclusions were drawn from this study, which are as follows:

1. A 2-D model that uses beam-column elements to represent the column and foundation shafts and compression only springs satisfactorily captured the measured response of the column/foundation system in warm and freezing conditions. This correlates well with the design recommendations presented in AASHTO (2007 and 2009) in which a method involving soil springs is the primary recommendation.
2. With respect to warm weather conditions, the response of a column to drilled shaft system at -1 °C (30.2 °F) to -20 °C (-4 °F) will change the lateral response as follows:
    - Increase the effective lateral stiffness by 40% - 188%;
    - Reduce the lateral displacement capacity by 17% - 63%;
    - Increase the lateral load resistance and shear demand in the column by 25% - 30%;
    - Increase shear demand in the foundation shaft by 25% - 80%;

- Shift the maximum moment upwards; and
- Reduce the length of plastic action in the foundation shaft.

3. The change in soil stiffness plays a more significant role in dictating the lateral response of column/foundations systems than the change in concrete and steel properties.
4. The depth of frozen soil and axial load do not greatly alter the response of the system in the frozen state (see Figure 2-10).

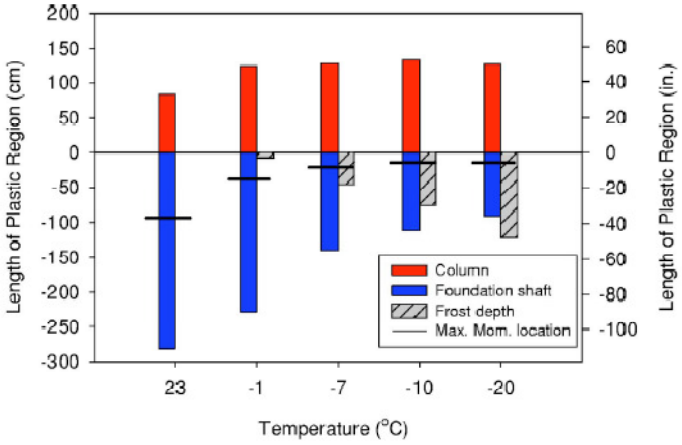

Figure 2-10: Frost depth, maximum moment location and plastic hinge length at ultimate condition (Sritharan et al., 2007)

5. Seasonal freezing will significantly alter the seismic response of integrated bridge column-foundations systems and, therefore, will have serious implications in areas where seasonal freezing occurs around the world (see Figure 2-11).

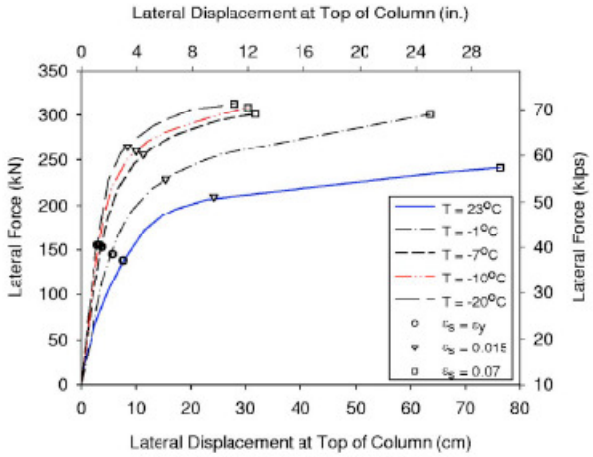

Figure 2-11: Global force-displacement response as temperatures decrease (Sritharan et al., 2007)

In addition to the monotonic analytical modeling performed by Sritharan et al. (2007), a secondary analytical approach was conducted by Wotherspoon et al. (2009) to construct a full cyclic model of the lateral force-displacement response of the two systems examined by Suleiman et al. (2006). The research was conducted using Ruaumoko and the Winkler soil spring concept. The springs in this method were established as a series of detachable springs so that the gap opening and reattachment that occurs during the cyclic loading would be accurately captured. Each soil spring response was uniquely defined using the methodology of Reese and Welch (1975) since CPT and experimental soils testing data was provided in Sritharan et al. (2007). The structural behavior of the reinforced concrete column and foundation shafts were modeled using experimental material properties through the use of moment-curvature responses constructed using a fiber based approach available in OpenSees. Cyclic loading was applied to the top of the column based on the experimental testing by applying increasing target displacements with no less than three cycles at each target displacement.

The authors concluded that through the use of elements available in Ruaumoko, the full-scale cyclic response of a column/foundation shaft could successfully capture the outdoor testing in both summer and winter conditions. This was accomplished by modeling structural nonlinearity, gap development and soil nonlinearity in compression. Each model was verified using multiple output parameters on the global and local level to ensure accuracy of the model. The model further validated the findings of Sritharan et al. (2007) in which the range of temperatures experienced by the system must be included in the design process to ensure an adequate response during a seismic event.

2.4 Impacts of Seasonal Freezing on the United States and Japan

To better understand the broad impacts of seasonal freezing, an investigation was undertaken that examined the potential of seismic events and seasonal freezing to occur simultaneously within the United States and Japan (Sritharan and Shelman 2008). In the United States, one commonly assumes that a significant freezing condition would only occur within the Central and Eastern United States and Alaska, but this is not an accurate assumption. In fact, a depth as small as 10 cm (4 in.) can alter the lateral loading response of integrated bridge column/foundation systems according to Sritharan et al. (2007).

DeGaetano and Wilks (2001) have suggested that a depth of this nature can be expected in the seismic region of the western United States including the state of California (see Figure 2-12). In Japan, the northern portion of Honshu Island and the Island of Hokkaido should experience seasonal freezing and high seismic activity as well (see Figure 2-13).

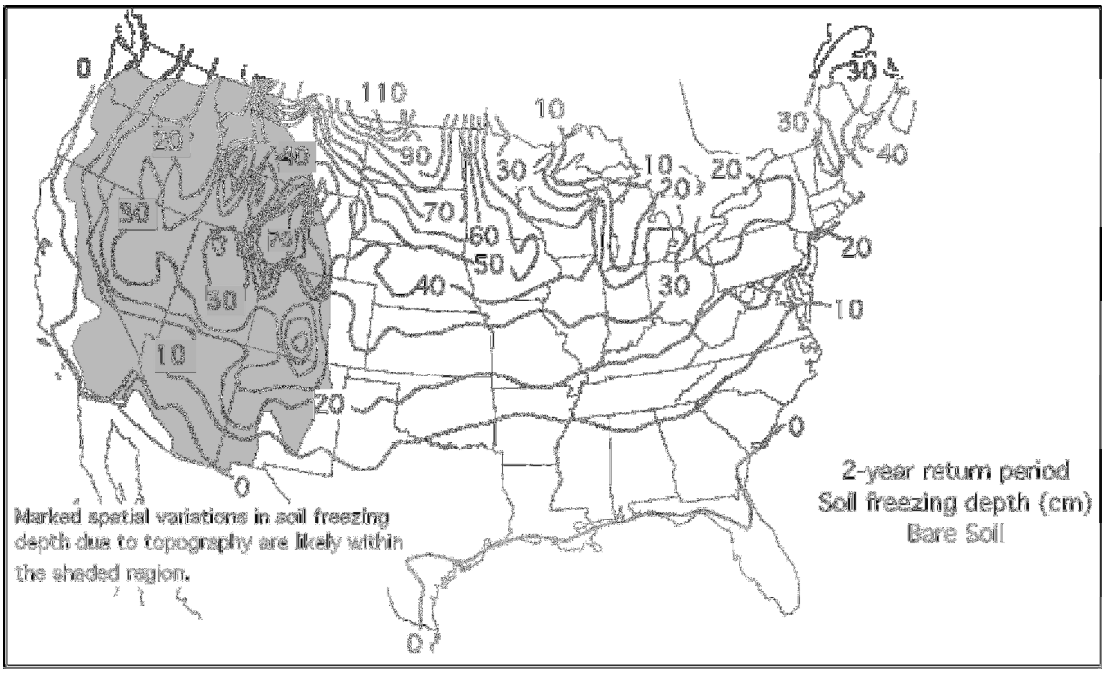

Figure 2-12: Frozen soil depth contours produced for a two-year return period by DeGaetano and Wilks (2001)

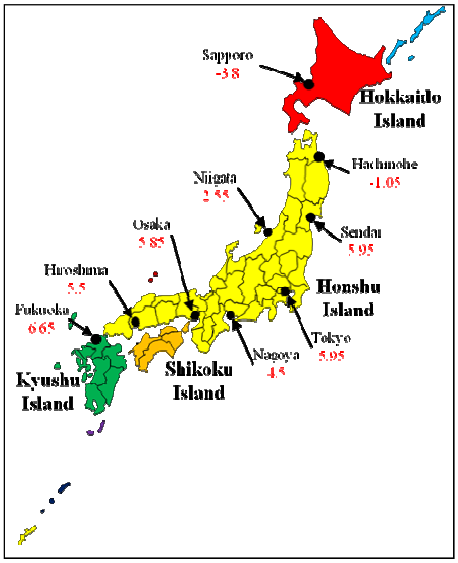

Figure 2-13: Average winter temperatures for Japan's Larger Cities (Japanese Meteorological Agency, 2009)

Despite the presence of frozen ground in winter months, all seismic regions of the United States, Japan and other countries around the world ignore the effects of seasonally frozen conditions on SFSI and the seismic response of bridges. To better understand the significance of freezing soils and seismic response of bridges, an impact study was performed for the United States and Japan. For the United States, the number of bridges within each state was determined and then compared to frost depth contour map in Figure 2-12 and a seismic hazard map. Due to lack of information, it was assumed that the bridges shown in Figure 2-14 were uniformly distributed within each state. The chosen seismic map for this study was the 0.2-second spectral acceleration map with a 10 percent probability of exceedance in 50 years as published by the United States geological Survey (2002). With a limiting criterion that the bridges should experience at least 0.2g spectral acceleration at a period of 0.2-second, 66,000 bridges were estimated to be in the seismic region. To examine how many of these bridges would be affected by seasonally frozen condition, the frost contours were overlaid on the seismic hazard map, as shown in Figure 2-15, and the number of bridges that may experience both a minimum of 10 cm (~ 4 in) of frost depth and 0.2g spectral acceleration was estimated. This combination showed that seismic response of approximately 50% of the 66,000 bridges in active seismic regions would be affected by seasonal freezing, which is a significant finding. When only the minimum of frost depth condition was used (i.e., the bridge site should experience a frost depth greater than or equal to10 cm [~ 4 in.]), over 400,000 bridges or two-thirds of all bridges in the US were found to be affected by seasonally frozen condition, yet this issue is seldom addressed in routine design methods.

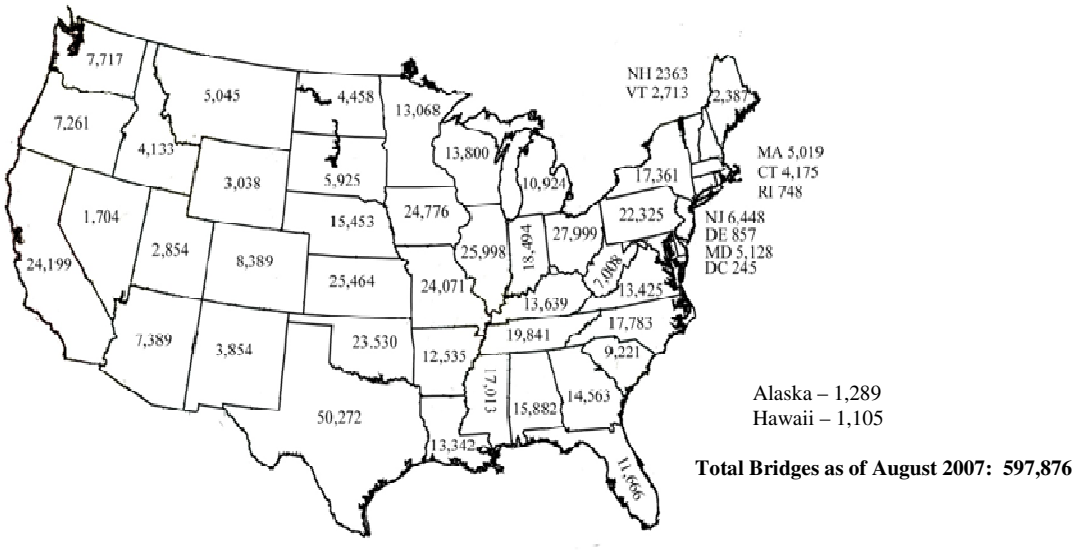

Figure 2-14: Statewide distribution of bridges in the United States (Bureau of Transportation Statistics, 2007)

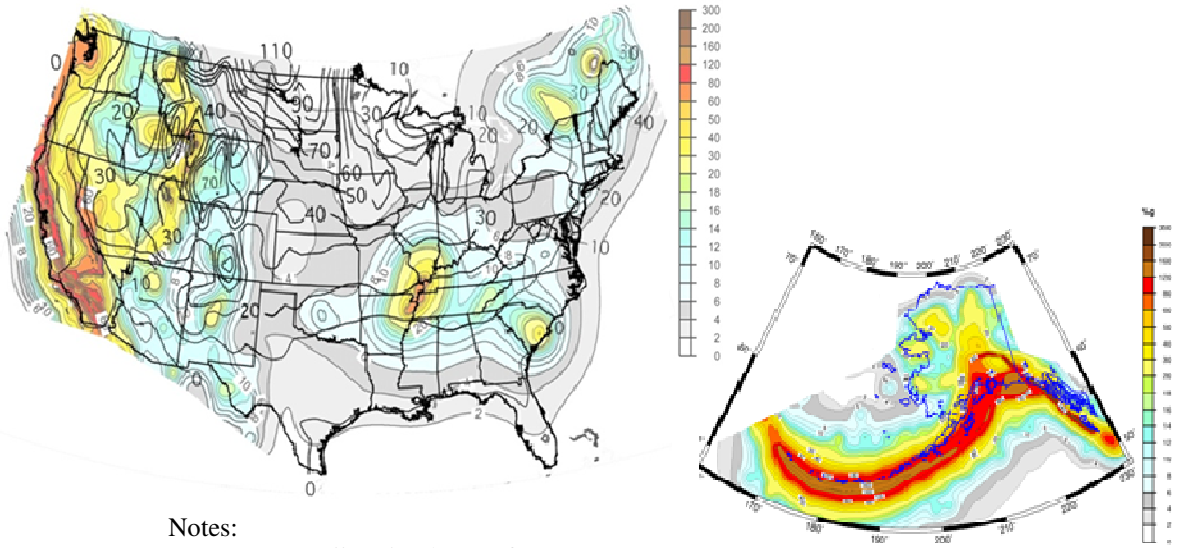

Notes:

1. Hawaii omitted as no frost concerns.
2. Entire State of Alaska would experience greater than 10cm frost depth

Figure 2-15: USGS seismic hazard map (2002) overlaid with frost depth contours

The broad impact study of Japan consisted of examining the average winter temperatures and comparing the locations of possible frozen soils to seismic hazards and population distribution. Figure 2-13 demonstrated the locations for possible frozen soils were Hokkaido

Island and the northern part of Honshu Island. Within this region, the seismic hazards were found, using the National Earthquake Information Center's historical and present data, and compared to the frozen soils area. With this information, the population distribution was examined to provide a risk estimate, as bridge locations were unavailable. It was noted that some major cities were located within this region, such as Sapporo. A final map correlating with Figure 2-13 was produced that shows the population distribution and seismic events in the area in Figure 2-16. It appears that bridges in four major cities and south eastern part of the island may be affected by both earthquakes and seasonally frozen condition.

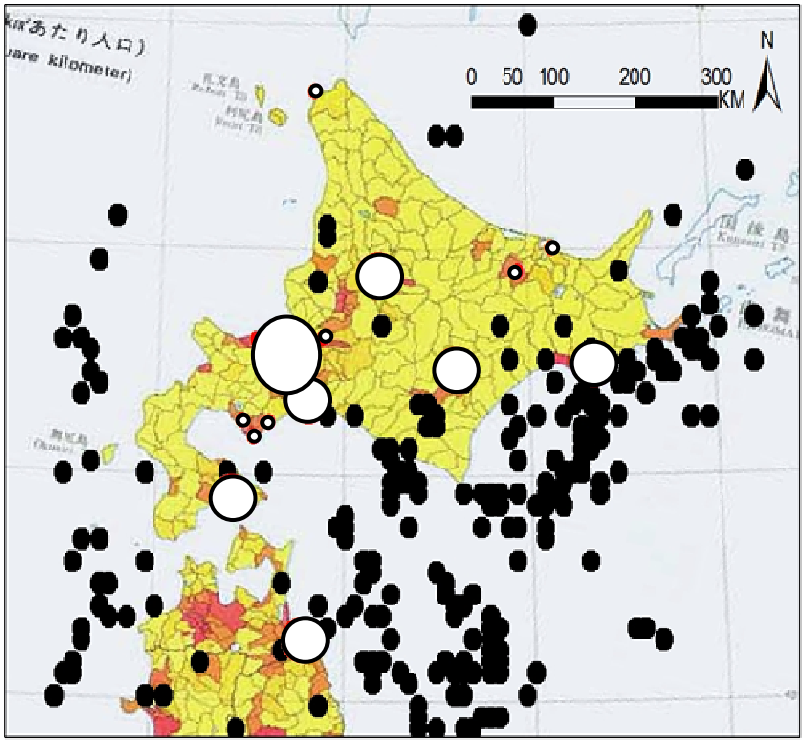

Key:

1. Small Black Circles are Earthquakes
2. Open Circles are High Population Density

Figure 2-16: Seismic activity of Japan near Hokkaido Island circa year 2000

2.5 Material Behavior

When examining the lateral response of columns supported on CIDH shafts, the material behavior must be defined for concrete, soil and steel. These definitions are even more critical during times of seasonal freezing in which material properties are markedly different

from warm weather conditions. The section below provides information on the limited amount of studies that have been performed in freezing conditions. These studies are critical in understanding the local response of a confined concrete member so that the moment-curvature response is correctly captured. By accounting for freezing effects in the moment-curvature response and the soil parameters, the development of the new methodology presented in Chapter 4 will give consideration to all seasons of the year.

2.5.1 Concrete

Sritharan et al. (2007) demonstrated in an exploratory research program that concrete material properties will change as temperature decreases. Although they state that these changes in the material properties do not cause as significant an impact as the change in soil properties, they must be accounted for to correctly handle the effects of seasonal freezing in design. Currently, a limited amount of research is present to show the influence of cold temperatures as warm weather conditions are generally used for the design process. The following section will discuss the prior research that has been completed on the effects of cold temperatures to concrete material properties.

Sehnal et al. (1983)

Prior research in material testing of concrete has shown that as temperature decreases the compressive strength, elastic modulus and bond strength of concrete increases. Sehnal et al. (1983) demonstrated that as temperature decreased, concrete compressive strength increased according to a polynomial curve in normal strength concrete. The curve produced by this study, reproduced in Figure 2-17, showed that between 20 °C (68 °F) and -25 °C (-13 °F) an increase of 25% in compressive strength could be expected. Although experimentation was performed on 41.4 MPa (6 ksi) concrete, it was assumed that this was applicable over varying strengths as the testing was done on plain Type II Portland cement concrete. They also provided evidence based on statistical modeling that the rate at which concrete test specimens were cooled to testing temperature was independent of the compressive strength (1983).

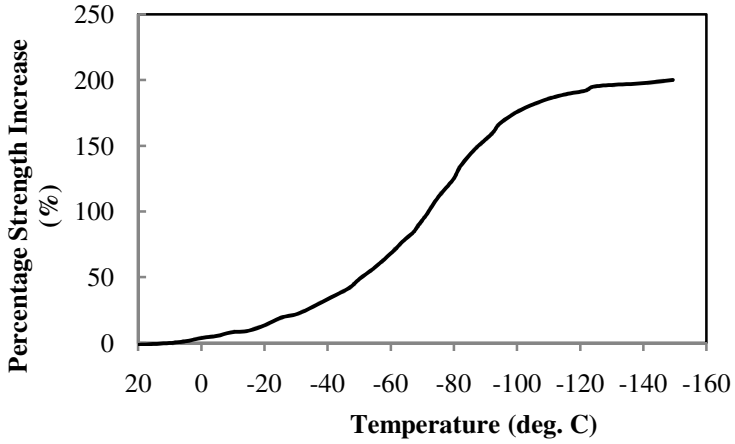

Figure 2-17: Percentage increase of concrete strength with reduction in temperature (after Sehnal et al., 1983)

Lee et al. (1988)

The information provided by Sehnal et al. (1983) was validated in 1988 by Lee et al. (1988a). This research demonstrated that the compressive strength increased in a polynomial manner as suggested by Sehnal et al. (1983). Lee et al. (1988a) further concluded that the modulus of elasticity and bond strength would increase at lower temperatures. These researchers noted that the increase in modulus of elasticity occurred at a slower rate than the rate of increase of concrete compressive strength (e.g., at -70 °C [-94 °F] the compressive strength increased by 151.3% compared with the elastic modulus increase of 114.7%). The bond strength in confined concrete was also noted to increase with lower temperatures since bond strength is correlated with the unconfined compressive strength of concrete. In the study it was found that at -70 °C [-94 °F] the bond strength would increase by 145.1% compared with the 128.6% increase of the concrete compressive strength. The data also demonstrates that a non-uniform increase of bond strength was experienced as temperature decreased from ambient room temperature.

In a follow-up paper published by Lee et al. (1988b), the effects of high strength concrete at low temperatures provided conclusions in terms of compressive strength, modulus of elasticity and bond strength. The main conclusions drawn were that the respective properties increased at a similar rate to that of normal strength concrete; however, the percent of increase tended to be lower than those of normal strength concrete at similar temperatures. This difference may be due to the variation in water to cement ratio between

the normal strength, w/c = 0.48, and high strength, w/c = 0.35, tests; however, the authors do not provide any reasons to the differences experienced between the two types of concrete.

In the two pieces of literature published by Lee et al. in 1988 (a & b), the researchers expanded the information available on Poisson's ratio. They reported that the past studies conclude that Poisson's ratio should be taken to be approximately 0.20 regardless of compressive strength and that Poisson's ratio will decrease as the compressive strength of the concrete increases. This suggests that no matter the temperature of concrete a constant value of 0.20 should be used for Poisson's ratio in concrete. However, Lee et al. (1988a, 1988b) has shown that in both normal strength concrete and high strength concrete that as temperature decreases and unconfined compressive strength increases, the Poisson's ratio will increase. The researchers provide data that suggests that at a temperature as low as -70 °C [-94 °F], Poisson's ratio will increase by approximately 150% in normal strength concrete and 125% in high strength concrete.

2.5.2 Steel

Understanding the behavior of steel at low temperatures is the other key component needed to perform a moment-curvature analysis that is able to account for the effects of seasonal freezing on the section response. Although a key component, very little research has been performed in this area. Filiatrault and Holleran (2001) experimented on CSA 30.16 reinforcing steel and found that the yield and ultimate tensile strengths would increase by 20% and 10%, respectively, at -40 °C when compared to 20 °C. In addition, the research concluded that Young's modulus and the ultimate tensile strain were unaffected by temperature. Another study performed by Bruneau et al. (1997) on American Society for Testing and Materials (ASTM) A572 Grade 50 steel found that the yield and ultimate tensile strengths increased by nine percent and five percent, respectively, at -40 °C when compared to 20 °C. Bruneau et al. (1997) also noted that the ultimate tensile strain and Young's modulus would not be affected when temperature is decreased.

These results, although comparable, were not performed on steel reinforcing bars that are now commonly used in high seismic regions, ASTM A706 Grade 60 steel. In companion research, to that presented in this report (Levings and Sritharan, 2009) this issue is addressed through experimental testing performed at low temperatures and varying loading rates. The

researchers concluded the following when temperature is decreased from 20 °C (68 °F) to -40 °C (-40 °F):

1. Young's modulus of elasticity, yield strain and ultimate strain are unaffected;
2. Yield and ultimate tensile strengths will increase following a quadratic trend. The trend shows an increase in the yield tensile strength of 5.1% and the ultimate tensile strength of 6.3% at-40 °C (-40 °F)when compared to 20 °C (68 °F).
3. Yield and ultimate tensile strengths were noted to increase with a higher rate of loading and appear to be affected by temperature, but further investigation is required;
4. The strain hardening region is unaffected by temperature, but will dissipate as loading rate is increased; and
5. Bar size was noted to possibly affect the yield and ultimate strengths increase in cold temperature, but more tests are needed to establish a reliable relationship.

2.6 Sectional Analysis Tool

In an attempt to handle the multiple issues associated with determining the moment-curvature behavior of a confined concrete section such as the column and foundation shafts, a section analysis tool was developed at ISU by Levings (2009). The program, Versatile Section Analysis Tool (VSAT), has been designed to handle typical cross-sections used in the seismic design of reinforced concrete as well as some unusual sections including circular concrete filled steel shells and H-shaped ultra high performance pile sections. In addition to being able to handle multiple types of cross-sections, the effects of soil confinement pressure and cold temperature on concrete and steel behavior properties are included in the program. Steel temperature effects are handled based off of the conclusions found by Levings and Sritharan (2009), whereas the concrete temperature effects are handled based off of data found through a literature review in Levings (2009). Any of the moment-curvature analyses reported within the remainder of this report were performed using VSAT which has gone through extensive verifications as provided in Levings (2009).

CHAPTER 3: EXAMINATION OF EXISTING METHODS

3.1 Introduction

In today's engineering practice, many models are available for use in the design and analysis of drilled shafts subjected to lateral loading. Many of the common models that are currently used for design and analysis purposes were introduced in Chapter 2: Literature Review. This chapter illustrates that each of these methods uses different procedures and techniques to account for the effects of SFSI. To better understand the models and the underlying rationale, this section further examines the different methods presented within the literature review through an example problem of a continuous bridge column supported by a CIDH shaft.

3.1.1 Example Problem

In order to compare the different methods to an experimental baseline, the identical full-scale systems (i.e., SS1 and SS2) used in the exploratory research program by Suleiman et al. (2006) and Sritharan et al. (2007) were chosen as the integrated column-shaft system. The column and foundation shafts, depicted in Figure 3-1, were originally designed taking into consideration average column and foundation reinforcement details used in the Midwest and high seismic regions as well as the seismic design recommendations included in the Applied Technology Council (ATC) 32 guidelines (1996) and AASHTO (1998). Due to the limitations of the different models, soil profiles were varied based on the method being examined and are presented in the respective sections below.

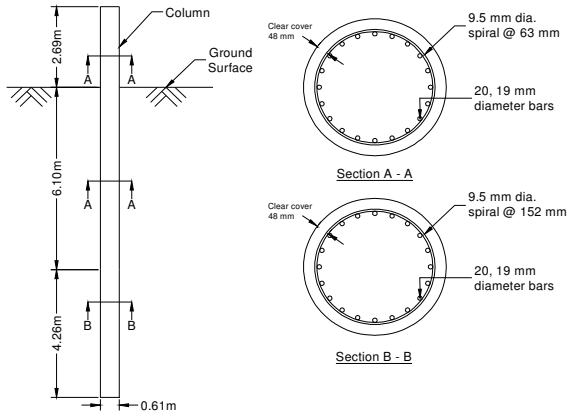

Figure 3-1: Details of experimental test units SS1 and SS2 (after Sritharan et al., 2007); (1 in. = 2.54 cm)

3.1.2 Moment-Curvature Analysis

In order to create an accurate analytical model that can characterize the nonlinearity in the system, moment-curvature analyses must be performed for the different cross-sections depicted in Figure 3-1. To perform these analyses, VSAT (Levings 2009) was used with the loadings and material properties provided in Table 3-1. The material properties and loadings were taken from the analytical study performed by Sritharan et al. (2007) for the warm weather integrated column-shaft system, SS1. The results of the moment-curvature analyses are provided within Figure 3-2 and were idealized later depending on the requirements of the specific model being examined. Although soil confinement pressure alters the moment-curvature response, it is ignored in the initial detailed analyses and therefore ignored in this section. The effects of soil confinement and how they included, however, are described in the sections that follow so that a more accurate model is developed.

Table 3-1: Loading and material properties used for moment-curvature analyses of SS1 cross-sections

	Location (Cross-Section)		
Material Property	**Column (A-A)**	**Foundation (A-A)**	**Foundation (B-B)**
Axial load, P [kN (kip)]	0 (0)	0 (0)	0 (0)
Concrete compressive strength, f'_c [MPa (ksi)]	57.9 (8.4)	56.5 (8.2)	56.5 (8.2)
Concrete cracking strain, ε_{co}	0.002	0.002	0.002
Ultimate concrete strain, ε_{cu}	0.01367	0.01386	0.0086
Concrete tensile strength, f'_t	$7.5(f'_t)^{0.5}$		
Steel yield stress, f_y [MPa (ksi)]	471.5 (68.4)		
Steel ultimate stress, f_u [MPa (ksi)]	748.4 (113.8)		
Ultimate steel strain, ε_{su}	0.12		

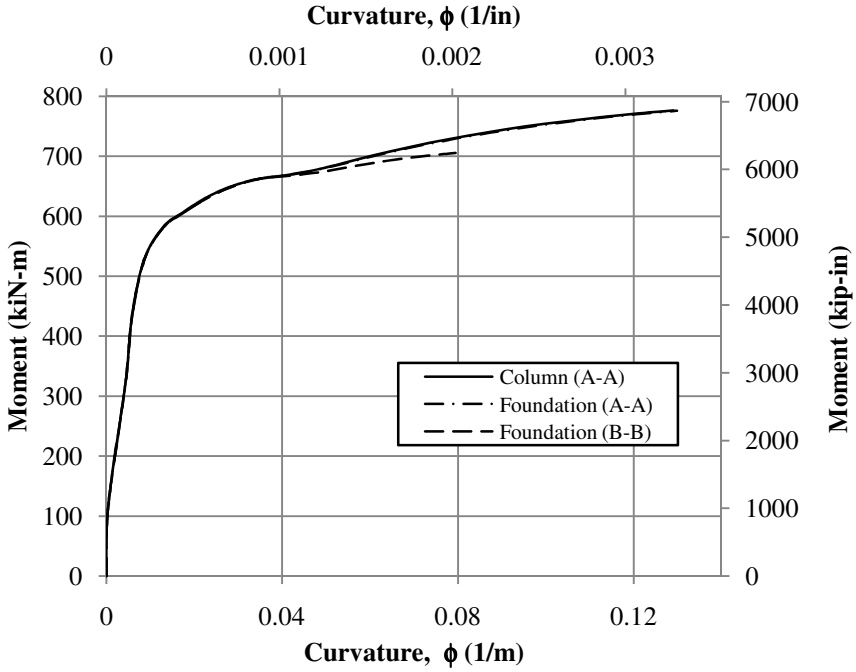

Figure 3-2: Moment-curvature response of SS1 cross-sections without soil confinement

3.2 Detailed Analysis of AASHTO 2007

The current bridge design specifications in use today, AASHTO (2007), suggest that a detailed analysis involving soil springs is the way to correctly model the lateral load response of drilled shafts in soil. In order to use this method, a computer program such as LPILE (Reese et al. 2004) is needed to perform a numerical analysis that will find the structural equilibrium at a given loading condition, force or displacement. These computer programs require a significant amount of information about the site to complete the analysis. This section will further discuss the needs of such a detailed method by examining the use of LPILE (2004) in determining the lateral response of the example column/foundation system presented in Section 3.1. As a basis of comparison, analysis results obtained for a model of SS1 in LPILE will be compared with the experimental results of this system as reported by Suleiman et al. (2006).

To use a computer program such as LPILE, the first step in determining the lateral behavior of a drilled shaft foundation is to define the type of analysis needed for the project. For the example problem, a full nonlinear static analysis was chosen in order to represent the inelastic action expected within the foundation shaft due to the lateral loading. After

defining the type of analysis to be used by the program, the integrated column/foundation system and surrounding soil properties must be defined. The first step in this process was to define the structural parameters of the shafts (e.g., cross-sectional area, moment of inertia and stiffness).

A key component in defining the structural parameters was the modeling of the shaft stiffness. In LPILE, the full moment-curvature results are used to represent the stiffness of the system when performing a full nonlinear analysis. The inputs needed for this are the flexural rigidities and moments of the different cross-sections along the length of the shaft. The values taken for this step were initially specified within Section 3.1.2. After manually inserting this data, the next step is to define the soil parameters at the site.

Since the basis of comparison for this analysis was with the experimental research completed by Suleiman et al. (2006), the soil profile obtained for the field test location at the Spangler testing facility on the ISU campus was directly used in the analysis. Accordingly, the site contained a glacial till composed mostly of low plasticity clay with a permanent water table at 8.2 meters below the ground surface. In order to better define the entire soil profile along the length of the shaft, the CPT data provided by the authors is presented in Figure 3-3a. The undrained shear strength, c_u, of the soil was then computed by using the method presented by Robertson and Campanella (1983) with a soil unit weight of 21.2 kN/m^3 (0.078 lb/in^3), Figure 3-3b. To input the soil profile into LPILE, the graphs were broken into piecewise linear portions and the resulting data was used to define the soil parameters needed for the selected soil models. The soil model chosen for this analysis was Reese's stiff clay model with and without free water as needed. The soil parameters used by this method included the soil's effective unit weight, γ, undrained shear strength, strain at fifty percent of maximum compressive stress and possibly a p-y modulus, k. The p-y modulus and fifty percent strain value were chosen based off of recommendations by Reese et al. (2004). The final points and parameters chosen for the analysis are provided in Table 3-2.

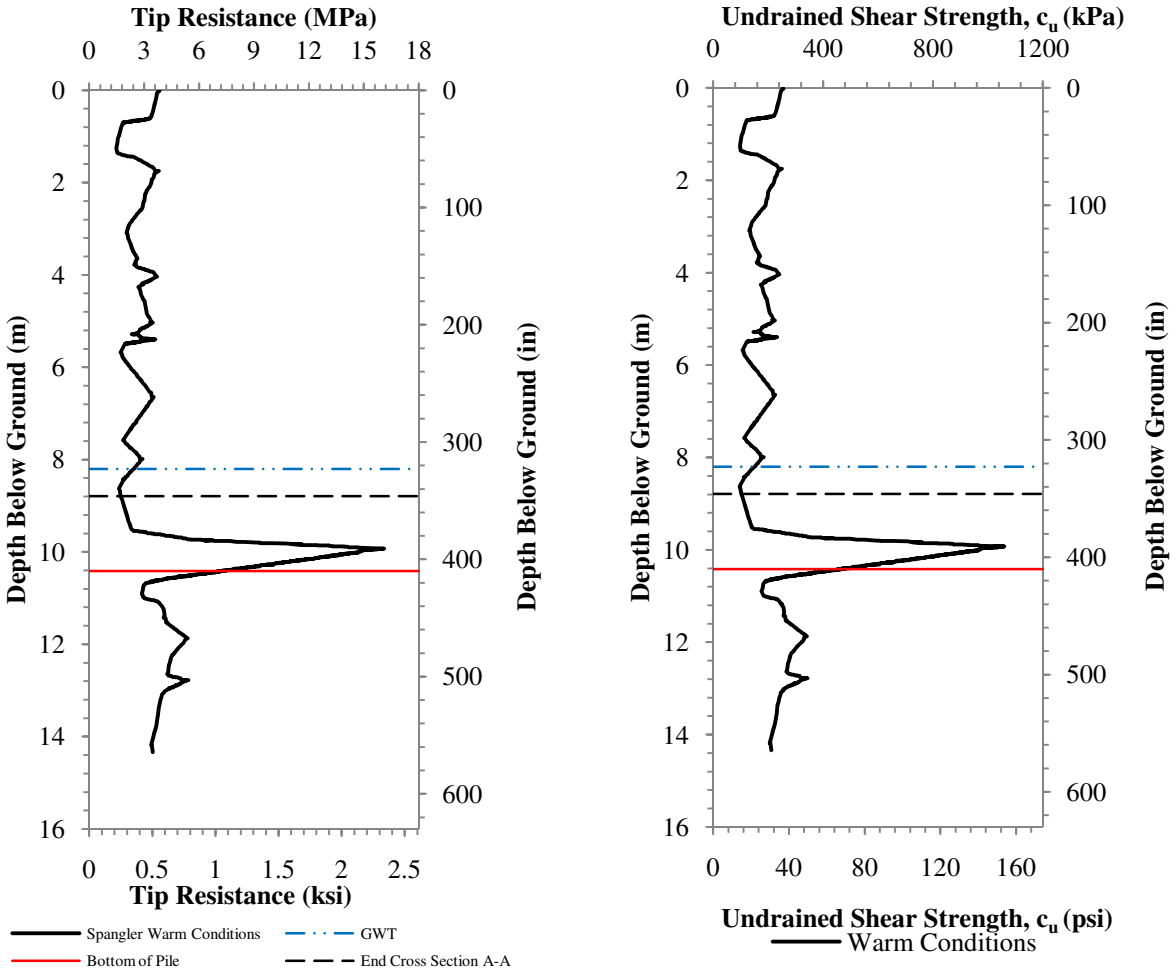

Figure 3-3: Soil profile with depth (a) CPT tip resistance (after Sritharan et al., 2007); (b) Undrained shear strength (GWT = Ground Water Table)

Table 3-2: Primary soil profile for soil spring method

Depth Below Ground Surface	Water Present	γ	c_u	ε_{50}	k
m (in.)		kN/m^3 (lb/in^3)	kPa (lb/in^2)	in/in	MN/m^3 (lb/in^3)
0 (0)	No	21.2 (0.078)	253 (36.7)	0.0045	N/A
0.61 (24)	No	21.2 (0.078)	193 (28)	0.005	N/A
1.22 (48)	No	21.2 (0.078)	96.5 (14)	0.007	N/A
1.40 (55)	No	21.2 (0.078)	115 (16.7)	0.005	N/A
5.33 (210)	No	21.2 (0.078)	186 (27)	0.005	N/A
8.23 (324)	Start GWT	21.2 (0.078)	152 (22)	0.005	271.5 (1000)
8.79 (346)	Yes	21.2 (0.078)	100 (14.5)	0.007	135.7 (500)
10.41 (410)	Yes	21.2 (0.078)	345 (50)	0.004	542.9 (2000)

Note: GWT = Ground Water Table

As part of the comparison, a secondary soil profile was created based off of the laboratory soils testing completed for this experiment. In Sritharan et al. (2007), stress-strain curves obtained from unconfined compression tests on soil samples were provided for the Spangler test site (see Figure 3-4a). Using this information along with the CPT, p-y curves were generated (see Figure 3-4b) using Reese and Welch's methodology (1975) for approximately the first two pile diameters below the ground surface, as the soils closest to the ground surface play a significant role in the lateral response of an integrated column-shaft system. The second soil profile is shown in Table 3-3.

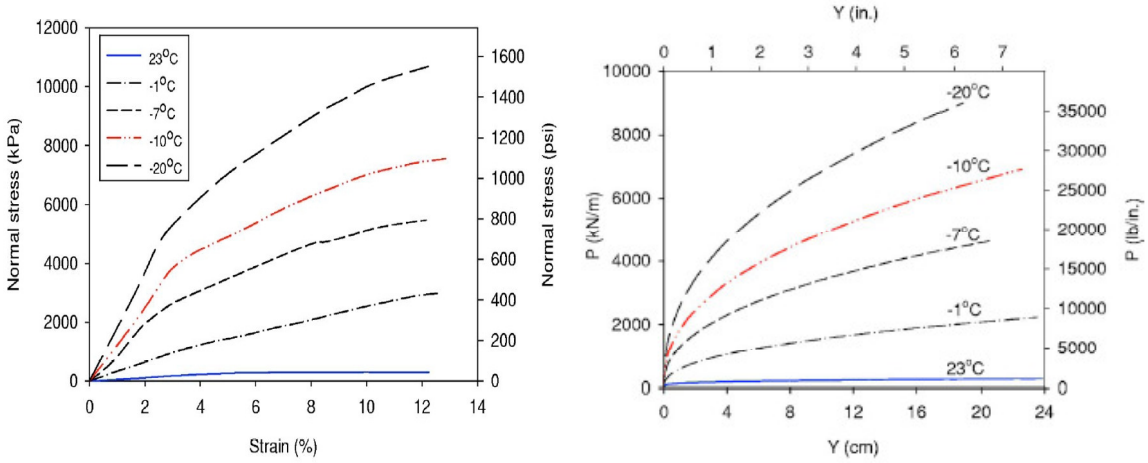

Figure 3-4: (a) Unconfined compression stress-strain curves (b) p-y curves generated for Spangler test site (Sritharan et al., 2007)

Table 3-3: Secondary soil profile for soil spring method

Depth Below Ground Surface	Water Present	γ	c_u	ε_{50}	k
m (in.)		kN/m^3 (lb/in^3)	kPa (lb/in^2)	in/in	MN/m^3 (lb/in^3)
0 (0)	No	p-y curve			
0.61 (24)	No	p-y curve			
1.22 (48)	No	p-y curve			
1.40 (55)	No	p-y curve			
5.33 (210)	No	21.2 (0.078)	186 (27)	0.005	N/A
8.23 (324)	Start GWT	21.2 (0.078)	152 (22)	0.005	271.5 (1000)
8.79 (346)	Yes	21.2 (0.078)	100 (14.5)	0.007	135.7 (500)
10.41 (410)	Yes	21.2 (0.078)	345 (50)	0.004	542.9 (2000)

Note: GWT = Ground Water Table

The final major step prior to completing the analysis of the integrated column-shaft system in warm weather conditions, SS1, was to define the boundary conditions enforced at the top of the column. Depending on the program, these conditions may be defined in a manner of different ways (e.g., shear and moment, shear and rotation, displacement and moment, pinned, fixed, etc.). The main boundary condition specified for the example problem was that a pinned connection was present between the superstructure and bridge column. With this as the basis, a pushover analysis was performed using the following criteria:

- The pushover analysis should be run by incrementally increasing the boundary conditions at the top of the column whether through force or displacement means;
- First occurrence of the extreme compression fiber in the concrete reaching a strain, ε_c, of 0.002. This value is important in the soil confinement process as this is where the unconfined and confined concrete curves begin to deviate from one another; and
- Ultimate lateral displacement occurs when the ultimate curvature, ϕ_u, of a cross-section is reached (typically within foundation shaft). This curvature assumes that a flexural failure in the system occurs at the in-ground hinge when a pinned superstructure is present in the analysis.

After running an initial analysis on the drilled shaft system, an iterative process that included changing the target pile head displacements was used to locate the third and fourth points listed in the above criteria. These points were critical to the analysis in that they are used to define the amount of soil pressure acting as confinement to the foundation shaft based on the study performed by Sritharan et al. (2007) and should therefore be included in the moment-curvature analysis. Using the procedure suggested by Sritharan et al. (2007) the average soil pressure experienced by the foundation shaft was found to be 372.3 kPa (54 psi) and 296.5 kPa (43 psi) for the primary and secondary soil profiles, respectively. The pressures were applied along the length of foundation shaft in which the concrete strain exceeded 0.002 at the ultimate condition as this is where the response of the shaft would be altered. This point typically occurred before the change in reinforcement properties and was therefore only applied to the foundation shaft of cross-section A-A. Although a non-uniform soil pressure more accurately represents the soil confinement, a uniform pressure was

specified for the different soil profiles based on the limitations of VSAT. Using these soil pressures, the moment-curvature analysis was repeated and the results indicated an increase in the ultimate moment and ultimate curvature for the foundation shaft. The ultimate moment and curvature increased by 3.7% and 7.5% in the primary soil profile analysis; whereas, an increase of 2.9% and 5.9% was experienced in the secondary soil profile analysis. The results of the moment-curvature analysis for the foundation shaft with cross-section A-A are shown in Figure 3-5.

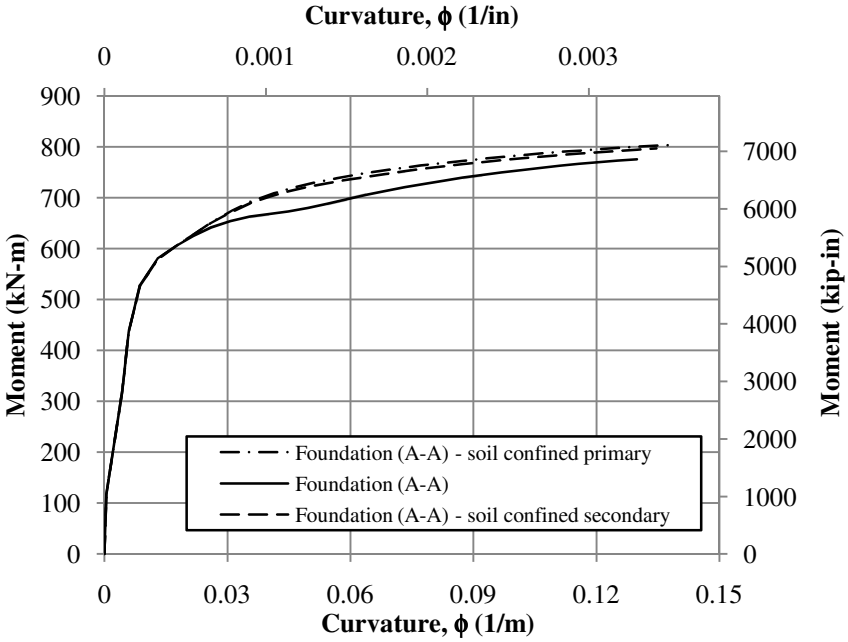

Figure 3-5: Moment-curvature analyses revised after adjusting for soil confinement in the foundation cross-section A-A.

Upon completion of the second moment-curvature analyses, LPILE was reconfigured with the new structural parameters and the soil profiles described in Tables 3.2 and 3.3. At this point, LPILE was run again and an iterative process was used to determine the lateral force-displacement response of the system. The results of two critical conditions, the point of first yielding and the ultimate point, are presented within Table 3-4 for the different soil profile models. The overall global lateral force-displacement responses of the final models are compared to the experimental data from Suleiman et al. (2006) in Figure 3-6.

Table 3-4: Lateral load response of SS1 at the critical conditions

		Soil Profile	
Critical Value	**Experimental**	**Primary**	**Secondary**
First yielding lateral load	137.75 kN (30.97 kip)	147.4 kN (33.14 kip)	138.15 kN (31.1 kip)
First yielding column head displacement	6.25 cm (2.45 in.)	5.54 cm (2.18 in.)	6.65 cm (2.617 in.)
Ultimate lateral load	Not pushed to failure	270.5 kN (60.80 kip)	252.6 kN (56.78 kip)
Ultimate displacement	Not pushed to failure	64.62 cm (25.44 in.)	78.87 cm (31.05 in.)
Max. moment location from top of column	3.69 m (145.28 in.)	3.32 m (130.72 in.)	3.67 m (144.48 in.)

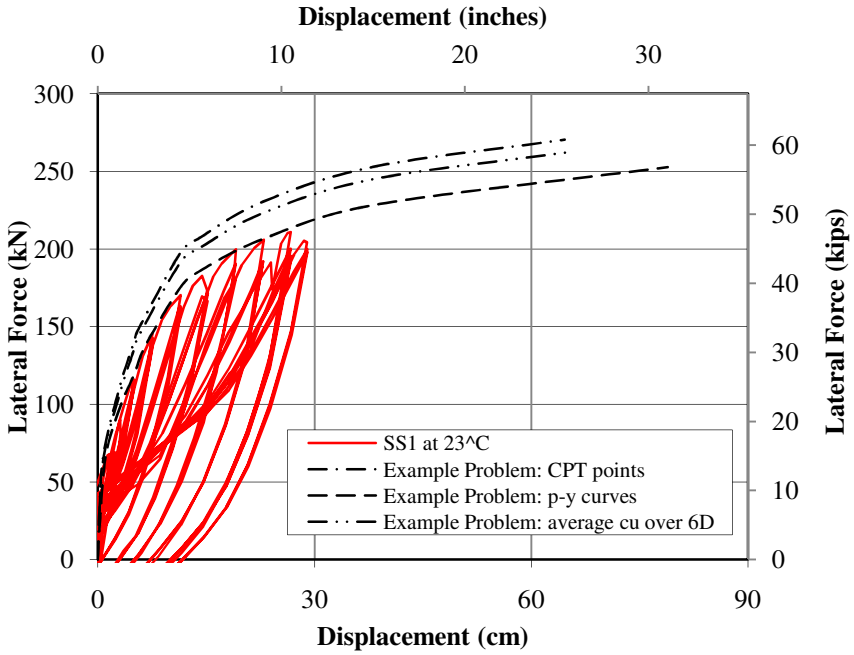

Figure 3-6: Global lateral load response of LPILE analyses compared to experimental results of Suleiman et al. (2006)

Besides the global responses mentioned above, a computer program using the Winkler soil spring method can also provide information regarding the localized responses. This is possible as the method employed by the computer uses a numerical process such as the finite difference method to find the structural equilibrium that occurs along the length of the shaft. Some of the more critical localized responses are provided in Table 3-5 for the different soil profiles.

Table 3-5: Localized responses of final models at the ultimate condition

	Soil Profile	
Local Response Values	**Primary**	**Secondary**
Elastic Curvature, ϕ_e	0.0098/m (0.0002486/in.)	0.011/m (0.0002749/in.)
Plastic Curvature, ϕ_p	0.13/m (0.003294/in.)	0.127/m (0.00322/in.)
Elastic Rotation below Max Moment, θ_{eb}	0.01783 rad	0.01987 rad
Plastic Rotation below Max Moment, θ_{pb}	0.08220 rad	0.08942 rad
Total Plastic Rotation, θ_p	0.15737 rad	0.17386 rad
Translation at Max Moment Location, Δ_{trans}	5.42 cm (2.132 in.)	6.07 cm (2.39 in.)
Length to First Zero Moment after Max, L_{m0}	6.84 m (269.35 in.)	7.19 m (283.13 in.)
Analytical Plastic Hinge Length, L_p	1.21 m (47.78 in.)	1.37 m (53.99 in.)
Actual Plastic Hinge Length, $L_{p,actual}$	3.77 m (148.48 in.)	3.85 m (151.37 in.)

The method discussed above, although it will provide significant results, has many issues associated with its use in design practice, which are as follows:

1. A significant amount of information is required about the structure and surrounding soil to create an accurate model that represents the real world conditions. This information includes the drilled shaft and column dimensions, reinforcing details along the length of the entire system, axial and lateral loading conditions, and boundary conditions at the column superstructure interface. The main issue, however, is that detailed information about the surrounding soil (e.g., CPT and laboratory testing) is needed to accurately capture the lateral load response.
2. The selected soil profile, especially near the ground surface, will greatly alter the overall response of the system. This is prevalent within Figure 3-6 where the soil profile based off of laboratory testing near the ground surface provided a more realistic soil response and therefore lateral load response. This is further established when examining the global displacement of the different curves generated for the system at an equivalent inertial force applied by ground movement. Take for example an inertial force of 200 kN (45 kip), at this force the displacements vary by approximately 60% which can cause an undesirable failure mechanism thus violating the capacity design principles. This variation is also significant in seismic design

where the displacements experienced by a system are extremely important to ensure that an adequate performance is maintained over the lifespan of the structure. Therefore, one may conclude that the model will only be as good as the information used during its creation.

3. The number of iterations needed to ensure structural equilibrium at a given loading condition using the finite difference method is not easily performed by hand calculations and expertise in using software such as LPILE (2004) is required.
4. Every time a structural or soil parameter is modified; a new model must be constructed in the appropriate computer software. This leads to numerous models being constructed so that an accurate representation of the lateral load response of a column supported on a CIDH shaft is obtained. New models must be created in order to make sure that the new system will effectively maintain the desired performance and adhere to the capacity design principles stated in Chapter 1.
5. The design process using this method will require a significant amount of time to complete. More time is required than with other methods due to the creation of multiple models because of the inherent iterative process between the foundation engineering and structural design.
6. Although the effects of wintry conditions were not considered in this section or the AASHTO code, Sritharan et al. (2007) addressed this concern. In the study, the researchers found that seasonal freezing could be modeled using LPILE when soil and structural parameters were modified for these conditions.

3.3 Chai (2002)

Since the method of designing and analyzing drilled shafts proposed by Chai (2002) was suggested for use in the AASHTO guidelines for seismic design (2009), an attempt was made to compare the model Chai provided to that of the more detailed soil spring model verified in Section 3.2 as well as the experimental data by Suleiman et al. (2006). In order to undertake Chai's method, two modifications were necessary to the soil and structural parameters used in the verification process. The first modification was that the soil needs to be represented as a single uniform layer, and the second modification was that the moment-curvature analysis needed to be idealized for an elasto-plastic response. The remainder of this section discusses

how these modifications were made and compares the results from the experimental data found by Suleiman et al. (2006) and the detailed soil spring model shown in Section 3.2 to the model suggested by Chai (2002).

In order to provide a realistic verification, the CPT data shown in Figure 3-3 was used to determine the properties of the uniform soil layer. Although the CPT data did not provide the closest lateral response in Section 3.1, this data is the best way of computing average soil properties. By using this information the soil profile was the same as the primary one presented in Table 3-2. The uniform soil layer was then constructed by finding a weighted average of the undrained shear strength of the soil within the first six diameters of the ground surface. This length was chosen as this was in the range for which Chai's method would be applicable. The final soil profile was found to be a soil with a unit weight of 21.2 kN/m^3 (0.078 lb/in^3) and an undrained shear strength, c_u, of 150.2 kPa (21.79 psi).

The structural parameters used for the model were modified by relating the area under the moment-curvature response with soil effects for the primary condition depicted in Figure 3-5 to that of an idealized elasto-plastic response. Similar to the detailed analysis, only the foundation with cross-section A-A was examined as this section develops the plastic action and will therefore dictate the inelastic response of the total system. The area under the curve was determined by generating a cubic function in Mathcad 14 (PTC 2007) that represents the moment-curvature response. This function was then integrated over the entire curvature spectrum to find an area that may be related to the elastoplastic response. Using this area, an elastoplastic response was found in which the yield moment, M_y, equals 739.9 kN-m (6549 kip-in), the yield curvature, ϕ_y, equals 0.00985/m (0.000255/in.) and the ultimate curvature, ϕ_u, equals 0.1396/m (0.003546/in.). The idealized elasto-plastic response is compared to the more accurate response shown in Figure 3-7 where it is noted that the idealized curve goes through the first yield point.

Upon determining the aforementioned modifications, Chai's model was completed following the procedures described in Section 2.2.4. The results found using this method are as follows:

- Modulus of horizontal subgrade reaction, k_h = 10.06 MPa (1459.7 lb/in^2);
- Shaft characteristic length, R_c = 164.54 cm (64.78 in.);

- Coefficient for aboveground height and depth to fixity, ξ_a and ξ_f = 1.636 and 1.464;
- Depth to point of fixity, L_f = 240.84 cm (94.82 in.);
- Normalized aboveground height and depth to fixity, L_a* and L_f* = 4.42 and 3.95;
- Normalized maximum moment, M_{max}* = 21.744;
- Normalized depth to maximum moment location, L_m* = 1.160;
- Depth to maximum moment, L_m = 70.72 cm (27.84 in.);
- Normalized ultimate shear at top of column, V_u* = 4.28;
- Ultimate shear at top of column, V_u = 238.84 kN (53.693 kip);
- Yield displacement, Δ_y = 14.33 cm (5.64 in.);
- Normalized plastic hinge length, λ_p = 1.442;
- Plastic hinge length, L_p = 87.88 cm (34.6 in.);
- Plastic curvature, ϕ_p = 0.13/m (0.003291/in.);
- Plastic rotation at ultimate condition, θ_p = 0.1139 radians;
- Plastic displacement at ultimate, Δ_p = 38.71 cm (15.24 in.); and
- Total displacement, Δ_u = 53.03 cm (20.88 in.).

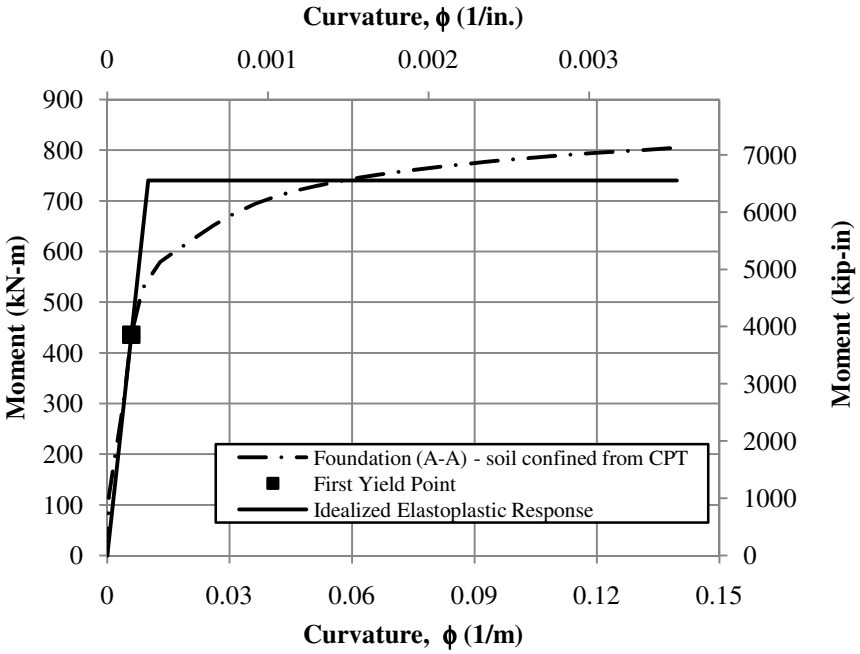

Figure 3-7: Idealized moment-curvature analysis for Chai's method

Based off of the analysis results presented above, the local and global responses of the example problem were compared. Chai's method provides an initial secant stiffness to the first yield point as 1667.2 kN/m (9.52 kip/in) compared with experimental results of 2213.6 kN/m (12.64 kip/in) a difference of 24.7%. If yielding for the experimental data is approximated at a displacement of 10 cm (3.94 in.) and a lateral force of 177.93 kN (40 kip) for a bilinear idealization, Chai's model over predicts the displacement and force at yield by 43.3% and 34.2%, respectively. At the ultimate condition, Chai's model under predicts the displacement and force by 32.8% and 5.4% when compared to the detailed analysis using the secondary soil profile. The global response comparison is presented within Figure 3-8 and when compared to a soil spring method or experimental data it is seen that the model does not accurately capture the global lateral loading response of the system. The results of the local responses of the detailed analyses and Chai's model are compared in Table 3-6, in which the data demonstrates that the inelastic range of the lateral loading is not accurately predicted. The localized information that can be compared with the experimental data, the maximum moment location, was under predicted by 29.3% thus stating that the point at which the most damage will occur is closer to the ground surface than what actually occurred.

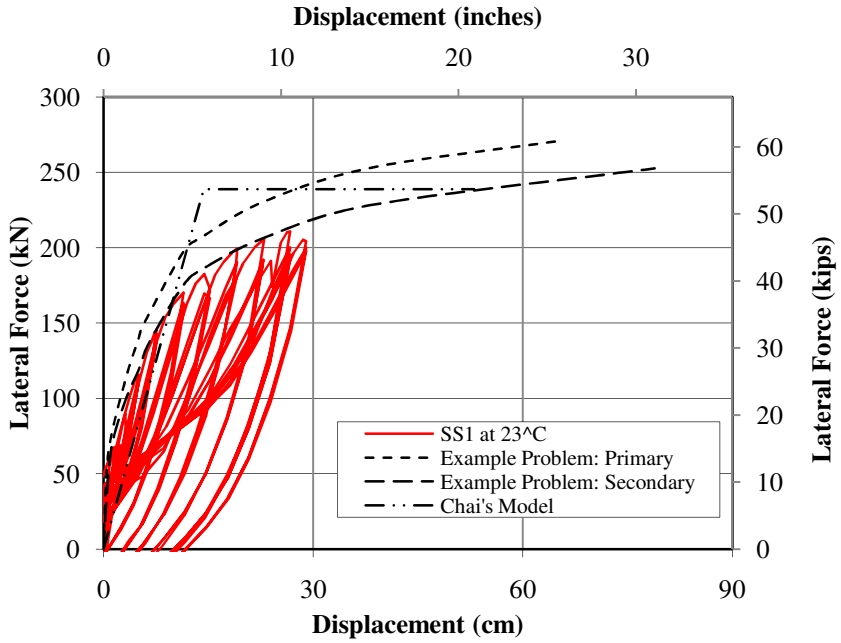

Figure 3-8: Global response comparison of Chai's method to experimental testing and soil spring models

Table 3-6: Local response comparison between Chai's method and soil spring method

	Soil Spring Method		Chai Method	% Difference	
Local Values	**Primary**	**Secondary**		**Primary**	**Secondary**
ϕ_e	0.0098/m (0.0002486/in.)	0.0108/m (0.0002749/in.)	0.0098/m (0.00025/in.)	0.56%	9.06%
ϕ_p	0.1297/m (0.003294/in.)	0.1268/m (0.00322/in.)	0.1296/m (0.003291/in.)	0.09%	2.20%
L_m	0.628 m (24.72 in.)	0.977 m (38.48 in.)	0.707 m (27.84 in.)	12.62%	27.65%
θ_p	0.15737 rad	0.17386 rad	0.1139 rad	27.62%	34.49%
Δ_{trans}	5.42 cm (2.132 in.)	6.07 cm (2.39 in.)	N/A	Cannot Compute	
L_p	1.21 m (47.78 in.)	1.37 m (53.99 in.)	0.879 m (34.6 in.)	27.58%	35.91%
$L_{p,actual}$	3.77 m (148.48 in.)	3.84 m (151.37 in.)	N/A	Cannot Compute	

The verification of Chai's model has demonstrated that there are some significant shortcomings associated with both the local and global lateral load responses over the entire range of loading. These shortcomings are found when applied to CIDH shafts in cohesive soils mostly due to the fact that the model was only verified against data from full-scale testing in cohesionless soils. The concerns associated with this method of predicting the local and global responses of CIDH shafts in cohesive soils are as follows:

1. The model assumption of an elasto-plastic moment curvature response is generally not an accurate assumption for integrated column/foundation systems. Unlike reinforced concrete members, this assumption introduces larger errors as it ignores the nonlinear behavior of reinforcing steel and soil leading to a perfectly plastic force-displacement response between the yield and ultimate limit states. The perfectly plastic response, however, is another inaccuracy when the experimental response of SS1 is examined and a second slope is seen between the yield and ultimate limit states.
2. The maximum moment location is over predicted by 12.6% when compared directly to the detailed analysis performed in LPILE using just the CPT data. The location was also under predicted by 27.7% when compared with the detailed analysis using the soil profile with p-y curves generated from laboratory testing. In addition, the

maximum moment location was found to be under predicted by 29.3% when compared with the experimental data produced by Suleiman et al. (2006). The inaccurate prediction of the maximum moment location will change the total displacement, although not as significantly as the other criteria, of the system as the plastic rotation is assumed to be concentrated at this location.

3. When compared to the primary and secondary soil profile analyses in LPILE, the plastic rotation in the system was under predicted by 24% and 31% respectively. Although this is conservative in a design process, this will generally lead to a higher cost of construction due to the increase in materials needed to obtain the appropriate lateral response of the system. An inaccurate plastic rotation value will also under predict the plastic displacement of the system.
4. The analytical plastic hinge length was also largely under predicted, 24.5% and 32.5%. This is rather significant as this value largely dictates the amount of plastic rotation concentrated at the maximum moment location and therefore the lateral plastic displacement of the system at the top of the column. By not providing enough plastic displacement in the system, the ultimate displacement was found to be invalid as this is where most of the total displacement comes from in this type of integrated column/foundation system. The difference in plastic rotation causes the final displacements to differ by 13.4% and 27.8% when compared to the primary and secondary soil profiles, respectively.

As part of the comparison between Chai's model and the detailed analyses, the sensitivity of the plastic rotation variation was examined. This was done by assuming that the detailed methods would provide a more realistic value of plastic rotation and therefore the values presented in Table 3-6 for the primary and secondary soil profiles were assumed to be the correct amount of plastic rotation experienced by the system. By using the plastic rotations from the detailed analyses and decreasing them by a known percentage, a new plastic displacement for Chai's model was computed assuming no variation in the maximum moment location. This new plastic displacement was then added to the original yield displacement found through Chai's methodology to find an ultimate displacement of the column supported on a CIDH

shaft. The new ultimate displacement value was then compared to the ultimate displacement of the detailed analyses based on the assumption that these were the values expected at the top of the column for a flexural failure at the maximum moment location. The results of this sensitivity analysis are provided in Table 3-7 where the displacement comparison shows that with minor changes in Chai's plastic rotation, the lateral displacement at the ultimate limit state is significantly altered. For example if the plastic rotation was equivalent to that of the detailed analyses, the ultimate displacement in Chai's model would be 105% of the ultimate displacement found in the primary soil profile analysis and 93.14% of the ultimate displacement found in the secondary soil profile analysis.

Table 3-7: Sensitivity of plastic rotation on ultimate displacement capacity

Error in Plastic Rotation	Percentage of Ultimate Displacement	
	Primary Soil Profile	Secondary Soil Profile
0%	105.0	93.14
2%	103.3	91.64
4%	101.7	90.14
6%	99.99	88.64
8%	98.34	87.14
10%	96.68	85.64
15%	92.54	81.89
20%	88.40	78.14
25%	84.26	74.39
30%	80.12	70.65
35%	75.98	66.90

5. Another major challenge associated with Chai's model is that the experimental verification and determination of plastic hinge length were done using data from testing in cohesionless soils (Chai and Hutchinson 2002). By testing in this type of soil, the plastic hinge length, although recommended for use in all soil types, has effectively been under predicted in cohesive soils. This arises since cohesive soils are generally less stiff and therefore develop a larger plastic rotation in the foundation shaft. In addition, the model suggested by Chai (2002) was never verified in cohesive soils, most likely leading to the inaccuracies within locating the maximum moment location.

6. The final shortcoming associated with this method is that the effects of temperature variation are not considered anywhere within the model development as presented in Section 3.2. This is an issue as a temperature variation as large as 60 °C (110 °F) commonly occurs across the United States as the weather and seasons change. The changes in material properties, however, should be given consideration as Sritharan et al. (2007) demonstrated that the overall lateral response of the system will be significantly altered.

3.4 Priestley et al. (2007)

Another common approach to handling soil-foundation-structure-interaction in cohesive soils is to use the method suggested by Priestley et al. (2007). The method is recommended for a limited range of cohesive soils and therefore a new soil profile was needed for a basis of comparison as the previous profile falls outside this range. The selected profile was chosen to be a uniform layer of soil to a depth of 10.4 m (410 in.) below ground with an undrained shear strength of 40 kPa (5.8 psi) and an effective unit weight of 18.85 kN/m^3 (0.069 lb/in^3). Using this new soil profile, the suggested method was compared against an LPILE analysis using a modified version of the procedure discussed in Section 3.2.

In order to minimize the amount of time required to perform an LPILE analysis, the moment-curvature response from column tip to bottom of foundation was constant. In addition, simplification was further included by maintaining consistent material and using a soil confinement value of 372.3 kPa (54 psi) found in the detailed analysis using the primary soil profile. The modification was done as the effects of soil confinement would not significantly alter the moment-curvature response of the shaft with differing soil pressures as stated by Sritharan et al. (2007) and as depicted in Figure 3-5. The main difference, however, was that an axial load of 400 kN (90 kips) was applied to the cross-section. The remaining soil parameters, k and ε_{50}, for Reese's stiff clay model were determined as necessary based off of recommendations by Reese et al. (2004). The results of the detailed analysis performed in LPILE are presented below in Table 3-8 and will be used for the basis of comparison.

Table 3-8: Results of detailed analysis using LPILE

Global Response	
First Yielding / Ultimate Lateral Load	127 kN (28.6 kip) / 137.4 kN (30.9 kip)
First Yielding / Ultimate Column Head Displacement	12.7 cm (4.98 in.) / 112.1 cm (44.1in.)
Local Response at Ultimate	
Maximum Moment Location from Column Tip, H_{IG}	4.54 m (178.88 in.)
Elastic Curvature, ϕ_e	0.011/m (0.0002701/in.)
Plastic Curvature, ϕ_p	0.114/m (0.002902/in.)
Total Plastic Rotation, θ_p	0.1938 radians
Translation at Max Moment Location, Δ_{trans}	9.1 cm (3.58 in.)
Analytical Plastic Hinge Length, L_p	169.6 cm (66.78 in.)
Actual Plastic Hinge Length, $L_{p,actual}$	4.77 m (187.94 in.)

To further establish a basis for comparison, the yield and ultimate locations for the moment-curvature analysis were found through a bilinear idealization of the response. Using this method of idealization, the yield moment was found to be 747.25 kN-m (6613.7 kip-in) at a curvature of 0.00909/m (0.0002309/in.) and the ultimate moment was found to be 875.06 kN-m (7744.92 kip-in) at a curvature of 0.125/m (0.003172/in.). These values were based off of the foundation shaft response obtained with soil confinement. The actual curve produced by VSAT for the shaft is compared with the bilinear idealization in Figure 3-9.

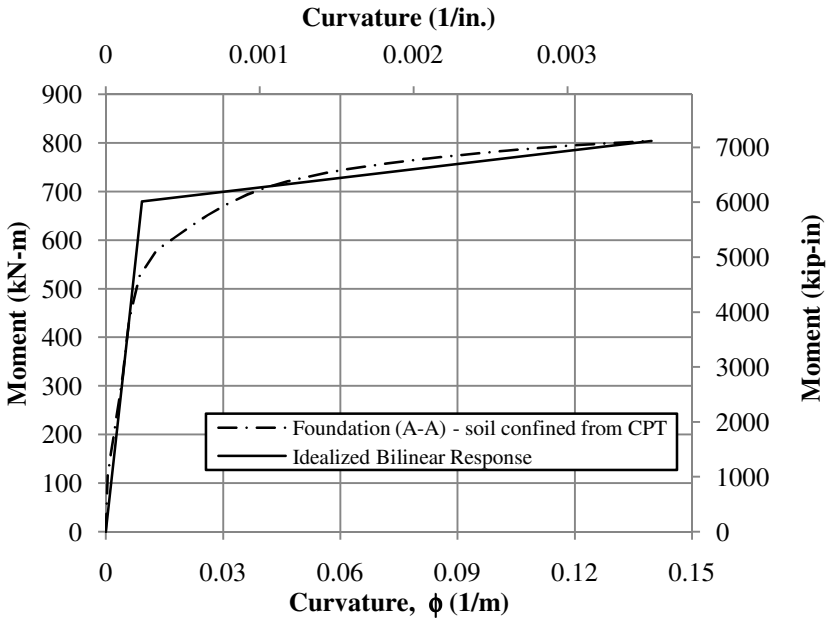

Figure 3-9: Bilinear idealized moment-curvature response

At this point, all of the information needed to perform the suggested method and appropriate comparisons with a detailed analysis were obtained allowing for the method to be completed. Following the procedures suggested in Priestley et al. (2007) and Section 2.2.5, the lateral response of the system was determined. The results of the proposed method are as follows:

- Location of in ground hinging from column tip, H_{IG} = 4.94 m (194.3 in.);
- Damage control strain limit in concrete and steel, $\varepsilon_{dc,c} = 0.01382$ and $\varepsilon_{dc,s} = 0.07$;
- Estimated neutral axis depth, c = 13.15 cm (5.14 in.);
- Concrete curvature limit state, $\phi_{ls,c} = 0.105$/m (0.00267/in.) [Controlling limit state since this is the maximum curvature obtainable before section failure according to equations provided in Priestley et al. (2007)];
- Steel curvature limit state, $\phi_{ls,s} = 0.166$/m (0.00423/in.);
- Plastic hinge length, $L_{p,IG}$ = 87.88 cm (34.6 in.);
- Yield curvature, $\phi_y = 0.0087$/m (0.000221/in.);
- Coefficient needed to account for fixity conditions, $C_1 = 1.232$;
- Yield displacement based off of in ground hinging, $\Delta_{y,IG}$ = 26.12 cm (10.28 in.);
- Plastic curvature, $\phi_p = 0.0963$/m (0.00245/in.);
- Plastic rotation, $\theta_p = 0.0846$ rad;
- Plastic displacement, $\Delta_{p,IG}$ = 41.77 cm (16.44 in.); and
- Total design displacement, $\Delta_{D,IG}$ = 67.88 cm (26.73 in.).

The results of the method suggested by Priestley et al. (2007) for determining the design displacement were then compared with the results of the LPILE analysis, Table 3-8, and bilinear idealization of the moment-curvature response, Figure 3-9, as the model uses the ultimate limit states to find the design displacement. The global information is compared numerically in Table 3-9 while the localized information is compared in Table 3-10.

Table 3-9: Global comparison between LPILE and Priestley models

Value	LPILE	Priestley et al.	Error
Yield Displacement	18.56 cm (7.31 in.)	26.12 cm (10.28 in.)	40.63%
Yield Lateral Load	187.3 kN (42.1 kip)	Not Computed	N/A
Ultimate Displacement	112.1 cm (44.1 in.)	67.88 cm (26.73 in.)	39.45%
Ultimate Lateral Load	137.4 kN (30.9 kip)	Not Computed	N/A

Table 3-10: Localized comparison between LPILE and Priestley models

Value	LPILE	Priestley et al.	Error
Max. Moment Loc. from Column Tip, H_{IG}	4.54 m (178.88 in.)	4.94 m (194.3 in.)	8.62%
Yield Curvature, ϕ_y	0.00909/m (0.0002309/in.)	0.0087/m (0.000221/in.)	4.29%
Elastic Curvature at Ultimate, ϕ_e	0.011/m (0.0002701/in.)	0.0087/m (0.000221/in.)	18.18%
Plastic Curvature, ϕ_p	0.114/m (0.002902/in.)	0.0963/m (0.00245/in.)	15.58%
Total Plastic Rotation, θ_p	0.1938 radians	0.0846 radians	56.35%
Translation at Max. Moment Location, Δ_t	9.1 cm (3.58 in.)	N/A	N/A
Analytical Plastic Hinge Length, L_p	169.6 cm (66.78 in.)	87.88 cm (34.6 in.)	48.2%
Actual Plastic Hinge Length, $L_{p,actual}$	4.77 m (187.94 in.)	N/A	N/A

The following conclusions were drawn about the method suggested by Priestley et al. (2007) for determining the lateral response of a continuous bridge column into a drilled shaft foundation in cohesive soils:

1. A full global force-displacement curve cannot be easily generated, as the method does not include how to handle shear force along the length of the column/foundation system. This means that the necessary shear reinforcement needed to prevent an undesirable failure mode may not be correctly accounted for in the design process.
2. The controlling curvature limit state in concrete is under estimated by 16% when compared to the bilinear idealization of the moment-curvature analysis. This under prediction causes the plastic curvature to be lower thus causing the plastic displacement to be lower than what will actually occur within the system. Although not the main contributor to the error in the plastic displacement, it will cause additional deviation from the more detailed analysis performed in LPILE.
3. Although the yield curvature is 4.3% lower than the idealized response, this will not have a significant impact on the final design displacement or yield displacement. In this case, the two displacement values would increase by half an inch which correlates to a 4% increase in the yield displacement and 2% increase in the total design displacement.
4. The analytical plastic hinge length is approximately 50% less than the length determined using the more detailed methodology. Due to this error, the plastic

rotation and plastic displacement will be significantly under predicted. The issue with the plastic hinge length arises due to the fact that it is determined in accordance with Chai's methodology which was shown to be inappropriate for use in cohesive soils in Section 3.3.

5. The overall design displacement of the system was found to be 39.5% lower than that found using the detailed methodology. A significant portion of the missing displacement is most likely due to the under estimation of plastic action within the inelastic range of the lateral displacement.
6. The last issue, besides those discussed within the literature review, associated with this method is that seasonal temperature variation was once again not considered in the development of the model. This is a major concern once again as the lateral loading response is significantly altered in sub-freezing temperatures.

3.5 ATC 32 (1996)

In the guidelines of ATC 32 (1996), it is suggested that an alternative method, equivalent cantilever length, can be used to design a pile shaft foundation instead of the detailed method using soil springs. This approach works on the concept of defining a fixed-base cantilever system that does not include soil in the model but is equivalent to a more detailed model which includes soil resistance. To use this method, the designer is redirected toward bridge design aids published by the California Department of Transportation (Caltrans) [Caltrans 1990], which use estimated depth to fixity found through a simplified or rigorous process to determine the lateral response.

The bridge design aids use a one of two nomographs, based on the type of soil (i.e., clay or sand), to define a depth below ground to the fixity location. These graphs, however, are limited by the following parameters:

- pile diameter must fall within four to ten feet;
- above ground column height shall fall between twenty and one hundred feet;
- modulus of elasticity of the concrete should be approximately 468,000 ksf; and
- the stiffness of the soil (shear strength or blow count) should be known.

The example problem presented in Section 3.1 does not meet the criteria specified in the above list and this method was therefore not used as a basis of comparison within this report.

The simplified design process starts by defining the structural and geotechnical parameters (e.g., shaft diameter and soil stiffness) to be used for the design. The next step in the process would be to use the nomographs to estimate the number of diameters to effective fixity based off of the soil stiffness parameter and appropriate column diameter. After defining the effective fixity location, the designer would use programs available through Caltrans to determine the appropriate loading and thus finalize the design of the system.

The more rigorous method of design follows the same procedures as outlined above, but determines the effective fixity location using a more detailed method. The more detailed method consists of running a program similar to LPILE, available through Caltrans, to define the top lateral deflection of the column and rotation at the top of the column at service loads. These deflection and rotation values are then placed in equations related to the shear and moment applied to the system to determine the point of effective fixity for the system. No matter the method used, ATC 32 further recommends that the effective cantilever length be taken to be no deeper than two pile diameters below the ground surface when determining the shear load. If a concrete sidewalk is present, it was further stated that the shear load should be determined using a cantilever that does not penetrate into the ground.

Although the model was not compared to the example problem, an elastic analysis was performed in LPILE to determine the efficiency in locating the effective point of fixity. This consisted of creating a system in LPILE with a six-foot diameter shaft, a twenty foot column height, a foundation length of twenty pile diameters below ground and a uniform layer of cohesive soil with a strength of 95.76 kPa (13.89 psi) and unit weight of 18.85 kN/m^3 (0.0694 lb/in^3). The analysis consisted of pushing the top of the column to a displacement of three inches while maintaining a pinned head condition. The results concluded that the maximum moment would form at a depth of approximately two pile diameters compared with the simplified method which predicts a fixity location at 2.4 pile diameters below the ground. This is a 20% error between the detailed analysis and simplified approach. The other challenge associated with this method is that a constant shear is assumed along the entire length of the shaft. This is not a valid assumption as the resistance of the soil causes a variable shear to occur along the length of the shaft once the shaft enters the ground level to

act as the pile foundation. The shear and moment profile of the detailed analysis performed in LPILE (see Figure 3-10) demonstrate the shortcoming in the model.

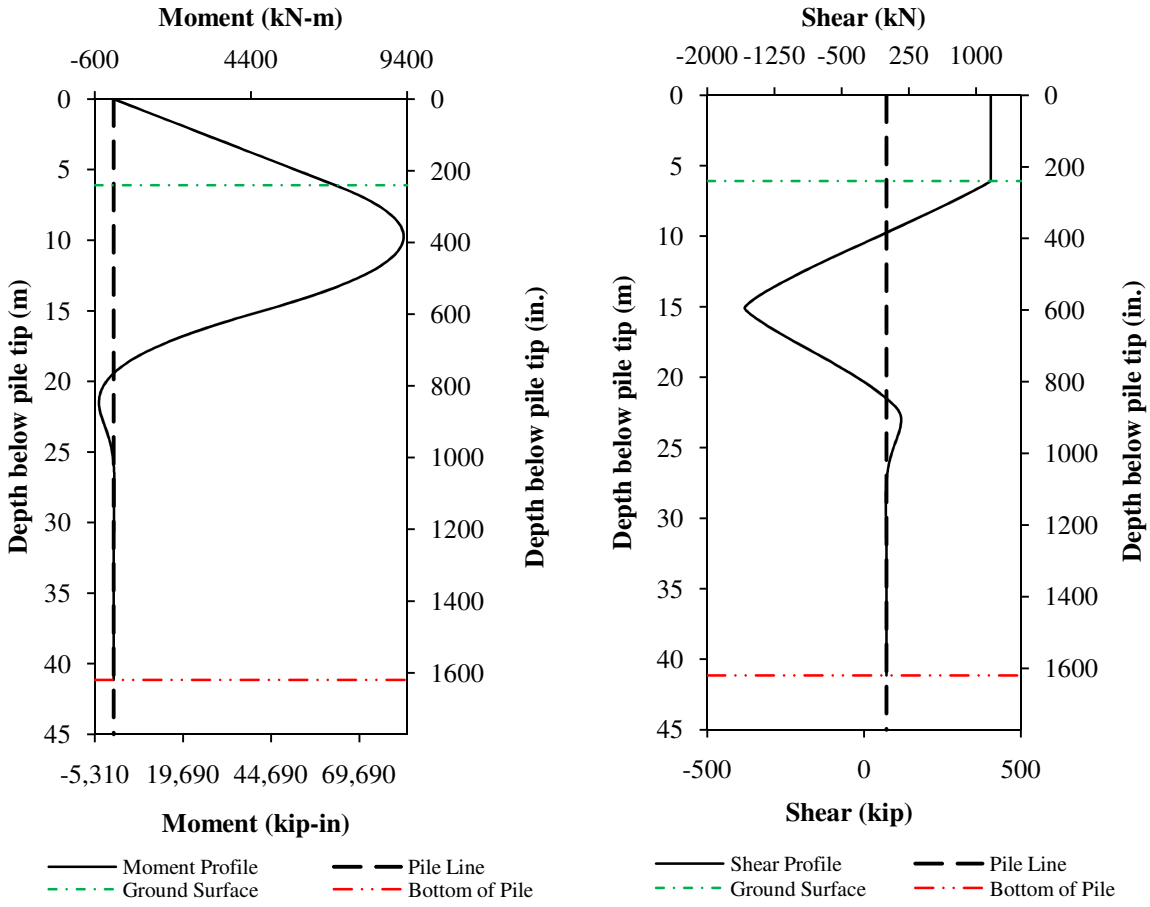

Figure 3-10: LPILE detailed analysis results (a) moment profile; (b) shear profile

3.6 AASHTO (2009)

In the guidelines available in AASHTO (2009), it is suggested that alternative methods to soil springs may be used to determine the lateral response of the integrated bridge column to foundation shaft. Within the guidelines, multiple alternative methods are presented [Chai (2002), Priestley et al. (2007) and AASHTO (2007) –fixity] for determining the lateral behavior of a column/foundation shaft; however, this section is going to focus on the common approach of estimating a depth to fixity for the system. These guidelines state that the estimated depth to fixity may be used in lieu of a more detailed method such as the soil spring method and is determined by means of a simplified equation that was previously

presented in Section 2.2.6. These equations, however, are only applicable as long as the system and all of its components follow a linear elastic behavior.

For this method, the soil profile used in verifying Chai's methodology was selected as this is an average value of the soil's undrained shear strength within the top six pile diameters and was the area where the largest influence on the lateral response would occur. Therefore, the soil was a cohesive low plasticity clay with c_u = 150.2 kPa (21.79 psi) and a unit weight of 21.2 kN/m^3 (0.078 lb/in^3). Using the structural parameters depicted in Figure 3-1 with elastic material properties and the equation produced by Davisson and Robinson (1965), in Section 2.2.6 the following results were obtained:

- Soil modulus for clays, E_s = 10.06 MPa (1.46 ksi);
- Concrete modulus of elasticity, E_c = 35.59 GPa (5161.6 ksi);
- Gross moment of inertia for weak axis, I_w = 0.00678 m^4 (0.785 ft^4);
- Effective depth to fixity, L_f = 3.10 m (121.97 in.); and
- Effective cantilever length, L_{cant} = 5.79 m (227.97 in.).

After determining the effective cantilever length, an estimate may be obtained for the lateral load resistance and displacement capacities using structural analysis software or standard cantilever equations derived from mechanics. For this verification, the standard cantilever equations developed through mechanics were used to compute the lateral resistance and displacement values. To determine these values, the model was originally defined to be fully elastic and therefore gross section properties and the concrete modulus of elasticity could be used. To ensure that the system was fully elastic, the maximum moment was assumed to occur before any yielding of the longitudinal reinforcement occurs. This meant that a moment of 435.76 kN-m (3856.8 kip-in) was attainable according to the moment-curvature analysis presented in Section 3.2. Based off of standard cantilever equations this correlates to a maximum lateral load of 75.26 kN (16.92 kip) at a displacement of 2.02 cm (0.80 in.).

If the designer were to assume that a linear elastic behavior was attainable up to the yield point from a bilinear idealization of the moment-curvature analysis, the method suggested by Davisson and Robinson could be performed again with different results. The idealized yield moment in this situation would be 801.6 kN-m (7094.76 kip-in) and an effective moment of

inertia of 0.0027 m^4 (0.240 ft^4). Using these aforementioned values, the following results were obtained for the effective point of fixity method suggested by AASHTO:

- Effective depth to fixity, L_f = 2.30 m (90.67 in.);
- Effective cantilever length, L_{cant} = 5.00 m (196.67 in.);
- Yield lateral load, V_y = 160.47 kN (36.07 kip); and
- Yield displacement, Δ_y = 9.04 cm (3.56 in.).

Although this method is very simple to use and will provide a result for design purposes, there are many shortcomings and limitations associated with its use, which are summarized below:

1. A key component concern with this method is that the model accounts for the effects of SFSI by creating a cantilever without soil in which the base is fixed against all deformation and the top is modeled based on the boundary conditions at the superstructure level. By modeling the system in this manner, the shear along the shaft length is therefore constant in order to maintain the static equilibrium. This assumption, however, is not valid once the shaft is below the ground surface where shear demands will vary with depth (see Figure 3-10b). In addition to the variable shear demands, the shear experienced in the foundation shaft may increase as is seen in Figure 3-10b after the maximum moment has occurred. Should a designer ignore this increase in shear, a brittle failure from shear may occur during the formation of plastic action which is against the principles of capacity design.
2. When the two different approaches to defining linear elastic behavior were compared with the experimental data produced by Suleiman et al. (2006), the following results were drawn:
   - lateral force at the point of first yielding was under predicted by 45.37%;
   - displacement at the point of first yielding was under predicted by 67.35%;
   - lateral force at idealized yielding was under predicted by 9.83%;
   - displacement at idealized yielding was under predicted by 10.67%; and
3. When moving from a purely elastic system in which the reinforcement does not yield to an idealized yield point, the effective point to fixity decreases by 25.7%. This difference is a major concern as this point in space needs to be clearly defined

because this is where the maximum moment will occur when using this method. An incorrect location of maximum moment may be devastating in the design process as this is the point at which most inelastic action will occur and must therefore be correctly confined to handle the large compressive strains expected to develop under design level or greater earthquakes.

4. Another shortcoming associated with this method is that the maximum moment location generally occurs at a point in the ground between this effective point of fixity and the ground surface. The experimental data from Suleiman et al. (2006) and the detailed analyses ran in LPILE states that the maximum moment location would form at approximately 1.02 m (40 in.) below the ground surface which is significantly less than either elastic method presented above. The method using the first yielding approach over predicts the location by 209.8% whereas the method using the idealized yield location over predicts the location by 130.3%. As previously stated the shaft design may violate capacity design principles as the shaft confinement reinforcement will not be located in the correct places or designed for the correct response.
5. A limitation of this approach is that inelastic action is not considered in determining the lateral displacement of the system. This is a concern as most of the lateral displacements for an integrated column/foundation system develop due to inelastic action that is expected with a large seismic event. By not including the effects of inelastic action, the plastic action developed due to in ground hinging at the maximum moment location is not included and the lateral response at the ultimate limit state cannot be defined.
6. Another limitation associated with this method is that no validation of the model is presented within the current guidelines (AASHTO 2009) and specifications (AASHTO 2007) for bridge design. For any form of validation, the designer must refer back to the research performed by Davisson and Robinson (1965).
7. In addition to no validation, this effective fixity model does not take into account the effects of seasonal temperature variations and it is believed was never included in the model development.

3.7 Summary of Examination

The examination that was undertaken within this chapter provided more information into the shortcomings and limitations of existing methods for determining the lateral load response of columns supported on CIDH shafts in cohesive soils. The methods presented ranged from simple to complex, but each method had shortcomings and limitations associated with their use. A summary of the findings within the confines of this examination are provided below:

- The detailed method suggested by AASHTO (2007), although able to accurately capture the lateral load response of a column-shaft system both globally and locally, had a number of shortcomings associated with its use and are as follows:
    - This method of analysis requires a significant amount of information about the structure and surrounding soil to accurately capture the response. The defining of properties for the soil surrounding the foundation shaft was found to be the area in which the most amount of information was needed. It was concluded that the lateral response of the system would experience significant differences in displacements for a given inertial loading based on the accuracy of the soil model used within the method. These differences in displacements are critical in a seismic based design where a designer must ensure that other components of the structure are not damaged from excessive lateral deflection.
    - Hand calculations are not easily performed for the detailed method. This means that expertise in computer programs such as LPILE is needed to perform the analysis.
    - The design procedure using this method takes more time due to the inherent iterative process between foundation engineering and the structural design. The iterations arise from the need to construct multiple models in LPILE as the structural design changes and more information is gathered on the surrounding soil.
    - The effects of seasonal wintry conditions on the lateral load response of columns supported on CIDH shafts in cohesive soils was not discussed in the specifications for bridge design. Although not discussed, Sritharan et al. (2007) demonstrated

that this method was capable of handling wintry conditions and the associated freezing when material properties (i.e., soil, concrete and steel) are adjusted correctly.

- The method proposed by Chai (2002) for determining the lateral load response of an integrated column/foundation system was found to have a number of challenges associated with its use. These challenges are summarized below:
  - The assumption of an elasto-plastic response between the yield and ultimate conditions based on the response of SS1 in the experiment performed by Suleiman et al. (2006). This response was inappropriate because unlike reinforced concrete members the combined nonlinearity response of soil, steel and concrete create a secondary slope over the inelastic loading range.
  - The method was only verified against a full-scale test in cohesionless soils although still recommended for use in cohesive soils. This means that no validation for the cohesive soil model was provided.
  - The plastic action within the system was significantly under predicted. Most of the error in this location was found to occur within the analytical plastic hinge length that dictates the plastic rotation and thus plastic displacement. The plastic hinge length was found to be the largest error source as it was defined based off of the full-scale testing of a column/foundation shaft performed by Chai and Hutchinson (2002) in a cohesionless soil. By basing the plastic hinge length off of testing in cohesionless soils, it was under predicted analytically due to the differences in stiffness common between a cohesive and non-cohesive soil.
  - Temperature effects were not given consideration in the development of the model even though they will alter the lateral load response of a column supported on a CIDH shaft.
- Priestley et al. (2007) suggested a method for handling the effects of SFSI in the determination of the design displacement for the lateral loading of column-pile shafts in cohesive soils. A summary of the shortcomings and limitations associated with the use of this method are presented below:

- The model was found to be applicable over a very limited range of geotechnical properties. This method should only be performed for cohesive soils with an undrained shear strength of 20 kPa (420 psf) or 40 kPa (840 psf) based on the information provided in the textbook. One could argue that the range could be expanded to handle soils that fall between these bounds, but no information was provided on how to handle this situation.
- Plastic action within the model was under predicted when determining the design displacement at the ultimate condition. This was found to be correlated with the way in which the plastic hinge length was determined for the suggested method. The authors of the textbook recommend the use of the plastic hinge length developed by Chai (2002) which was previously shown to be invalid for cohesive soils.
- Lateral force was found to not be easily computed. Without these forces the shear demands on the column and foundation shafts are unknown and could lead to a brittle failure of the structure which is in direct violation of the capacity design principles.
- Seasonal freezing was once again ignored in the development of the model that determines the lateral design displacement of a column-pile shaft in cohesive soils.

- The final two methods, ATC 32 and AASHTO, presented in the above chapter examine the effective point of fixity method. The shortcomings and limitations associated with the use of these models are summarized below:
  - Both methods produced a constant shear profile along the length of the column and foundation shafts. This profile, however, is not valid as the soil will cause a variable shear profile and may cause the shear demand to increase, depending on the location being examined within the system. This can lead to a brittle failure of the structure when subjected to a design level or greater earthquake, thus violating the capacity design principles.
  - The maximum moment location was found to occur between the point of fixity and the ground surface even though these models suggest that it would occur at

the effective point of fixity. By incorrectly defining the maximum moment location, insufficient confinement reinforcement may be provided at the actual location where the maximum moment develops and may cause a failure in the foundation shaft. This would violate the capacity design principles in which the designer wishes flexural yielding and plastic hinges to develop without failure.

- Neither method discusses how the inelastic action that is expected from a design level or greater earthquake will be handled. This limits the range of the models to the elastic loading range even though the most significant amount of displacement occurs after yielding in the inelastic range.
- The effects of seasonal freezing on the lateral response of an integrated column/foundation system were not included in the development of either method, thus limiting their use to warm weather conditions.
- The ATC 32 model requires the use of computer software available at Caltrans to determine the forces to be used in the design of the column. These programs, however, are not readily available to the common user. In addition to this, the model is only applicable over a limited range of structural parameters as described in Section 3.5 above.
- The AASHTO method is only applicable when the response of the system and materials fall within the linear elastic range. Although this is the case, no recommendations were made as to the range over which this occurs and the designer must ensure that this will be the case when using this method. In addition, no validation of the method was provided within the specifications and guidelines provided by AASHTO.

CHAPTER 4: DEVELOPMENT OF A NEW METHOD

4.1 Objective

The current state of practice, as described in Chapters 2 and 3, are unable to effectively capture the lateral load response of a bridge column supported on a drilled shaft founded in clay during all seasons of the year unless a detailed and time consuming methodology is used. The major issues within the current state of practice simplified models are as follows:

1. Plastic action within the inelastic range of the system is generally underestimated as the analytical plastic hinge length in some models is based off of experimentation in cohesionless soils;
2. Although recommended for use in cohesive soils, most of the current models were only verified against experimental testing performed in cohesionless soils as this is easier to control;
3. None of the current models considered the effects of seasonal temperature variation on material properties during their development;
4. The maximum moment location is generally found to not coincide with that of a detailed analysis in cohesive soils; and
5. Localized effects (e.g., curvature and translation) at the point of maximum moment are not accurately captured in most of the models although this is where the most damage will occur in an integrated column/foundation system subjected to design level or greater seismic events.

Due to these deficiencies within the current state of practice, a new simplified method for determining the lateral loading response of drilled shafts in cohesive soils is necessary. Taking the aforementioned issues into consideration a new methodology was created that would be able to effectively capture both the elastic and inelastic range of the lateral loading response of continuous bridge columns supported on CIDH shafts subjected to design level or greater seismic events. The new simplified method was also created such that effects of seasonally wintry conditions could be captured due to the impacts of seasonally frozen clay on the seismic response of these systems (Sritharan et al., 2007). By giving consideration to the effects of wintry conditions in the model development, the new method will be able to be used during all seasons of the year.

4.2 Background on Model Development

This section discusses in more detail the background information used in regards to the development of the model. This includes a general description of the new model as well as an introduction into the procedures that determined the critical parameters and their values needed for this method. The general description provides background as to why the selected model was chosen and brief information about the critical parameters and three springs used within the new methodology. The developmental process, on the other hand, presents a brief introduction on the procedures used to create the data necessary for determining critical parameters for use in the model.

4.2.1 Description of New Model

Model development began with the selection of the type of system to be used for determining the lateral loading response of a bridge column continued into the ground to act as a drilled shaft foundation. The premise used for the model was that it must be easy to use and generate a bilinear force displacement curve with sufficient accuracy while ensuring that the model would lead to conservative outcomes from design perspectives. In addition to these two main requirements, the new model had to be easily input into a structural analysis computer program. With these constraints in mind, the model, as depicted in Figure 4-1, was conceived for further development based on the FBD (Figure 1-9a) and reasons proposed in section 1.4.2; however, it did not initially include the translational soil spring as it was unclear whether or not it would be needed at the start of the project.

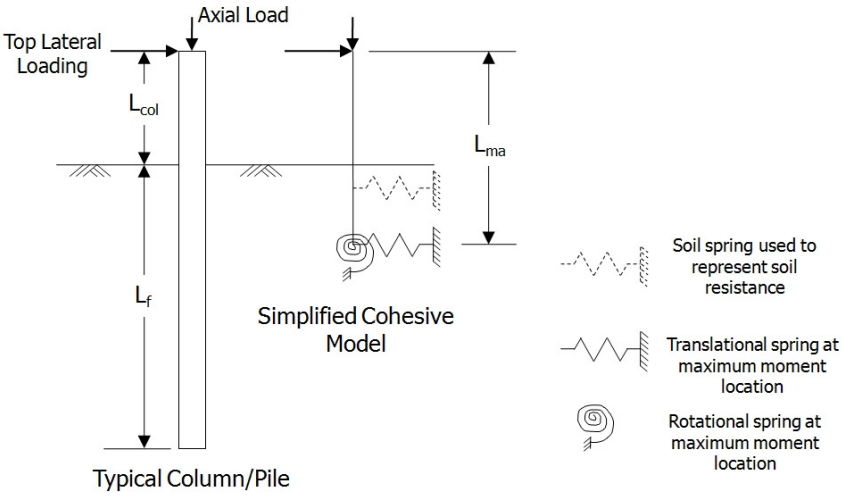

Figure 4-1: Proposed new simplified model

The model depicted in Figure 4-1 was decided on as the springs would allow the model to be easily input into a structural analysis program, while still being able to locate critical locations and produce a force-displacement response as desired. The parameters used within the final model are presented in Figure 4-2 and their development is discussed further in Section 4.4. The most critical point within the model, the maximum moment location, defines the effective height of the system but with a flexible base as opposed to a fixed base assumed in the current practice [Chai 2002, AASHTO 2007, AASHTO 2009]. This location was important as two springs, a rotational and a translational, were placed here. This point was given significant consideration, as this section in the drilled shaft is where the most damage due to seismic lateral loading occurs and all plastic action is assumed to act solely in this vicinity when determining the final displacement. The flexible base was chosen so that the local response, translation and rotation, at and below this point could be accurately represented in the final model. The second translational spring was added to the model later to represent the resistance to displacement provided by the soil above the maximum moment location as well as the variation in shear along the length of the shaft below the ground surface.

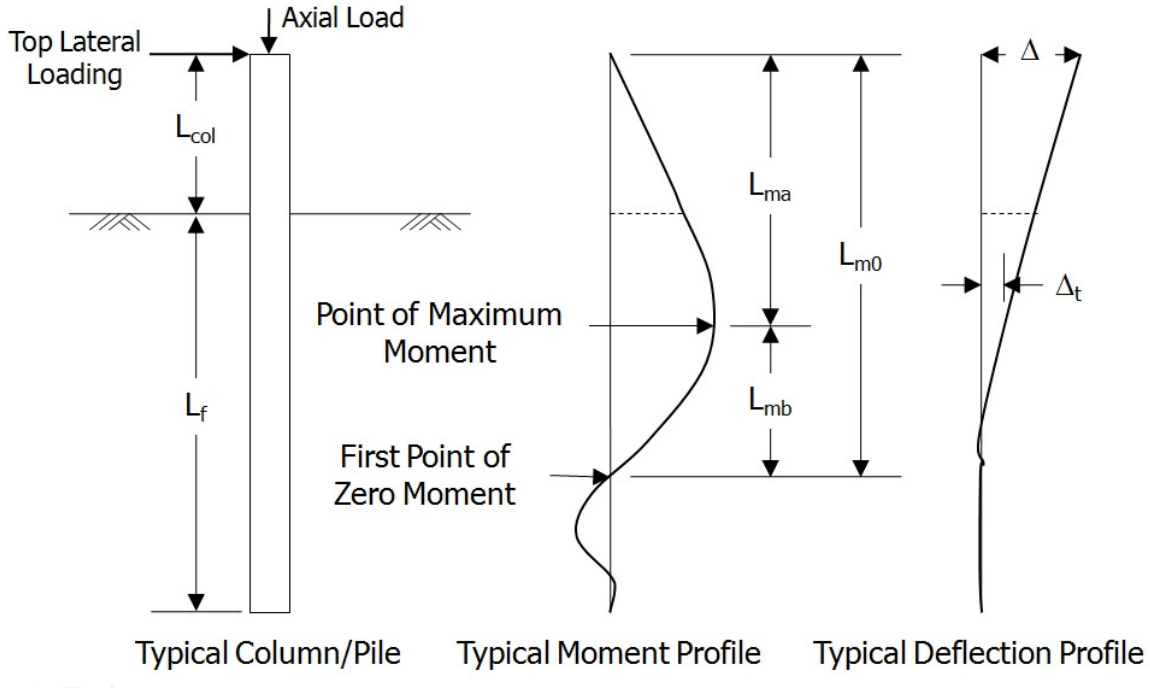

Figure 4-2: Definition of critical parameters used in the proposed simplified method

4.2.2 Process of Development

The development of the critical locations and values associated with the new simplified approach consisted of running a series of detailed analyses using LPILE plus 5.0 (Reese et al., 2004) and then examining the results of the different trials to identify appropriate trends within the data. The first step of the examination was to determine the overall local curvatures, ϕ, experienced within the system by dividing the moment with the flexural rigidity at each node produced by the analysis along the length of the shaft. At this point, the overall curvatures were broken down into elastic and plastic components, ϕ_e and ϕ_p respectively, in order to better identify the contributions of each component to the overall lateral response of the system. To break down the curvatures into elastic and plastic components, the elastic curvature, Equation 4-1, was subtracted from the total curvature to determine the amount of plastic curvature experienced at any given section. After obtaining these components, integrations were performed along the length of the column and foundation shaft from bottom to top to determine the elastic and plastic rotation and displacement values at each node. Once this step was completed, the data was compiled and normalized with respect to multiple parameters (e.g., column diameter and effective height) to help examine possible trends occurring within different data sets.

$$\phi_e = \frac{M}{M_y'}\phi_y' \tag{4-1}$$

where, M = moment at a given point along the shaft;
M'_y = moment at first-yield for concrete cross-section; and
ϕ'_y = curvature of concrete cross-section at first-yield moment.

4.3 LPILE Analyses

For the numerous detailed analyses run during the development of the new methodology for determining the seismic response of drilled shafts in clay soils, certain information was needed to perform the fully inelastic analysis with a displacement convergence tolerance of 2.54E-05 cm (1E-05 in.). This section discusses the parameters that were varied during the model development as well as the different tools used to represent the material properties within the system.

4.3.1 Analysis Parameters

In order to perform the detailed analyses, a series of structural and geotechnical parameters were needed to provide a significant amount of data for the development of the new methodology. Selections of the parameters needed to complete these analyses were based off of commonly occurring cases in practice. The structural and geotechnical parameters were varied in the analyses as follows:

1. Structural Parameters
    - Axial load ratio, ALR, varied from zero to ten percent for c_u = 168.6 kPa (24.45 psi) and was equal to five percent in all other cases;
    - Top of the column was taken to experience pinned head conditions;
    - Column diameter, D, was constant at 0.61 m (24 in.) as the critical parameters were often nondimensionalized with respect to D;
    - Above ground column height, L_{col}, varied from zero to 10D;
    - Length of foundation shaft, L_f, was long enough to ensure that a portion of the shaft would not experience any lateral movement in all trials. This length was kept constant at 10.41 m (410 in.);
    - Longitudinal reinforcement ratio, ρ_l, was maintained at two percent;
    - Horizontal reinforcement ratio, ρ_s, was constant at nine-tenths of a percent based off of a 5.03 cm (1.98 in.) cover to the main longitudinal bars. This satisfies recommendations made in ATC-32 (1996) and AASHTO (2007);
    - Expected concrete compressive strength, f'_{ce}, was kept constant at 27.6 MPa (4000 psi); and
    - Steel reinforcement was taken as ASTM A706 Grade 60.
2. Geotechnical Parameters
    - Uniform layer of clay soil with no groundwater present;
    - Effective moist unit weight of soil, γ_m, was constant at 21.2 kN/m^3 (135 lb/ft^3);
    - Undrained shear strength of soil, c_u, varied from 48.3 kPa to 380 kPa (7 psi to 55 psi) to represent clay soil from soft to stiff; and
    - Strain at fifty percent of maximum stress, ε_{50}, as suggested by Reese et al. (2004).

4.3.2 Moment-Curvature Analyses

A key component in defining the parameters for a full inelastic analysis is to define the structural behavior of the individual elements within LPILE. To define this, a moment-curvature analysis was undertaken in VSAT (Levings 2009) using the aforementioned structural parameters. The moments and corresponding flexural rigidities obtained from these analyses were then input into LPILE to represent the structural behavior. Within LPILE, the moment-curvature response of any section was assumed to be constant from column tip to bottom of the drilled shaft in order to reduce the number of variables being modified with each analysis. The three moment curvature responses and the corresponding input information for LPILE are provided in Figure 4-3.

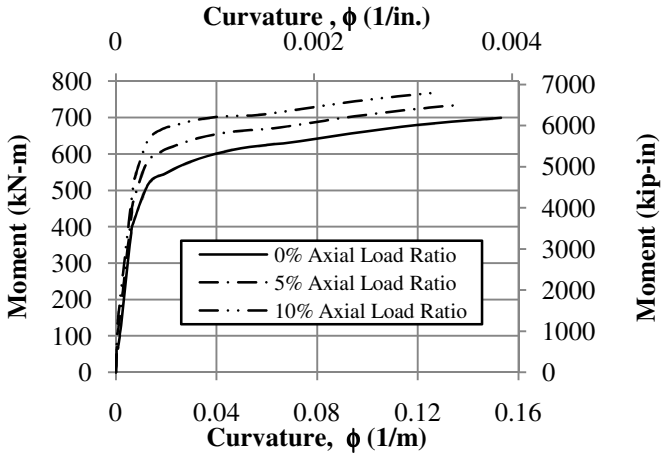

(a) Moment – curvature response using VSAT (Levings 2009)

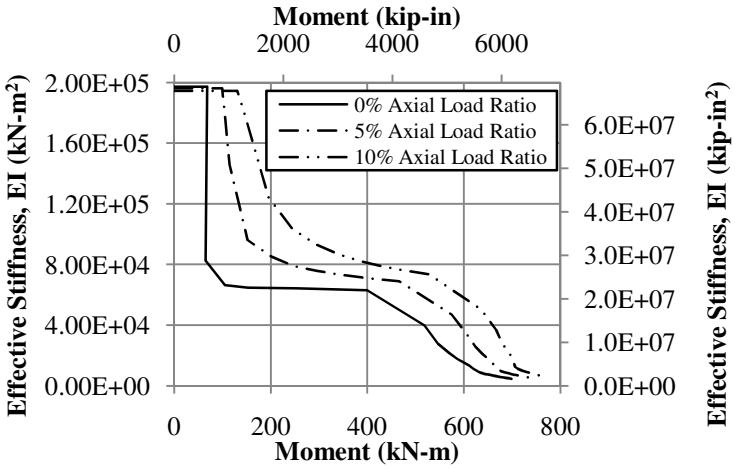

(b) Input parameters used in LPILE (Reese et al., 2004)

Figure 4-3: Structural behavior of column and foundation shafts

4.3.3 Soil Material Models

Each model used theoretically generated p-y curves to determine the nonlinear behavior of the soil. To develop these curves, the selected soil model in LPILE was that of Reese for Stiff Clay (Reese et al., 2004). This model requires the input of the soil's undrained shear strength, effective unit weight and strain at fifty percent of the maximum stress with depth. Since the soil was assumed to be a uniform layer of soil, the height of the soil layer was taken to be equal to the length of the foundation below the ground surface by varying the necessary soil parameters as stated in Section 4.3.1. After specifying the parameters, LPILE internally generates the p-y curves for each node along the length of the shaft using the method suggested by Reese and Welch (1975). Although this material model is stated to be for stiff clay, the original work by Reese and Welch (1975) does not specifically imply that this is the only area in which the soil material model is applicable and was therefore used over the entire range of soil stiffness parameters varied for the analyses.

4.4 Simplified Method for Determining Lateral Response

While performing the different analyses, the data was compiled in Microsoft Excel and different trends were examined to identify the suitable parameters for use in the new methodology. Each trial was individually examined and broken down into elastic and plastic components using the method described in Section 4.2.2. The remainder of this section presents the process undertaken to identify the critical locations as well as the final equations that were developed for use in the new method for determining the lateral response of drilled shafts subjected to design level or greater earthquakes.

4.4.1 Maximum Moment Location

The most critical portion of the model development was to define the effective height by locating the point of maximum moment. The process started by taking the different systems created in the detailed analyses and pushing them all to a pre-determined deflection, less than the ultimate displacement and greater than the yield displacement, to try and locate the maximum moment location. This method was chosen as it would remove the variability associated with having multiple displacement values to examine. Although this appeared to be a benefit when examining the data, no consistent trends could be developed for anything

other than the maximum moment location as it was found to consistently vary with above ground column height only as expected based on previous research. In addition, the method was not accurately predicting the maximum moment location when the pre-determined deflection was exceeded as the maximum moment location will typically shift towards the ground surface, albeit minimally, as a larger displacement is induced at the top of the pinned head column.

Due to these issues arising with the first method, an adjustment was made to the limit state at which the equations would be developed. The new limit state that was chosen was that of the ultimate condition defined by a flexural failure of the shaft when the ultimate moment capacity, M_u, and therefore ultimate curvature of the concrete cross-section, ϕ_u, was obtained anywhere along the length of the column and foundation shaft. The flexural failure was taken to be the ultimate limit state as this approach is consistent with the capacity design principles. By basing the decision off of the capacity design principles it was assumed that any other failure modes such as a shear failure would not occur prior to reaching the flexural failure of the system. After developing the equations at this limit state, the equations would then be verified against the yield limit state to see if the equations would still be valid for predicting the needed force-displacement point to construct a bilinear response for the entire system. The yield limit state was defined as the first occurrence of the yield strain being reached in the longitudinal tension reinforcement of the shaft. Since this limit state is different than the idealized yield limit state used in practice (Priestley et al., 1996), this particular state is referred to as the first yield limit state in the remainder of this report. It will be shown later that the first yield limit state was found to be more appropriate for defining the bilinear response of the column-shaft system as the response of this system is effected by both soil nonlinearity and that in the section response. From these first analyses, it was also noted that axial load ratio would not significantly change the maximum moment location and that the five percent ratio provided the average effective cantilever height. This was noted as there was only a minimal variation in the data for the different ALR examined at c_u = 168.6 kPa (24.45 psi).

Using the ultimate limit state and the five percent axial load ratio, a trend was found to be present within the data when the aboveground height, L_{col}, and the maximum moment

location, L_{ma}, were normalized with respect to the diameter of the continuous shaft. The diameter was chosen as the value for normalization as this is a common method between the different methods presented in Chapter 2 and this avoids investigating the new method for different values of D. The data points for both the ultimate limit state and the first yield limit state found through this examination are shown below in Figure 4-4. The trend that can be noted is that as the above ground height of the column increases the depth to the maximum moment location will increase in a non-linear manner. The trend further demonstrates that the location of the maximum moment will be a function of the undrained shear strength for the soil as the lower this value gets at a similar above ground column height, the deeper the maximum moment location will be. This is expected as a less stiff soil will disperse the lateral loading over a longer shaft length, causing the maximum moment location to occur at a greater depth. The final trend depicted within Figure 4-4 is that the maximum moment location does not vary significantly when examining the yield of ultimate limit state of the integrated column/foundation system.

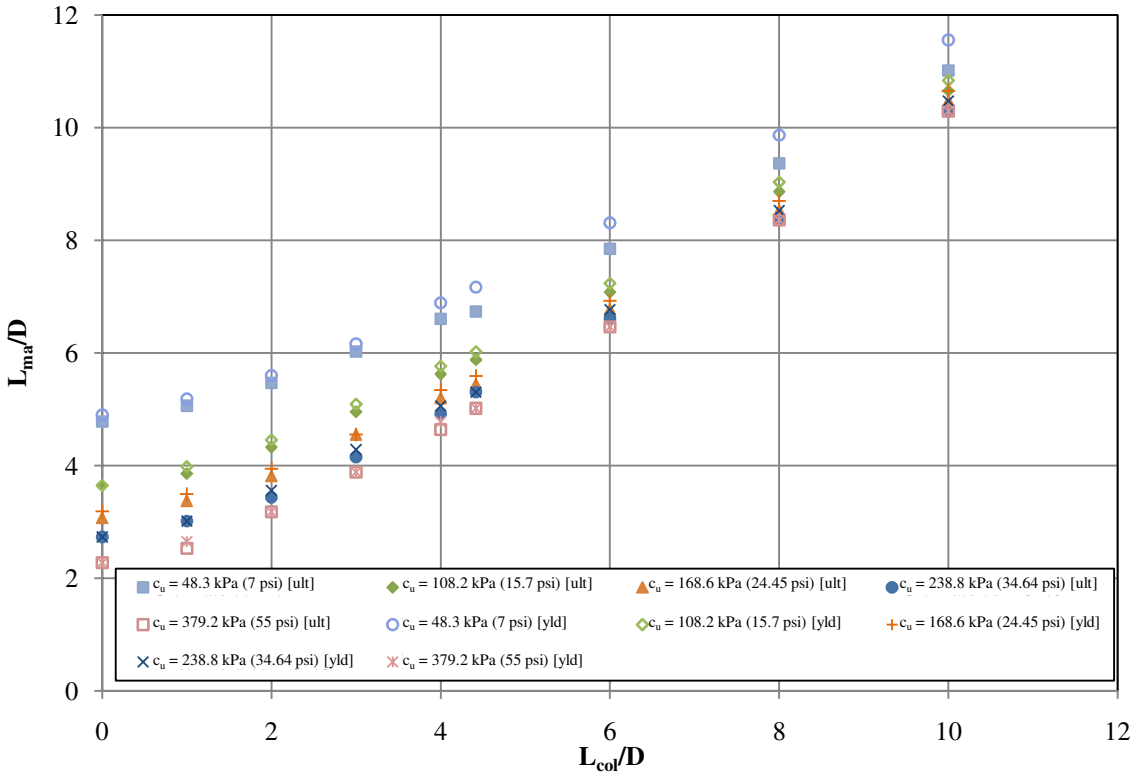

Figure 4-4: Location of the maximum moment at the first yield and ultimate limit states at 5% ALR

Based on the trends noted in Figure 4-4 equations were developed that would locate the point of maximum moment for a given design problem by creating a series of best fit lines for the different ultimate limit state data sets and then ensuring that all factors noted to influence the location were included. A linear trend was tried initially to represent the differing data sets, but this was found to under predict the maximum moment location at the extremes while over predicting the location in the middle. Due to these issues, a series of second order equations were created that fit the data as shown in Figure 4-5. These equations were found to well represent the data and therefore used to create a final equation that takes the form of $y(x) = ax^2+bx+c$ where x is defined as the normalized above ground height of the column, L_{col}/D; y is defined as the normalized depth to maximum moment taken from the top of the column, L_{ma}/D; and a, b and c are coefficients that account for the soil parameters based on the soils undrained shear strengths and the established trend lines.

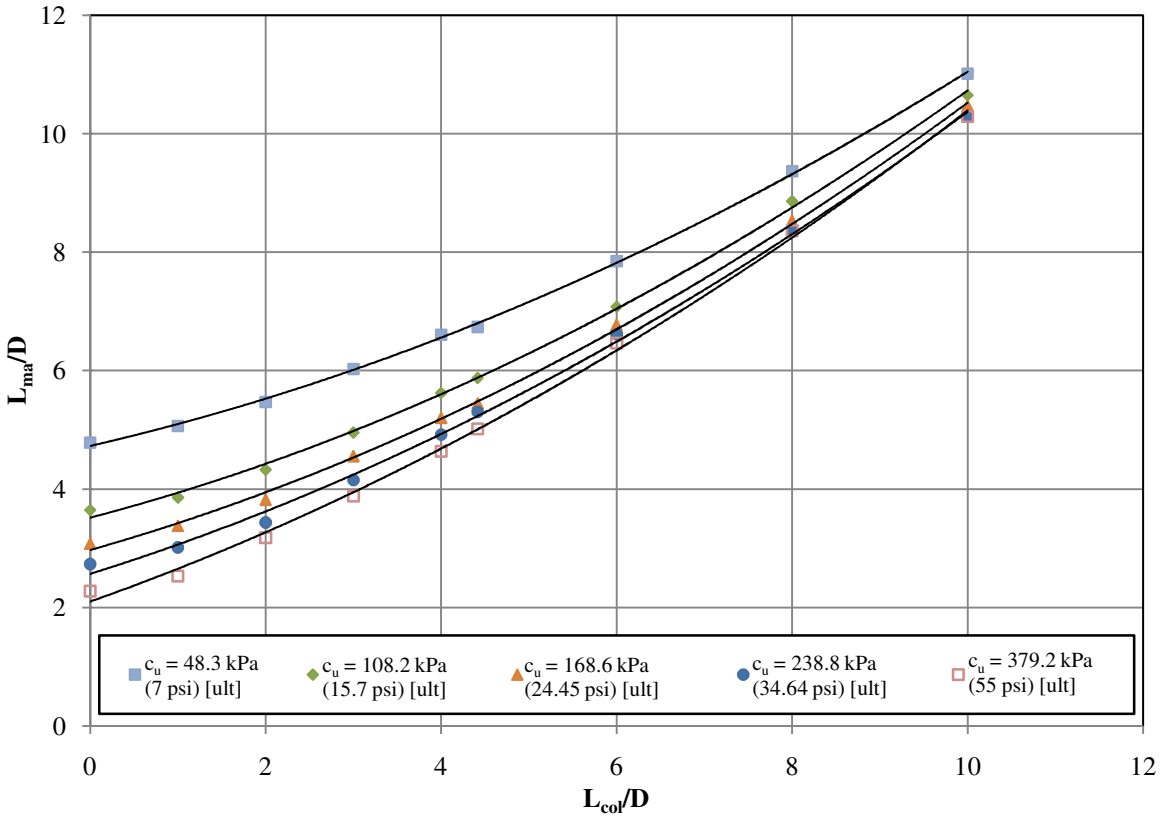

Figure 4-5: Location of the maximum moment with second order polynomial trendlines

The final step in the equation development was to define the coefficients needed to complete the second order polynomial equation. This was accomplished by taking the

individual coefficients for each of the lines shown in Figure 4-5 and graphing them against the undrained shear strength so that the effect of differing soil properties could be handled within a single equation. The effective unit weight and fifty percent strain values of the cohesive soil were not included as the first of these variables remained constant in all analyses while the second variable was chosen based off of the undrained shear strength following the recommendations of Reese et al. (2004). After plotting the data, trends were then created that would allow for the coefficients (α_{ma}, β_{ma} and χ_{ma}) used to locate the maximum moment location to be computed based off of the undrained shear strength of the soil. These coefficients ensure that the correct polynomial line is used. The data points and the trends for the different coefficient relationships are provided in Figure 4-6.

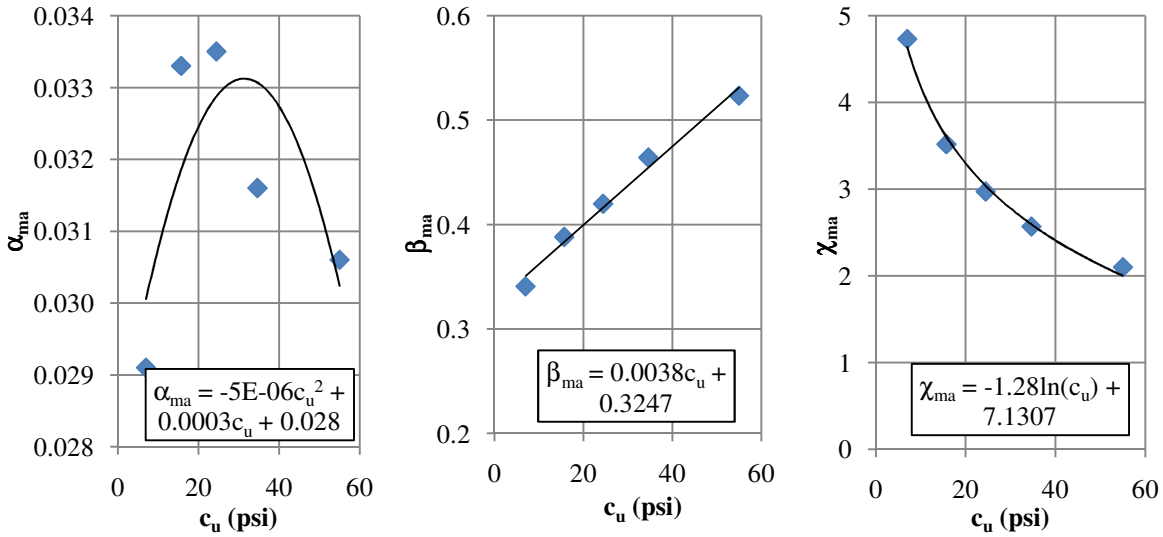

(a) α_{ma} coefficient (b) β_{ma} coefficient (c) χ_{ma} coefficient

Figure 4-6: Soil coefficient relationships used to locate the point of maximum moment (1 psi = 6.895 kPa)

At this point, the final equation for locating the point of maximum moment and therefore the effective height of the system was completed. The second order equation is provided here as Equation 4-2 with the left and right hand sides of the normalized equation multiplied by D to provide a solution that has a length dimension. The final equation was then used and compared with the ultimate limit state data to ensure that the equation would accurately locate the point of maximum moment. This comparison is provided in Figure 4-7, where it

can be seen that the new equation correlates well with the maximum moment location found through the detailed analyses.

$$L_{ma} = D\left[\alpha_{ma}\left(\frac{L_{col}}{D}\right)^2 + \beta_{ma}\left(\frac{L_{col}}{D}\right) + \chi_{ma}\right] \quad (4\text{-}2)$$

where, $\alpha_{ma} = -0.000005ac_u{}^2 + 0.0003bc_u + 0.028$;
$\beta_{ma} = 0.0038bc_u + 0.3247$;
$\chi_{ma} = -1.28\ln[c_u(\text{psi})] + 7.1307$;
$\chi_{ma} = -1.28\ln[c_u(\text{kPa})] + 9.6021$;
a = 1.0 for c_u in psi and 0.021 for c_u in kPa; and
b = 1.0 for c_u in psi and 0.145 for c_u in kPa.

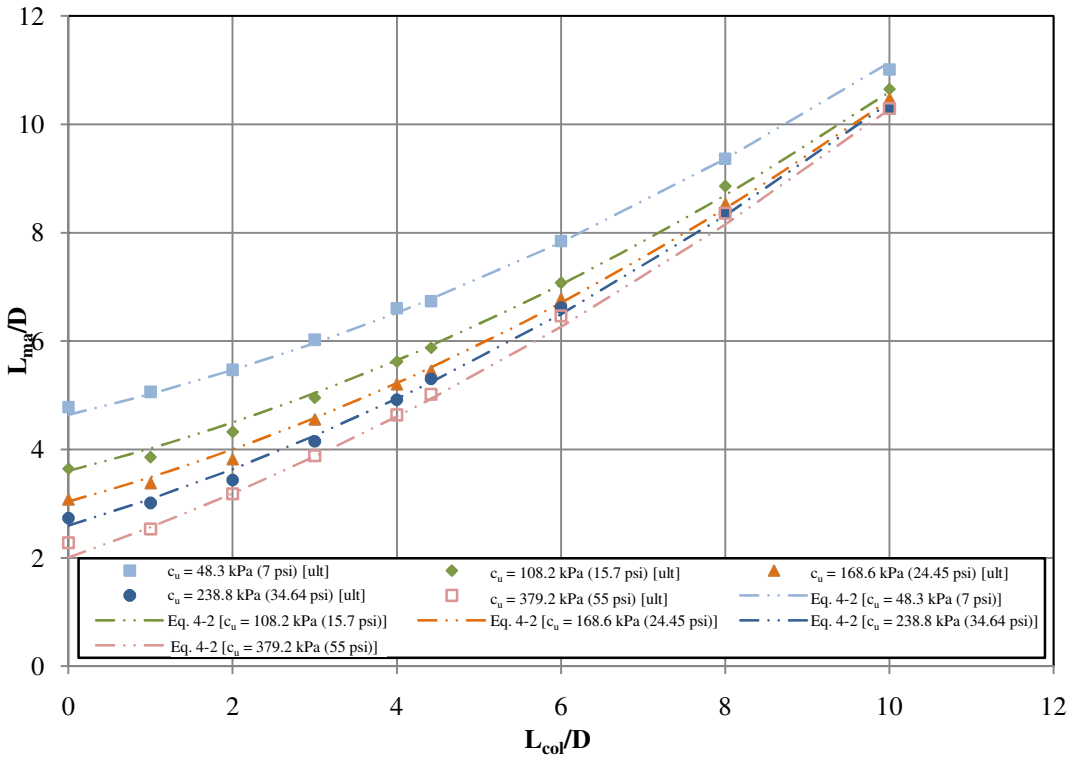

Figure 4-7: Comparison of maximum moment location using the developed equation and detailed analysis results

4.4.2 Plastic Hinge Length and Zero Moment Location

After establishing the maximum moment location, the next critical step in the development of the new model was to define the analytical plastic hinge length above and below the maximum moment location, L_{pa} and L_{pb}, respectively. This step was deemed to be the next crucial step as this will define the amount of plastic rotation and therefore plastic displacement experienced within the inelastic range of the system's behavior. The analytical

plastic hinge length, however, should not be used to determine the area over which confinement reinforcement should be provided as it is strictly to find an equivalent length that will determine the plastic rotation when multiplied by the plastic curvature, ϕ_p, at the maximum moment location. The lengths above and below the maximum moment location were treated separately in this manner in case it was necessary to define two different trends based on the data and the original plan was for the rotational spring to only model the system deformation below the maximum moment location.

The plastic rotation below the maximum moment location, θ_{pb}, was first obtained by performing an integration of the plastic curvatures along the length of the shaft to the maximum moment location. Since a function is not directly obtained through the data, the integration was performed by averaging the plastic curvature at the point being considered with the plastic curvature at the previous point thus creating a series of rectangular areas that could be summed. Once this plastic rotation was obtained, the analytical plastic hinge length was determined by dividing with the plastic curvature at the maximum moment location obtained at the ultimate condition. This is presented algebraically in Equation 4-3 where x is the length along the shaft.

$$L_{pb} = \frac{\int_{L_f}^{Lma} \phi_p(x)dx}{\phi_p} = \frac{\theta_{pb}}{\phi_p} \tag{4-3}$$

After establishing the analytical length to be used for comparison purposes, trends were examined to establish an equation or graph that would easily provide a numerical value for the analytical plastic hinge length. During the iterative process, a number of comparisons were examined. The comparisons were undertaken using normalized data and trends that other researchers had previously established. The comparisons, as presented in the following list, did not provide consistent trends when plotted and separated by differences in the analyses. In the following list, k_h is a horizontal subgrade modulus taken in units of force per length cubed based off of Vesic's equations reproduced in Bowles (1988) and L is the total length of the system.

- L_{pb}/D versus k_hD^5/EI_e;
- L_{pb}/D versus $1000[k_hD^6/D'(EI_e)]$ (Priestley 1996);
- L_{pb}/D versus L_{col}/D (Chai 2002);

- L_{pb}/D versus (L-Lma)/D;
- L_{pb}/D versus $c_u D^2/\gamma_m$;
- L_{pb}/D versus c_u;
- $[3.7D-0.2(L-L_{ma})]/(L-L_{ma})$ versus c_u, where $3.7D-0.2(L-L_{ma})$ was a conservative lower limit on L_{pb} that does not capture the full plastic action; and
- $[3.7D-0.2(L-L_{ma})]/[D(L-L_{ma})]$ versus c_u.

At this point, a new approach was undertaken in which the analytical plastic hinge length below the maximum moment location was compared to a length within the system that might be determined through an equation based approach. Using this method as a basis it was found that the analytical plastic hinge length ranged from 0.16 to 0.20 times the distance between the first point of zero moment, L_{m0}, after the maximum moment is obtained and this variable is defined as, L_{mb} (see Figure 4-2). This is clarified in the bar graph shown in Figure 4-8 where the analytical plastic hinge length was divided by L_{mb} and then compared for all of the ultimate limit state trials. Recognizing that the column-shaft displacement capacity will be rarely reached in seismic loading due to the influence of soil flexibility, the analytical plastic hinge length below the maximum moment location was conservatively specified at the lower limit of this ratio. The final equation developed for L_{pb} is provided below as Equation 4-4.

$$L_{pb} = 0.16 L_{mb} \tag{4-4}$$

The first point of zero moment after the maximum moment location was chosen as this is where the moment profile reverses direction. The reversal of the moment profile means that soil resistance has now completely overcome the external lateral loading demand. In addition, the plastic action within the system has typically dissipated by this point. This means that all of the plastic action is seen within the specified length thus allowing for a better understanding of the distance over which plastic action may occur within the system. Finally, the zero moment location was chosen as the analyses typically demonstrate that deflections at this point are essentially negligible as they are generally about a 0.25 mm (~ 0.1 in.).

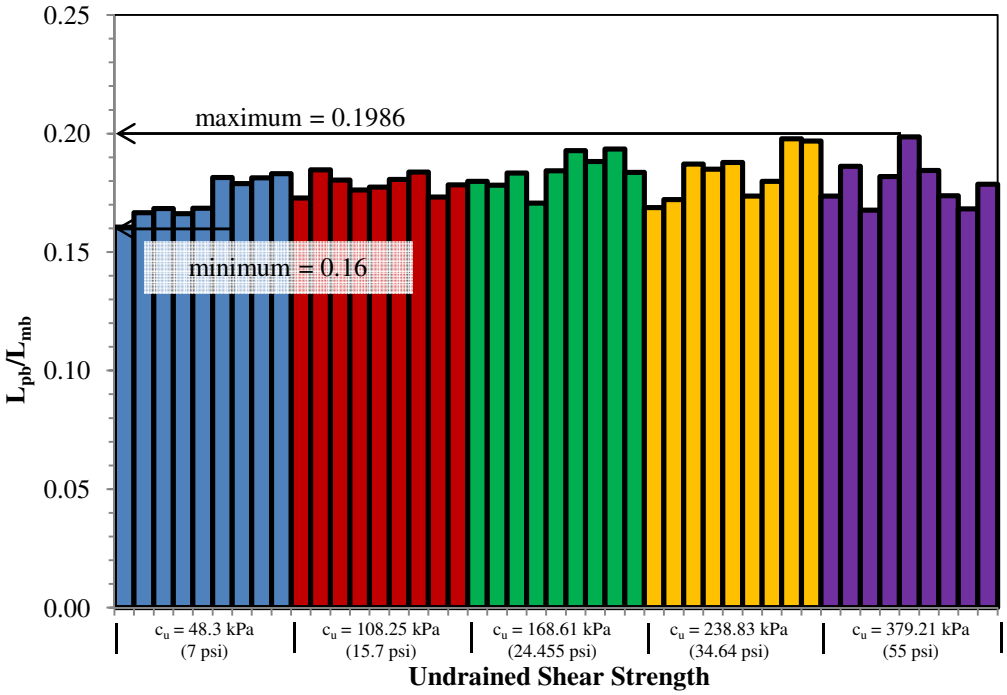

Figure 4-8: Analytical plastic hinge length compared with L_{mb} for all above ground column heights at the ultimate limit state

Using the data from the detailed analyses at the ultimate limit state, the zero moment location was defined in the data set by a linear interpolation between the positive and negative moments on either side of the zero point. The value was then normalized with respect to the shaft diameter and plotted against the normalized above ground height and the undrained shear strength of the soil. The plot against the undrained shear strength provided a better correlation when the trends were examined in detail (see Figure 4-9). The values at the first yield were included for the first two series to demonstrate that only the ultimate limit state needed to be analyzed since the data is nearly identical. Similar to the maximum moment location, the effects of the ALR were examined at an undrained shear strength of 168.6 kPa (24.455 psi). This comparison found that the ALR did not significantly alter the zero moment location and an average value for the ALR of 5% was used in the remainder of the analyses. The two main trends demonstrated in the figure are: (a) as the undrained shear strength increases the zero moment location decreases, and (b) as the normalized above ground column height increases the zero moment location increases.

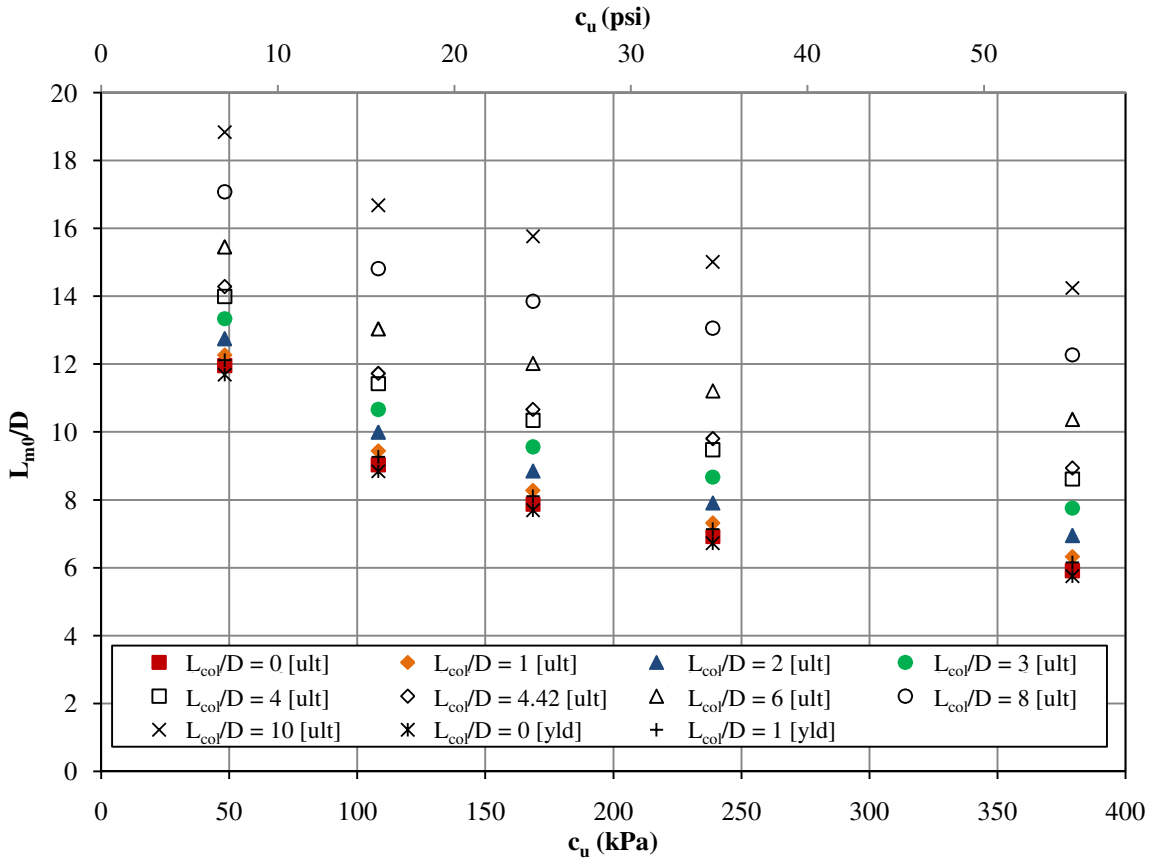

Figure 4-9: Normalized zero moment location versus undrained shear strength at the ultimate limit state and 5% axial load ratio

After establishing the desired plot for locating the first point of zero moment after the maximum moment, different trends were examined including functions following linear, second order polynomial and power series trends. During this process, it was found that a power series function would best capture the trend depicted by the data, Figure 4-10. This was the case as the linear and second order polynomial functions could not accurately capture the curvilinear behavior of the data. A higher order function was not chosen to maintain an equation that would be easier to use for determining this location. This means that the final equation takes the form of $y(x) = ax^b$, where y is the normalized length to the first zero moment location; x is the undrained shear strength of the soil; a is a coefficient determined based on the normalized above ground height and b is an exponent based on the normalized above ground height.

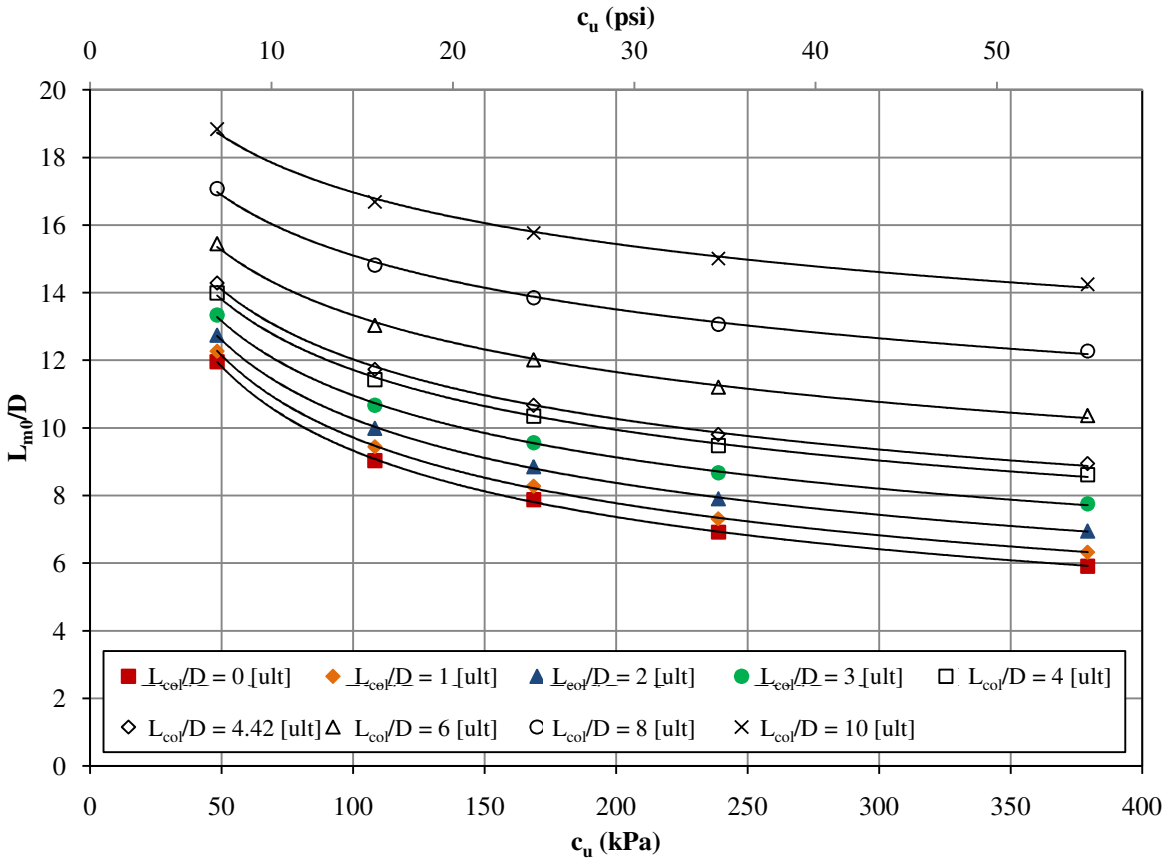

Figure 4-10: Normalized zero moment location with the established power series trend lines at the ultimate limit state

Similar to the maximum moment location, the final step in determining the first zero moment location equation was to create a way to incorporate the influence of soil and determine the coefficient value, α_{m0}, and the exponent value, β_{m0}, to be used in the proposed equation. To define these variables, the coefficients for each trend were taken and plotted against the normalized aboveground height as this was the main factor missing in the equation development and the soil effects are already being accounted for in the overall equation. By accounting for the column height in this manner, the coefficients effectively establish the equation on the correct power series shown in Figure 4-10. The data and the relationships chosen for each coefficient are provided in Figure 4-11. The linear trend for the α_{m0} coefficient was selected as the data generally increases as the above ground column height increases.

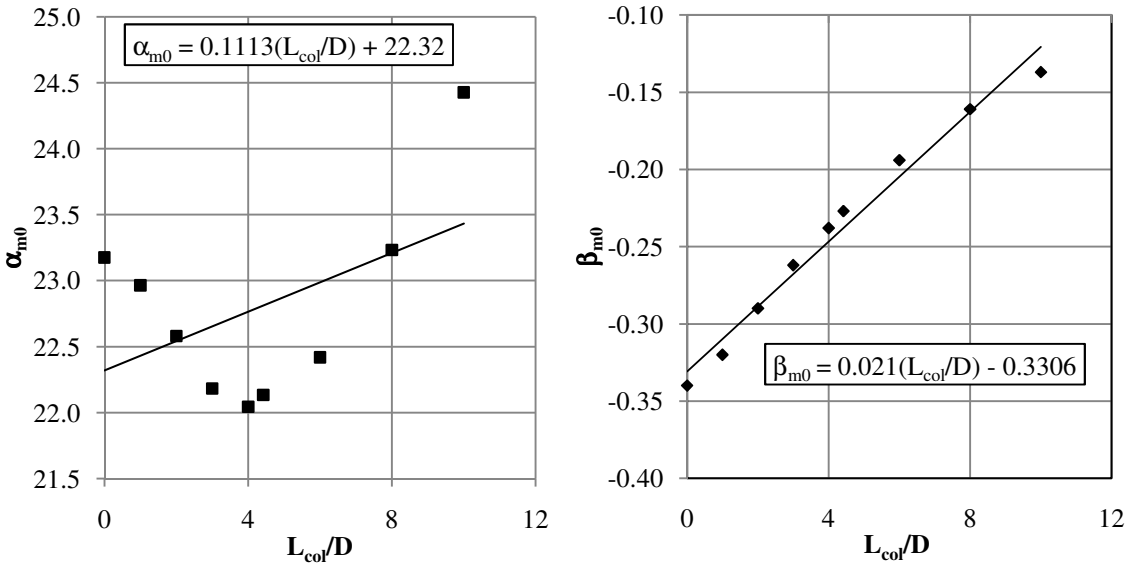

(a) α_{m0} coefficient (b) β_{m0} coefficient

Figure 4-11: Coefficient and exponent relationships used when locating the first zero moment location

Following establishment of these two relationships, the final equation was fully developed for locating the point at which the first occurrence of zero moment is reached after the maximum moment occurs. The developed equation is presented within the text as Equation 4-5 with some reorganization, moving the variable D to the right hand side of the equation, and manipulation of significant figures to provide a final value that has units of length. The equation was then used to determine the zero moment location and the results were plotted against the detailed analyses at the ultimate condition. This comparison is provided in Figure 4-12 where it can be seen that equation 4-5 correlates well with the actual data obtained from detailed LPILE analyses at the ultimate limit state. At this point the analytical plastic hinge length below the maximum moment location was fully developed as L_{mb} is defined as L_{m0} minus L_{ma}.

$$L_{m0} = D\alpha_{m0}[\mathrm{c_u(psi)}]^{\beta_{m0}} \quad \text{or} \quad L_{m0} = D\alpha_{m0}[0.145\mathrm{c_u(kPa)}]^{\beta_{m0}} \tag{4-5}$$

where, $\alpha_{m0} = 0.11\left(\frac{L_{col}}{D}\right) + 22.3$; and

$\beta_{m0} = 0.021\left(\frac{L_{col}}{D}\right) - 0.33.$

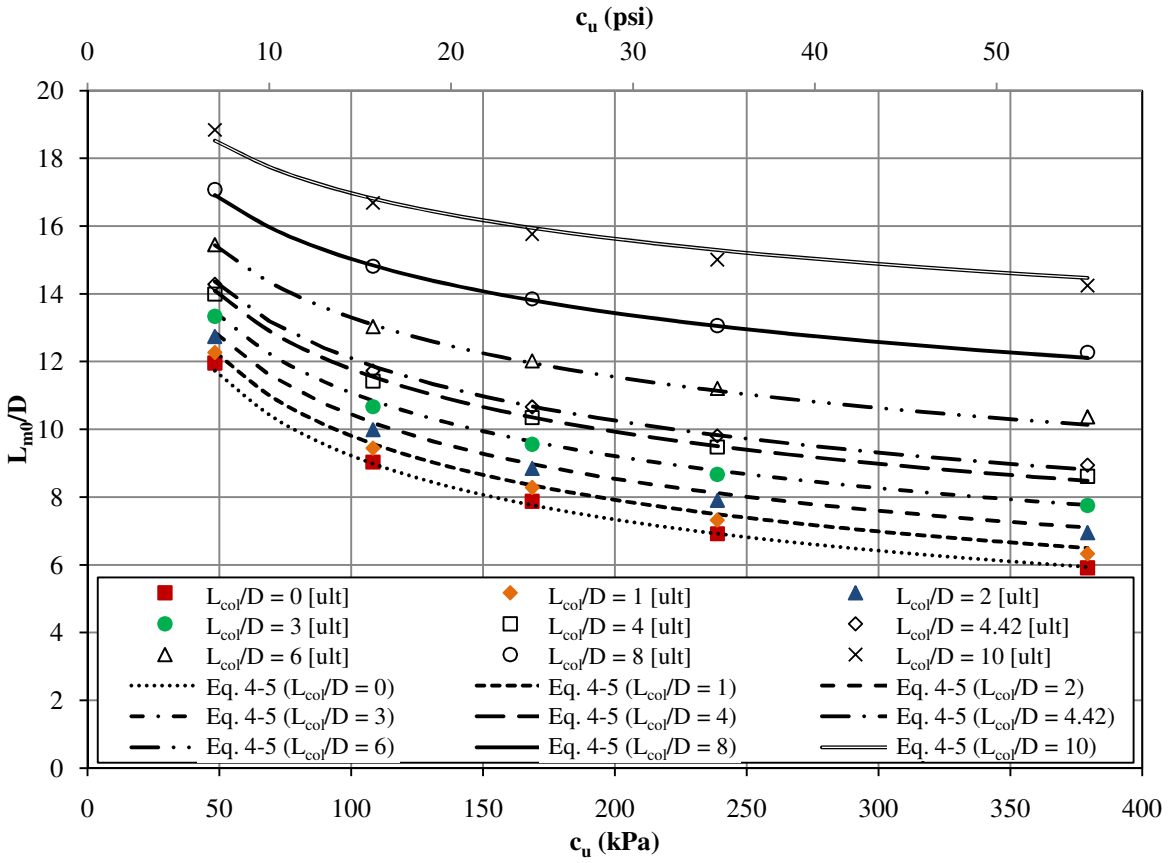

Figure 4-12: Comparison of normalized zero moment location using Equation 4-5 and detailed analyses

4.4.3 Rotational Spring at Maximum Moment Location

The next step in the development of the model was to define the spring properties at maximum moment location. This process began by establishing the bilinear rotational spring that would be located at this point. A bilinear representation was selected for the moment-rotation response as this will provide a means to account for the strength gained due to material nonlinearity (e.g., soil and steel) between the first yield and ultimate limit states. The remainder of this section will discuss the development of the properties needed to define the bilinear moment-rotation behavior of the rotational spring at the maximum moment location.

The rotational spring was originally specified such that it would model the elastic and plastic rotations occurring in the shaft below the effective height of the cantilever but was later modified to further simplify the hand calculations. This simplification was

accomplished by including the effects of plastic rotation that will take place in the shaft and possibly column above the maximum moment location. Thus allowing all of the plastic action to be concentrated solely at this point and allowing the plastic displacement, Δ_p, of the system to be determined by multiplying the effective height of the cantilever with the total plastic rotation, θ_p, as shown in Equation 4-6.

$$\Delta_p = \theta_p L_{ma} \tag{4-6}$$

In order to establish the plastic displacement in this manner, it was necessary to define the analytical plastic hinge length for the region above the maximum moment so that an analytical plastic hinge length for all of the plastic action could be established as $L_p = L_{pa} + L_{pb}$. The above ground length was found through the integration method specified in the previous section thus establishing the plastic rotation to be specified as shown in Equation 4-7 with ϕ_p being determined from Equation 4-8.

$$\theta_p = L_p \phi_p \tag{4-7}$$

$$\phi_p = \phi - \phi_e \tag{4-8}$$

where, ϕ is the curvature at a given moment past the first yield point; and
ϕ_e is found using Equation 4-1.

At this point it was necessary to define the analytical plastic hinge length above the maximum moment location. To define this length, the normalized plastic hinge length, defined as the integral of ϕ_p between the appropriate upper and lower limits divided by the maximum plastic curvature obtained in the shaft, above and below the maximum moment location were compared using a bar graph. The bar graph used for this comparison, as presented in Figure 4-13, showed that the two normalized values are approximately the same. Based on this, the analytical plastic hinge length above the maximum moment location was defined as being equivalent to the analytical plastic hinge length below the maximum moment location. By defining the length in this manner the overall analytical plastic hinge length could be determined by doubling the equation developed for the plastic hinge length below the maximum moment location, Equation 4-9, and thus defined the plastic displacement of the system.

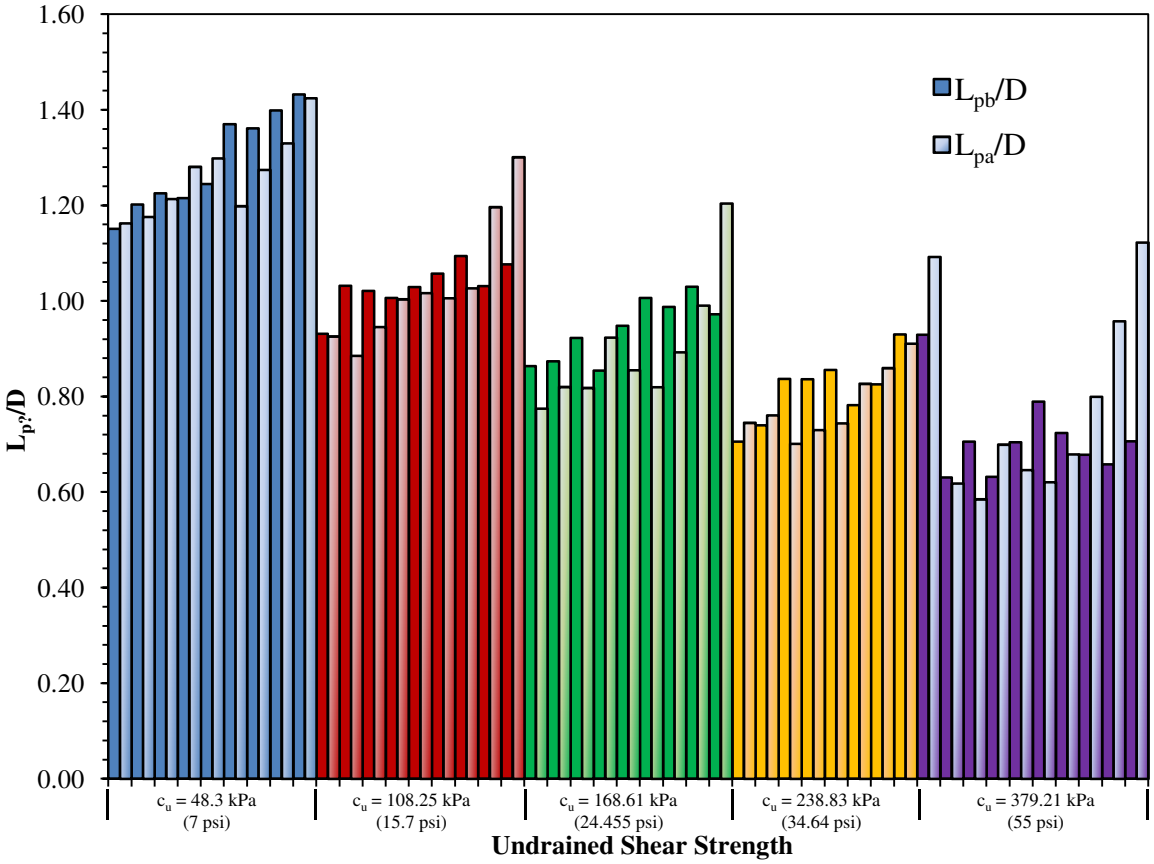

Figure 4-13: Comparison of normalized plastic hinge lengths where the gradient bars are L_{pa}/D and non-gradient bars are L_{pb}/D

$$L_p = L_{pa} + L_{pb} = 2L_{pb} = 2(0.16L_{mb}) = 0.32L_{mb} \quad (4\text{-}9)$$

The other two rotations needed for defining the rotational spring were the elastic rotations below the maximum moment location at the yield and ultimate limit states, θ_{eby} and θ_{ebu} respectively. The elastic rotation above the maximum moment location was not included in the rotational spring as it is accounted for later on when determining the elastic displacement above the flexible base. The limit states for the rotational spring were previously defined as the as the first occurrence of the yield strain in the extreme tension bar and the flexural failure of the system, respectively. In order to determine these values, the elastic curvature components of the detailed analyses were used to perform a first integration along the length of pile shaft from the bottom to maximum moment location to determine the elastic rotation in the system. This integration consisted of summing up average rectangular areas based off of the data at that point and the previous data point thus providing the elastic

rotation at the location being examined. Using this data, the elastic rotations were examined for trends.

The main trend examined for this process was a comparison of the elastic rotation with the normalized length L_{mb}/D. This trend was primarily examined as no other locations would have to be defined to determine the amount of elastic rotation below this point. The data demonstrated that two different linear trends could be developed for the yield and ultimate limit states. The data and linear trends found for the elastic rotations at yield and ultimate limit state are provided graphically in Figure 4-14. The linear equations that follow the trends are provided below as Equations 4-10 and 4-11.

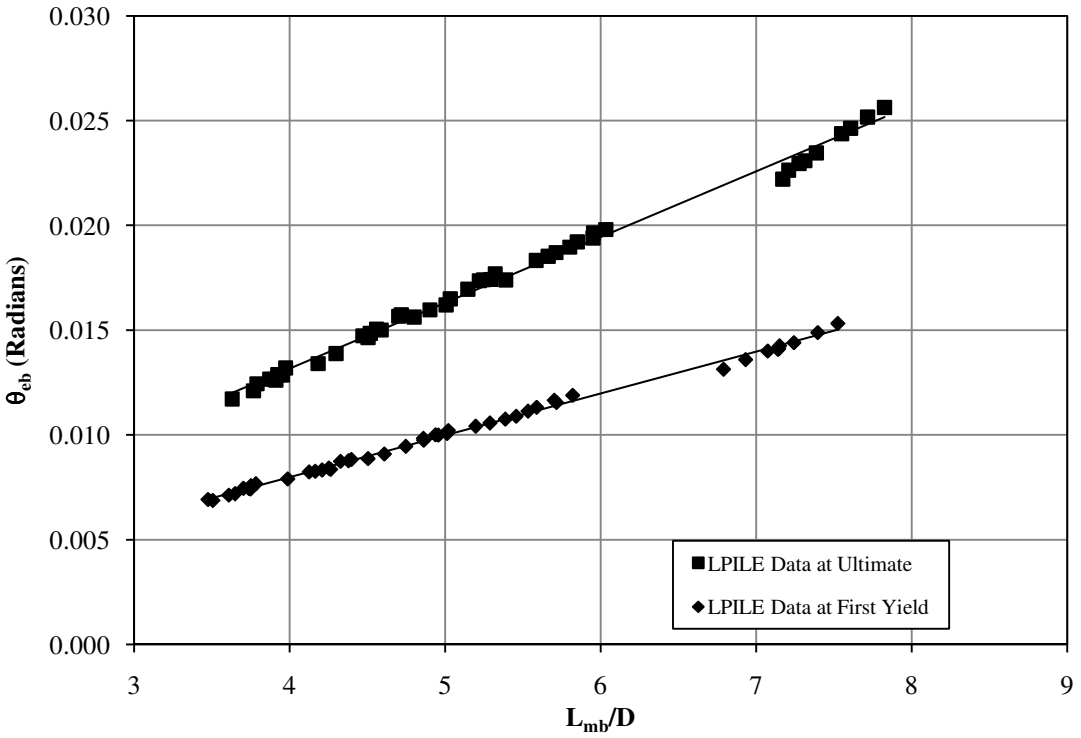

Figure 4-14: Data and trends obtained for the elastic rotation below the maximum moment location

$$\theta_{eby} = 0.002\left(\frac{L_{mb}}{D}\right) + 0.00001 \tag{4-10}$$

$$\theta_{ebu} = 0.0031\left(\frac{L_{mb}}{D}\right) + 0.0006 \tag{4-11}$$

The bilinear moment-rotation spring can now be fully defined as all of the components have been defined, with the exception of the moments which are to be taken based off of a

moment-curvature analysis. The three points that will define the rotational spring are the initial point, the yielding point and the ultimate point. These points are defined as follows:

- The initial point is defined by the point of zero radians and zero moment;
- The first yielding point is defined by the yield rotation, θ_y, and the first yielding moment, M'_y, from the moment-curvature analysis. The yield rotation is defined as the elastic rotation below the maximum moment location at first yield, θ_{eby}; and
- The ultimate point is defined by the ultimate rotation, θ_u, and the ultimate moment, M_u, from the moment-curvature analysis. The ultimate rotation is defined as θ_{ebu} plus θ_p.

4.4.4 Translational Spring above the Maximum Moment Location

The translational spring used to represent the soil above the maximum moment location (see Figure 4-1) was originally to be included in the model when dealing with the effects of seasonal freezing with the intent of capturing the necessary changes needed to relocate the point of maximum moment. Although this was the original intent behind the translational spring used to represent the soil pressure, it was quickly determined that this would not be the only case in which the soil spring was needed. The need for the spring became evident when attempting to compute the top lateral force resistance using static equilibrium of the proposed new model. Due to the large differences experienced in the top lateral force without this spring, it was specified for use in all temperature conditions that an integrated column/foundation system may be modeled for design purposes.

A single spring is used to represent the resistance of the soil to lateral movement over the height of the soil, h_s, between the ground surface and the maximum moment location. Since this spring represents the average stiffness of the soil over this height, it is placed halfway between the ground surface and the maximum moment location, $h_s/2$. By locating the spring in the system in this manner, the influence of seasonal freezing on the soil properties are accounted for and thus the modified behavior of the system can be captured. Even though seasonal temperature variation affects the behavior of construction material properties, their influence is relatively small on the overall response of the integrated system (Sritharan et al., 2007). If the inclusion of construction material properties at freezing

temperature is desired, these changes are accounted for by modifying the moment-curvature response used in the analysis. If desired, the designer may replace this single spring with multiple springs to represent the soil stiffness above the maximum moment location, which can increase the accuracy of the analysis especially when the temperature gradient is significant in this region. Each spring used would still be developed in a similar manner, to that presented below, with the main difference being the length over which the passive soil pressure is activated for each spring.

The properties of the translational spring are determined following the methodology presented by Reese and Welch (1975) with modifications that create a force-displacement curve as opposed to the p-y curve presented in the research by modifying the developed curve through the multiplication of the soil subgrade reaction value, p, by the length over which the soil is being developed. For the model, this length is equal to the distance between the ground surface and the maximum moment location, h_s. When using multiple springs, the distance in the multiplication would be equal to half the distance between adjacent springs plus the distance to a second critical location (e.g., flexible base and halfway to another spring) By performing this multiplication, a force value, V_s, at each displacement can be determined for representing the average soil resistance above the maximum moment location. Once this multiplication is completed, the force-displacement curve is fully developed for use in a computer program.

Although force-displacement response of the soil spring was previously defined, a simpler method for determining the soil force, V_s, was needed for the hand calculations at the ultimate and yield limit states. For the ultimate limit state, the soil was assumed to be fully activated and therefore the ultimate soil subgrade reaction, p_u, found using the Reese and Welch methodology (1975) would be expected in the passive loading of the soil. With this assumption in mind, the ultimate soil shear force, V_{su}, would be equal to the ultimate soil subgrade reaction multiplied by the height of the soil above the maximum moment location, Equation 4-12. In the model proposed by Reese and Welch (1975) this value is obtained and the soil proceeds to deform in a perfectly plastic manner with no ultimate displacement being reached for the translational spring and a designer must make an appropriate decision on the final displacement of the soil in the region above the maximum moment location.

$$V_{su} = p_u h_s \quad (4\text{-}12)$$

where, p_u = ultimate soil subgrade reaction, minimum of Equations 2-2 and 2-3; and
h_s = height of soil between the maximum moment location and ground surface.

In order to determine the resistance of the soil at the first yield condition, the ultimate soil subgrade reaction was compared with the soil reaction found at the first yield limit state, p_y, in the detailed analyses. The averages for each limit state were found by averaging the subgrade reaction at the individual points along the length of the foundation shaft from the ground surface to the maximum moment location. This was deemed appropriate since the subgrade reaction was essentially constant in this region. In order to compare the two limit states, the average value of the first yield to ultimate soil subgrade reaction was compared to the undrained shear strength of the soil. This comparison, as presented in Figure 4-15, found that as the undrained shear strength of the soil increased the ratio of the first yield to ultimate soil subgrade reaction would decrease in a logarithmic manner. Since the comparison is made based off of a ratio of the first yield to ultimate limit state a coefficient, η, could be developed that would relate the yield soil shear force, V_{sy}, to the ultimate soil shear force, as given in Equation 4-13. The value of η is then determined through Equation 4-14, which was developed based off of the best fit trend line shown in Figure 4-15.

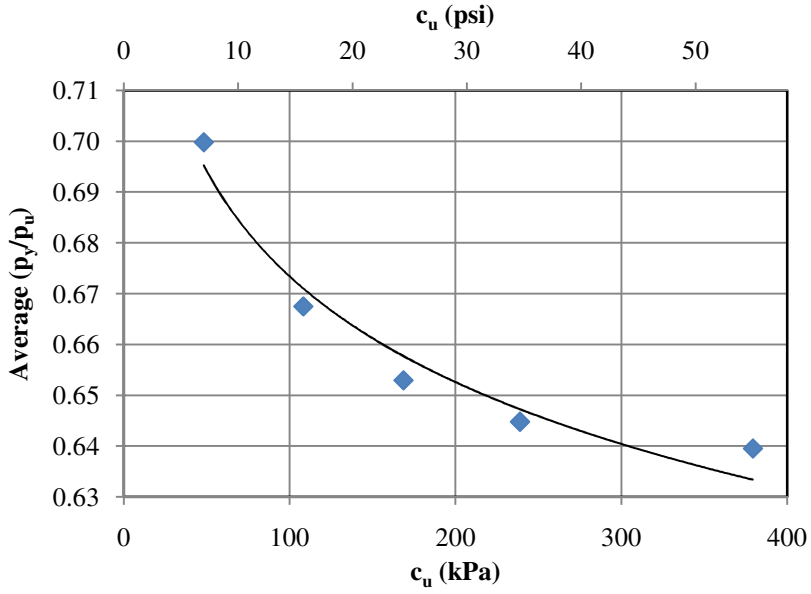

Figure 4-15: Average first yield to ultimate subgrade reaction comparison including data points and best fit trend line (1 psi = 6.895 kPa)

$$V_{sy} = \eta V_{su} \tag{4-13}$$

$$\eta = -0.03\ln[c_u(psi)] + 0.7536\ or\ -0.03\ln[c_u(kPa)] + 0.8115 \tag{4-14}$$

4.4.5 Translational Spring Representing Effects below Maximum Moment

The last major component in the development of the new model was to specify the properties of the translational spring located at the point of maximum moment. This translational spring is a bilinear representation of the force and displacement that is taking place at the maximum moment location due to the behavior of the soil and foundation shaft below this point. The properties of this bilinear spring were specified so that the changes between the first yield and ultimate limit states due to material nonlinearity, soil and structural, are more realistically captured. In addition to the effects of material nonlinearity, the bilinear system was chosen as this requires definition of only three points. The remainder of this section discusses the development of the translational spring that is located at the point of maximum moment.

The initial development of the displacement components of the bilinear force-displacement spring were determined based off of the common moment profile for an integrated system subjected to lateral loading (see Figure 4-2). By using the moment profile in the development, the idea was to create an equation that would be solely based off of the structural parameters of the foundation shaft. For this method, the soil parameters were included in the definition of the critical locations (i.e., maximum moment and zero moment locations). In order to determine a displacement value in this manner, a visual integration method was employed over the length of shaft between the first zero moment and maximum moment location. The aforementioned length was chosen as the displacement at the zero moment location is typically negligible as found in the results of the detailed analyses, thus suggesting that the lateral displacement at the maximum moment location would be mostly due to the induced moment above the zero moment location and the curvature change along L_{mb}. The visual integration was performed by using different geometric profiles, such as parabolic and triangular, and relating them to the typical moment profile of an integrated column/foundation system (see Figure 4-2) to determine the translational displacement. Although equations were developed using this method, they proved to be unreliable at both the first yield and ultimate limit states when compared to the detailed analysis results.

To correct the issues associated with this method, empirical equations were developed by normalizing the translation at the maximum moment location with the foundation shaft diameter (i.e., Δ_t/D) and relating it to the normalized length between the maximum moment location and zero moment location (i.e., L_{mb}/D). The relationship was determined by plotting the normalized translation against the normalized length value for the first yield and ultimate limit states. These relationships are presented in Figure 4-16 and a linear trend for both the first yield and ultimate limit states exists. The linear trend prevalent in the graph shows that as the length L_{mb} increases, the translation at the maximum moment location would also increase. This is expected because the increase in the translation occurs with softer soil where the length between the maximum moment location and the zero moment location will increase based on the relationships developed in Section 4.4.2. It is also noted that the softer soils deviate further away from the apparent linear trend than the stiffer soils.

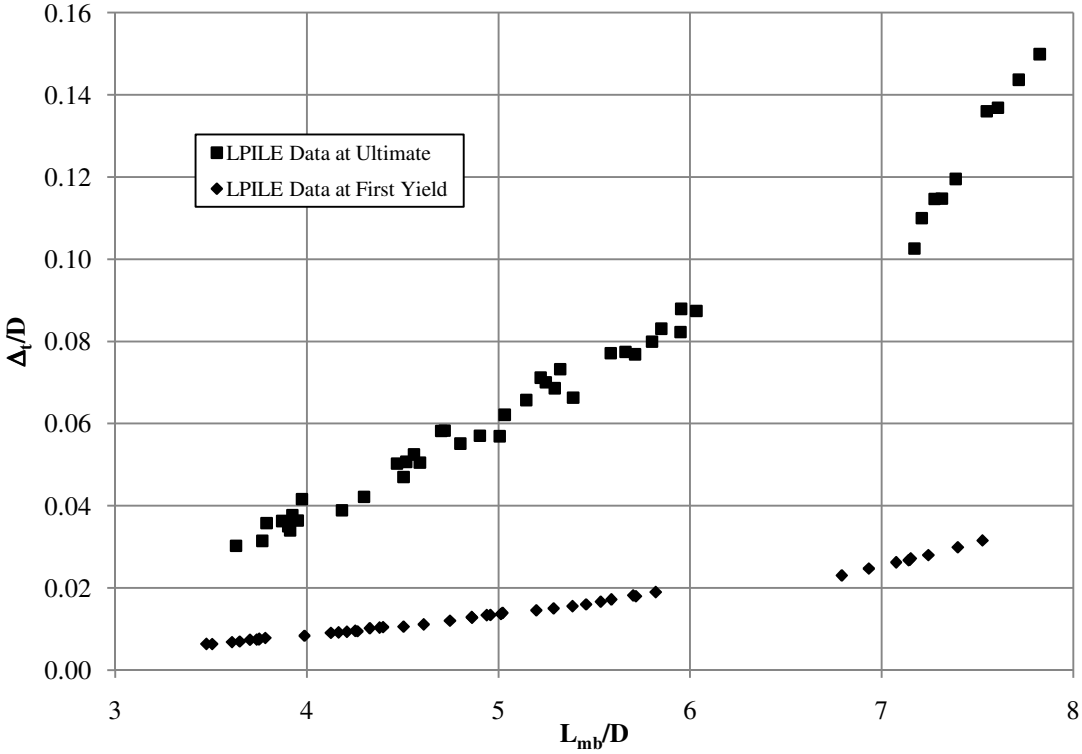

Figure 4-16: Normalized translation at first yield and ultimate limit states versus normalized length L_{mb}/D

The next step in developing the displacement components of the translational spring was to determine a set of equations that defines the translation at both the first yield and ultimate

limit states. To determine equations that would represent the displacement for these limit states, best fit linear trend lines were individually created that would represent the entire data sets including the soft soil range. The trends are shown in Figure 4-17 with the developed linear equations provided herein as Equations 4-15 and 4-16, where Δ_{ty} and Δ_{tu} are the translations at the maximum moment at the first yield and ultimate limit states, respectively.

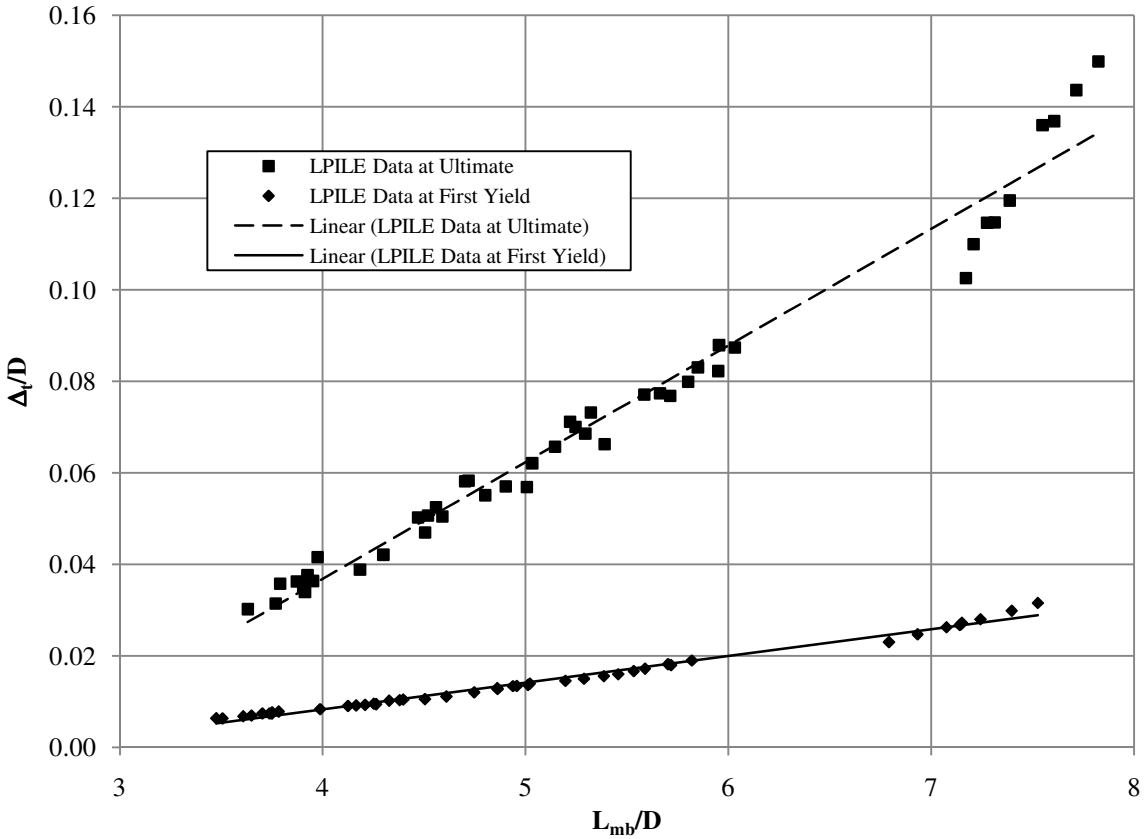

Figure 4-17: Linear trend lines associated with the yield and ultimate limit state translation at the point of maximum moment

$$\Delta_{ty} = 0.0058\left(\frac{L_{mb}}{D}\right) - 0.015 \quad (4\text{-}15)$$

$$\Delta_{tu} = 0.0255\left(\frac{L_{mb}}{D}\right) - 0.0652 \quad (4\text{-}16)$$

Although two equations that represent the average displacement of the system at the point of maximum moment were found, modifications were made to better capture the effects of the soft soil and to further simplify the hand calculations. The first modification undertaken was the simplification of the two equations by relating the first yield translation to the ultimate translation. By dividing Δ_{tu} with Δ_{ty} it was found that the slope would differ

by a factor of 4.397 and the intercept would differ by a factor of 4.347. Since these values are relatively the same, they were averaged and resulted in a value of 4.372. The first yield translation in the model was therefore specified as the translation at the ultimate condition, as previously defined, divided by the constant 4.37, Equation 4-17.

$$\Delta_{ty} = \frac{\Delta_{tu}}{4.37} \tag{4-17}$$

Upon completion of this simplification, the modification for a soft soil was examined. The goal of the examination was to determine a coefficient, ψ, which could be included in the ultimate translation equation so that the relationship defined in Equation 4-17 would still be valid. In order to do this, it was determined that the normalized length between the zero moment and the maximum moment locations should be adapted such that the coefficients already developed in Equation 4-16 for the linear trend at the ultimate limit state would remain unchanged. The new relationship would then take the form shown in Equation 4-18. The coefficient, ψ, was also specified to only be used if the soil had an undrained shear strength less than or equal to approximately 70 kPa (10 psi) based off of the better fit of the linear trend to the detailed analyses at higher shear strengths as presented in Figure 4-17.

$$\Delta_{tu} = 0.0255\psi\left(\frac{L_{mb}}{D}\right) - 0.0652 \tag{4-18}$$

To determine a value in this manner, the actual data points were compared to the linear trend line and the relative percentage of the normalized length was computed at each data point as demonstrated in Figure 4-18. By examining the data and possible trends presented within this figure, a secondary graph of the relative percentages of the normalized length was then plotted against the normalized above ground column height. The secondary plot, Figure 4-19, depicts a linear trend in which the relative percentage of the normalized length increases as the above ground column height increases. This response allowed the coefficient, ψ, to be determined as a linear function of the above ground height and is presented in Equation 4-19.

$$\psi = 0.0157\left(\frac{L_{col}}{D}\right) + 0.9342 \tag{4-19}$$

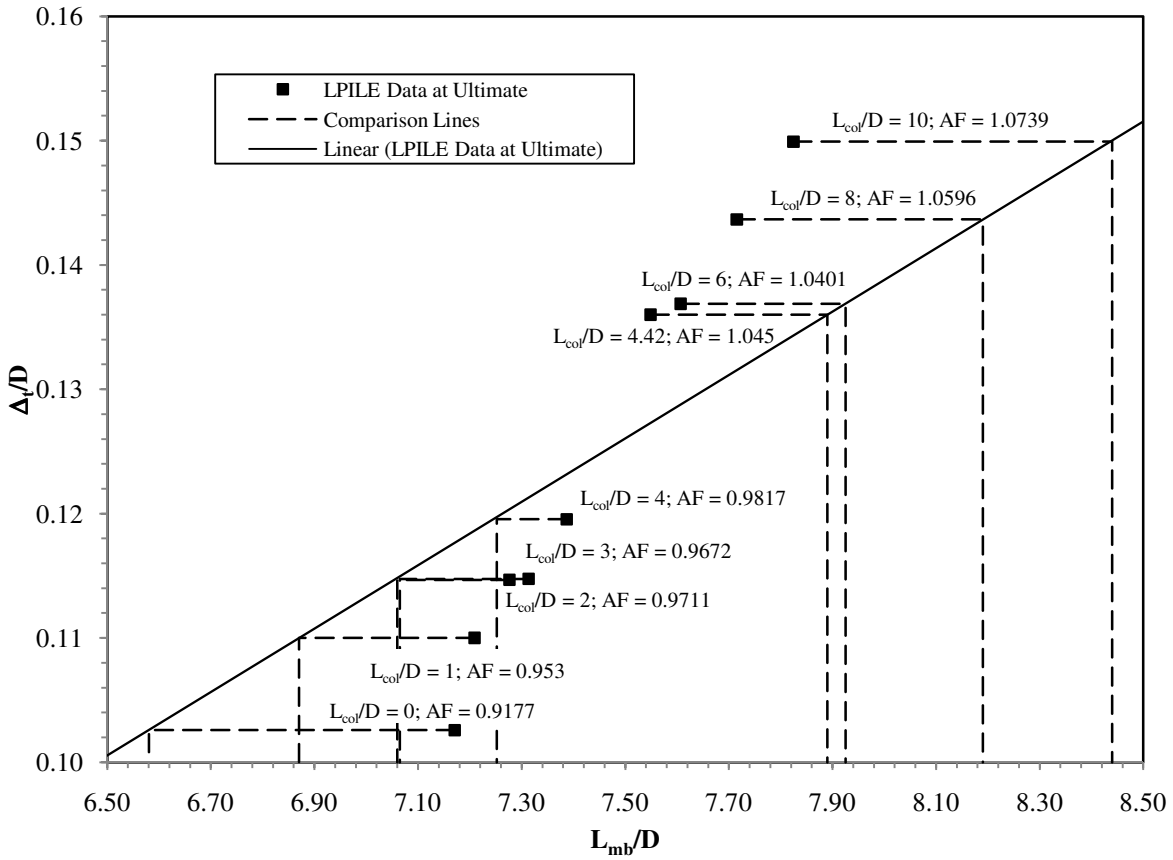

Figure 4-18: Soft soil correction information for coefficient ψ (Note: AF = Adjustment factor)

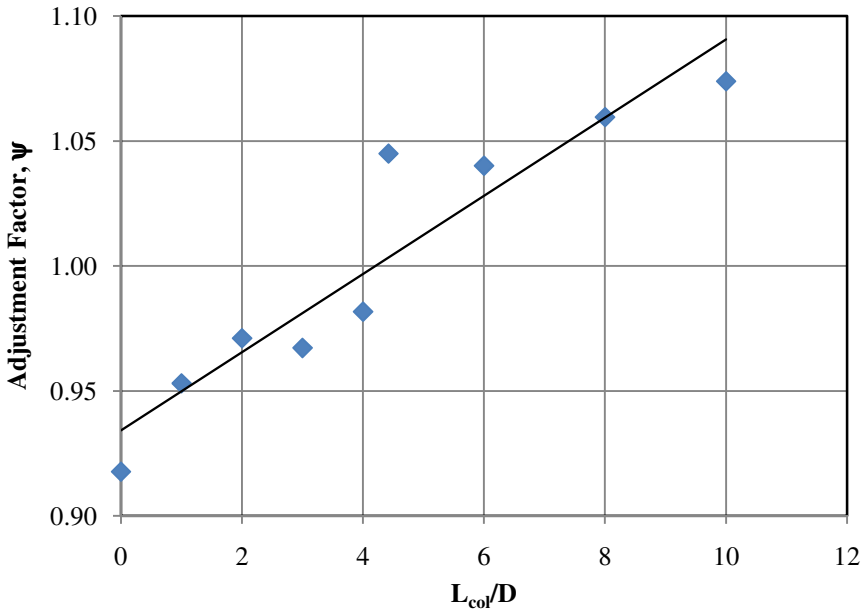

Figure 4-19: Soft soil adjustment factor data and a linear fit curve

Equations 4-18 and 4-17 were verified graphically in Figure 4-20 and mathematically in Table 4-1 to ensure that it would provide a satisfactory result over the range of the soil shear strengths. A graphical and mathematical representation were both needed to ensure that the modification factor, ψ, would capture the correct data if the soil had a shear strength less than 70 kPa (10 psi). Therefore, the mathematical verification was performed by using the normalized length L_{mb}/D obtained from the detailed analyses at an undrained shear strength of 48.3 kPa (7 psi) and determining the translation through Equations 4-18 and 4-17 depending on the limit state. Both the graphical and mathematical comparisons agree well with the detailed analyses.

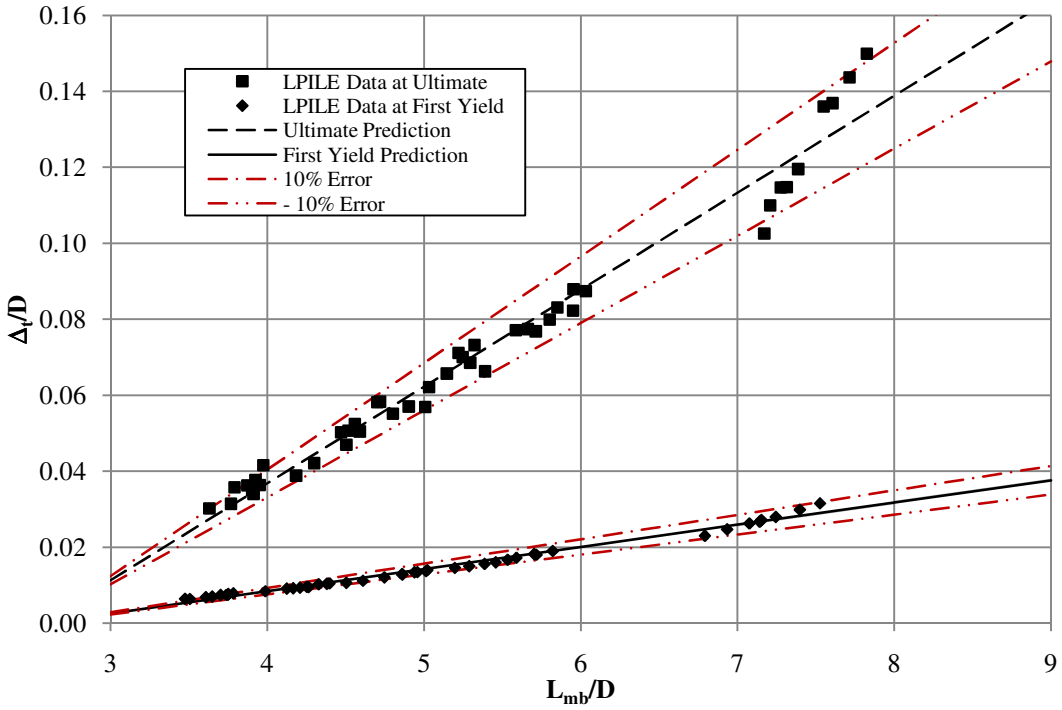

Figure 4-20: Graphical verification of proposed translation equations at the maximum moment location

The final step in defining the properties for the bilinear spring is to specify the forces at which the first yield and ultimate translations will occur. These forces are specified by ensuring that structural equilibrium is maintained at each limit state. Therefore, the horizontal shear forces used in specifying the bilinear spring behavior are found by making sure that the summation of the horizontal forces are equal to zero at each respective limit state.

Table 4-1: Mathematical verification of the proposed translation equations at the maximum moment location for c_u = 48.3 kPa (7 psi)

			Δ_{tu}/D			Δ_{ty}/D		
L_{col}/D	L_{mb}/D	ψ	LPILE	Eqn.	Error	LPILE	Eqn.	Error
0	7.1707	0.934	0.1026	0.1056	2.96%	0.0230	0.0242	4.94%
1	7.2090	0.950	0.1100	0.10942	0.53%	0.0247	0.0250	1.30%
2	7.2763	0.966	0.1147	0.1140	0.61%	0.0263	0.0261	0.67%
3	7.3135	0.981	0.1148	0.1178	2.66%	0.0272	0.0269	0.89%
4	7.3869	0.997	0.1195	0.1226	2.56%	0.0267	0.0281	4.92%
4.42	7.5489	1.004	0.1360	0.1280	5.90%	0.0269	0.0293	9.04%
6	7.6070	1.028	0.1369	0.1343	1.89%	0.0280	0.0307	9.74%
8	7.7153	1.060	0.1437	0.1433	0.25%	0.0299	0.0327	9.74%
10	7.8246	1.091	0.1499	0.1525	1.74%	0.0316	0.0349	10.58%

4.4.6 Global Bilinear Force-Displacement Response

The necessary individual components have now been fully developed and are ready to be used to determine the global bilinear force-displacement response. This process combines the elastic, plastic and translation components of the displacement (i.e., Δ_e, Δ_p and Δ_t respectively) to determine the total displacement, Δ, at the top of the system for the yield and ultimate limit states (see Equation 4-20).

$$\Delta = \Delta_e + \Delta_p + \Delta_t \tag{4-20}$$

In this process, a minor iteration on the elastic displacement of the system is used to more accurately capture the additional displacements and forces developed due to the applied axial load at the top of the column. In addition to computing the ultimate displacement of the system, the lateral load applied at the top of the column will be determined thus finalizing the global force-displacement response of the integrated column/foundation system.

The plastic displacement shall be specified first as this component of the total displacement requires no iterations at the first yield or ultimate limit states. When examining the first yield limit state, the system is expected to behave in a fully elastic manner which means no plastic displacement occurs at this limit state. Therefore the plastic displacement at first yield, Δ_{py}, is equal to zero and the total displacement is just that of the elastic displacement in the system. At the ultimate limit state, the model was created such that the plastic displacement, Δ_{pu}, was simply equal to the plastic rotation multiplied by the effective

height of the system as in Equation 4-21. The plastic rotation can be found using Equation 4-7 with the analytical plastic hinge length taken from Equation 4-9. The effective height of the system is the distance to the maximum moment location from column tip as specified in Equation 4-2.

$$\Delta_{pu} = \theta_p L_{ma} \tag{4-21}$$

The second component to be specified in the final displacement equation is the translational component. This component is used to specify the amount of translation that takes place at the maximum moment location due to lateral movement that occurs to the shaft below this point. Therefore, this value is simply taken as the displacement of the translational spring at the maximum moment location for the correct limit state. At the ultimate limit state, this displacement is equal to Δ_{tu} taken from Equation 4-18 thus allowing the first yield displacement, Δ_{ty}, to be determined using Equation 4-17.

The third and final component to be specified for the total displacement is the elastic displacement of the system. This component is defined as the summation of the elastic displacement occurring above the maximum moment location, Δ_{et}, and the elastic displacement caused by the elastic rotation below the maximum moment location, Δ_{eb}. The elastic component of translation at the flexible base is not included here as it was already accounted for as Δ_{ty}. The displacement caused by the elastic rotation does not require an iterative process and is equal to the elastic rotation below the maximum moment, θ_{eb}, at the appropriate limit state multiplied by the effective height of the system as in Equation 4-22. The elastic rotation for the appropriate limit state is found through Equation 39 or Equation 40.

$$\Delta_{eb} = \theta_{eb} L_{ma} \tag{4-22}$$

where, θ_{eb} = elastic rotation at the appropriate limit state using Equation 4-10 or 4-11

In order to determine the elastic displacement above the maximum moment location, Δ_{ea}, an iterative process must be used due to the large displacements expected within the system at the ultimate limit state. In order to define this deflection the top lateral force must be approximated based off of structural equilibrium including P-Δ effects. This initial estimate

can be found through the use of Equation 4-23 in which P is the applied axial load to the system, M_{max} is the ultimate moment capacity of the shaft at a given limit state and V_{t1} is the uncorrected lateral load at the top of the column. Once this lateral force is obtained, an estimate on the elastic displacement may be made by using the deflection of a free end of a fixed cantilever ignoring the resisting force from the soil, Equation 4-24 (first term only). A more accurate analysis can be performed with the inclusion of this force (second term of Equation 4-24) and a fixed base cantilever, but the second term is small in comparison to the first and may therefore be neglected when performing this step. The second term was considered negligible as the two displacement values typically vary by less than 10%.

$$V_{t1} = \frac{M_{max} - P(\Delta_p + \Delta_{eb}) + V_s(h_s/2)}{L_{ma}} \tag{4-23}$$

$$\Delta_{ea} = \frac{V_{t1} {L_{ma}}^3}{3EI_e} - \frac{1}{8}\frac{V_s h_s}{EI_e}(L_{ma} - 0.25h_s) \tag{4-24}$$

where, EI_e is the effective flexural rigidity of the system and is taken as M'_y/ϕ'_y

Although these values are a good approximation of the global lateral load and elastic displacement above the maximum moment location, the values should be corrected again due to the large displacement of the column tip at the ultimate limit state. The correction ensures that the moment caused by the P-Δ effects is captured correctly. In order to find a more appropriate displacement and the top lateral load, Equation 4-23 is modified to include the elastic displacement above the maximum moment location and the new lateral load input into Equation 4-24 to determine the elastic displacement above the maximum moment location, Δ_{eac}. The corrected lateral, V_t, is found through the use of Equation 4-25. By accounting for the elastic displacement in this manner, the rotation of the foundation shaft above the maximum moment location has also been accounted for.

$$V_t = \frac{M_{max} - P(\Delta_p + \Delta_{eb} + \Delta_{ea}) + V_s(h_s/2)}{L_{ma}} \tag{4-25}$$

The final step in specifying the global force-displacement response of an integrated column/foundation shaft is to combine the information presented above into a graphical format. The bilinear approximation for the system uses the following three points to define the response:

- The initial point of the curve is taken as the origin of a Cartesian coordinate system. This point is used because it is assumed that at no lateral load there will be no lateral displacement and vice versa.
- The second point is defined as the first yield location. The model presented above defines this point as the location at which the extreme tension bar first experiences a yielding strain. This point would use M'_y in Equation 4-25 to determine the lateral load at the top of the column and the displacement is obtained from Equation 4-20 and does not include any plastic displacement component.
- The third and final point defines the ultimate limit state. In the model, the ultimate limit state is defined as the full development of the flexural capacity in the foundation shaft at the maximum moment location. Therefore, the point would be defined using the ultimate capacity and curvature of the foundation shaft based off of a moment-curvature analysis. The lateral force is defined using Equation 4-25 and the lateral displacement is defined using Equation 4-20 with the inclusion of plastic action.

4.5 Model Verification

The new methodology for determining the seismic response of drilled shafts in clays has now been fully developed and its effectiveness still needs to be verified. Therefore, verification against the detailed analyses used in developing the model as well as the experimental data reported by Suleiman et al. (2006) was performed. Two different investigations were conducted to ensure that both the local and global responses of the system are actually captured by the proposed model. In addition to these responses, the comparison with the experimental data will demonstrate the models ability to handle both the frozen and the unfrozen state when dealing with seasonal freezing as well as its effectiveness in a real life situation. The remainder of this section will discuss in detail the results of the two different verifications that were performed for the proposed methodology.

4.5.1 Experimental Verification

The first key step in performing the experimental verification was to specify an equivalent soil profile to be used in the new method. This was done by taking the soil profile at the Spangler site on the Iowa State University campus in the frozen and unfrozen state, as illustrated in Figure 4-21, and determining an average undrained shear strength, moist unit

weight and strain at fifty percent of maximum stress for the cohesive soil within the first six pile diameters below the ground surface. This depth was chosen based on the assumption that the maximum moment location occurs within the specified length. In addition, to this the height of the soil between the ground surface and the maximum moment location was not used as this would require multiple iterations to define the response of the overall system. This length is also common within previous research (e.g., Chai 2002 and Das 2004) into the lateral load response of an integrated column/foundation system.

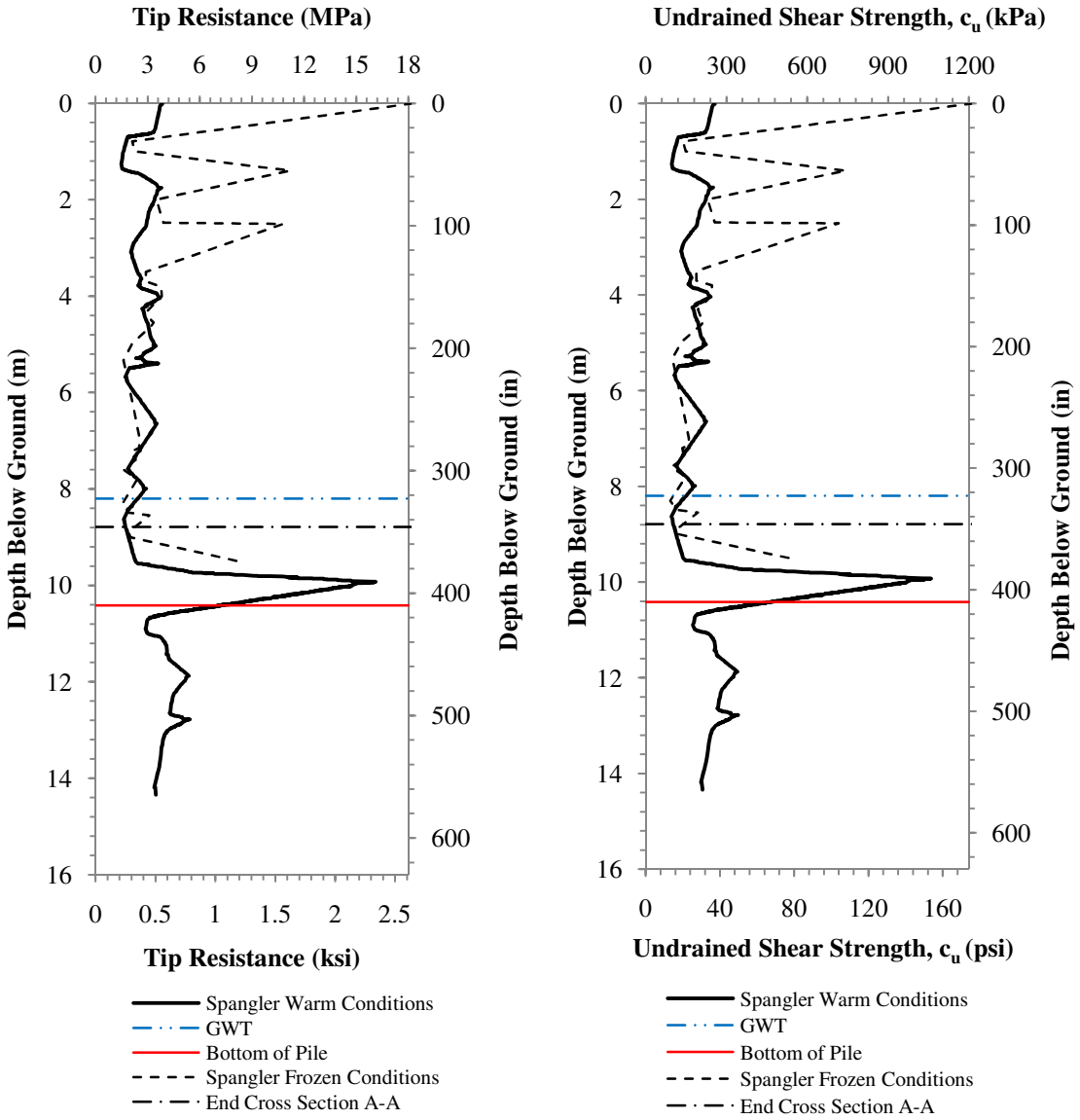

Figure 4-21: Spangler soil profile with depth in the unfrozen and frozen state (a) CPT tip resistance; (b) undrained shear strength (GWT = Ground Water Table)

The average undrained shear strength was found by using a weighted average method based on the length of the pile between two consecutive points. The undrained shear strengths for the system were thus found to be 150.2 kPa (21.79 psi) and 440.5 kPa (63.98 psi) for the unfrozen and frozen states respectively. The fifty percent strain value was based off of recommendations by Reese et al. (2004) and found that the values would be 0.005 and 0.004 for the unfrozen and frozen states. The last parameter, moist unit weight, was taken as 21.2 kN/m^3 (0.078 lb/in^3) based off of the laboratory testing performed by Suleiman et al. (2006).

The remaining information needed to perform the analysis is a definition of the structural response of the foundation shaft. This was performed by using VSAT (Levings 2009) to determine the moment-curvature response of the two systems. The cross-section and material properties used within this analysis were modeled off of the data presented in Sritharan et al. (2007) for the foundation shaft and then corrected for the effects of temperature as necessary. In addition, a soil confining pressure of 344.75 kPa (50 psi) was also specified based off the work done in Chapter 3 and a water percentage by weight for the concrete was assumed to be three percent in order to account for frozen temperatures using VSAT. The input parameters used in VSAT were previously provided in Table 3-1 as the Foundation (A-A) cross-section. To handle the temperature effects, VSAT internally computed the modified values based on the work performed by Levings (2009) for an analysis temperature of -10 °C (14 °F) and testing temperatures of 20 °C (68 °F).

The results of the analysis were then idealized using a bilinear representation as this will provide enough information to use the new method. The results of the bilinear idealization are provided in Table 4-2 and this is compared to the actual moment-curvature response in Figure 4-22.

Table 4-2: Bilinear idealization obtained for shafts from moment-curvature analyses

Value	SS1 at 23 °C	SS2 at -10 °C
First Yield Moment	435.30 kN-m (3852.72 kip-in)	451.18 kN-m (3993.24 kip-in)
First Yield Curvature	0.00591/m (1.50E-04/in)	0.006171/m (1.57E-04/in)
Yield Moment	678.14 kN-m (6002.01 kip-in)	705.78 kN-m (6246.70 kip-in)
Yield Curvature	0.009201/m (2.34E-04/in)	0.009654/m (2.45E-04/in)
Ultimate Moment	801.60 kN-m (7094.76 kip-in)	810.13 kN-m (7170.24 kip-in)
Ultimate Curvature	0.138865/m (3.53E-03/in)	0.125594/m (3.19E-03/in)

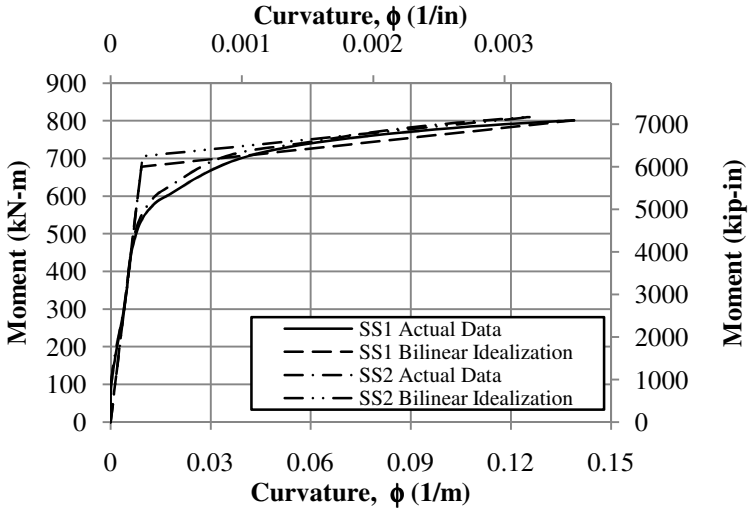

Figure 4-22: Moment-curvature analyses of SS1 and SS2 for Foundation (A-A) cross-section

At this point, the two different models were created and ran based off of the information provided in Table 2. The results of the analysis were then compared to the experimental data of SS1 in Figure 4-23 and SS2 in Figure 4-24, to examine the global lateral force-displacement trend in both the warm weather and cold weather conditions. In addition, the model was compared with the detailed analyses completed for SS1 and SS2 to demonstrate the accuracy of the other parameters involved in the model development. These comparisons are provided below in Table 4-3 and Table 4-4 for SS1 and SS2, respectively.

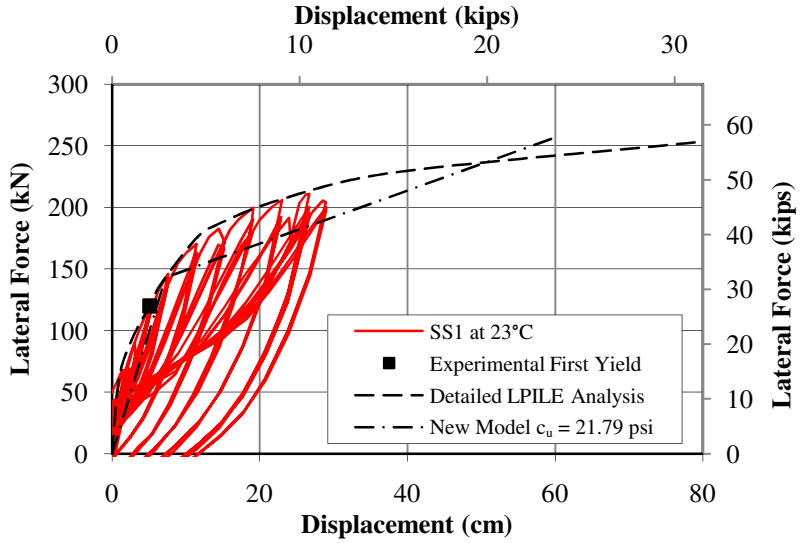

Figure 4-23: Global response comparison of new methodology with experimental response and detailed analysis of SS1 at 23 °C (1 psi = 6.895 kPa)

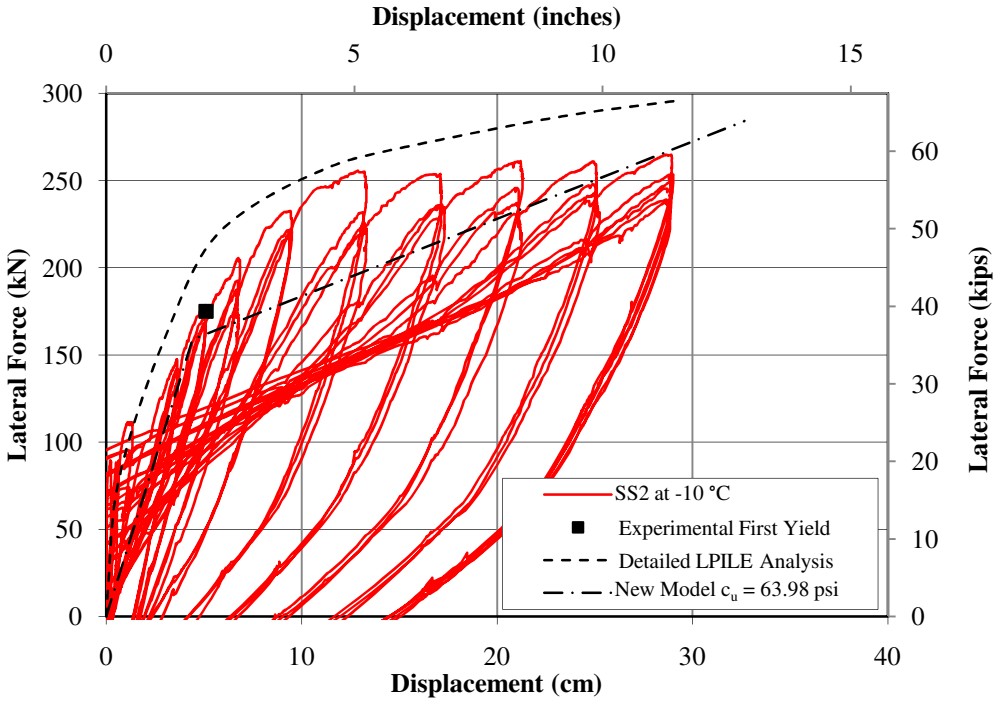

Figure 4-24: Global response comparison of new methodology with experimental response and detailed analysis of SS2 at -10 °C (1 psi = 6.895 kPa)

Table 4-3: Comparison of critical parameters of SS1 at the ultimate limit state

	Detailed Analysis		Proposed New Model		
Parameter	SI	English	SI	English	Error
L_{ma}	3.67 m	144.5 in	3.42 m	134.7 in	-6.81%
L_{m0}	7.19 m	283.1 in	6.69 m	263.3 in	-6.95%
L_{mb}	3.52 m	138.7 in	3.27 m	128.5 in	-7.10%
p_u	249.5 kN/m	1424.9 lb/in	306.4 kN/m	1749.8 lb/in	-18.6%
V_s	243.9 kN	54.8 kip	223.6 kN	50.3 kip	-8.32%
Δ_t	6.07 cm	2.39 in	4.35 cm	1.71 in	-28.3%
θ_{eb}	0.01987 rad		0.017 rad		-14.4%
Δ_{eb}	7.29 cm	2.87 in	5.89 cm	2.32 in	-19.3%
L_{pb}	0.71 m	27.8 in	0.52 m	20.56 in	-26.8%
θ_{pb}	0.0894 rad		0.067 rad		-25.1%
θ_p	0.1739 rad		0.1337 rad		-23.1%
Δ_p	0.64 m	25.3 in	0.46 m	18.01 in	-28.1%
Δ_{ea}	5.33 cm	2.10 in	4.68 cm	1.84 in	-12.20%
V_t	252.6 kN	56.8 in	258.1 kN	58.0 kip	2.18%
Δ_u	0.79 m	31.1 in	0.61 m	23.9 in	-22.8%

Table 4-4: Comparison of critical parameters of SS2 at the ultimate limit state

	Detailed Analysis		Proposed New Model		
Parameter	SI	English	SI	English	Error
L_{ma}	2.80 m	110.08 in.	2.95 m	116.1 in.	5.36%
L_{m0}	4.94 m	194.39 in.	5.18 m	203.9 in.	4.86%
L_{mb}	2.14 m	84.31 in.	2.23 m	87.8 in.	4.21%
p_u	2013.7 kN/m	11498.5 lb/in	839.4 kN/m	4739.2 lb/in	-58.3%
V_s	208.6 kN	46.9 kip	215.1 kN	48.3 kip	3.12%
Δ_t	1.24 cm	0.49 in	1.71 cm	0.67 in.	37.9%
θ_{eb}	0.0105 rad		0.012 rad		14.29%
Δ_{eb}	2.95 cm	1.16 in.	3.52 cm	1.39 in.	19.32%
L_{pb}	0.31 m	12.21 in.	0.36 m	14.05 in.	16.13%
θ_{pb}	0.0355 rad		0.041 rad		15.49%
θ_p	0.0839 rad		0.0817 rad		-2.62%
Δ_p	0.23 m	9.02 in.	0.24 m	9.49 in.	4.35%
Δ_{ea}	2.84 cm	1.12 in.	3.32cm	1.31 in.	16.90%
V_t	295.8 kN	66.5 kip	284.1 kN	63.9 kip	-3.95%
Δ_u	0.29 m	11.5 in.	0.33 m	12.9 in.	13.79%

The global comparison provided in Figure 4-23 and Figure 4-24 shows that the new model is able to capture the full range of elastic and inelastic action with slopes that correspond well with the experimental data produced by Suleiman et al. (2006). Therefore, the comparison is showing that the effects of nonlinearity within the system are being accurately captured as desired in both seasonal temperatures. In the more direct comparison of the two methods, it may appear at first glance that the data does not well correlate. However, this is not true based on the assumptions made within the model development. An examination of the plastic displacement and its components is the particular area within the model where the most error appears to occur. However, this is expected as the plastic hinge length was conservatively chosen based off of the information in Figure 4-8 for the entire range of data analyzed. A closer look at the experimental data in Figure 4-8 for a c_u = 150.24 kPa (21.79 psi), which is close to the value of c_u = 168.61 kPa (24.45 psi) shown in the figure, would suggest a longer analytical plastic hinge length thus creating a conservative plastic displacement. This conservatism in the displacement at the ultimate limit state will help in the design process and in turn help to guarantee that an undesirable failure

mechanism does not occur. The top lateral load, however, is not a conservative value so that the shear force is adequately captured and allows for the horizontal reinforcement to be correctly included. By maintaining conservatism in this manner, the proposed model better adheres to the capacity design principles by allowing flexural action to occur while preventing an undesirable failure mechanism. The more detailed method also demonstrates that the critical locations within the integrated column foundation system are accurately captured with an error of less than ten percent. In addition to the critical parameters, the effects of seasonal freezing were effectively captured during the modeling of SS2 even though c_u = 441.1 kPa (63.98 psi) falls outside of the range specified in the model development. Therefore, it can be said that the new method is effectively capturing the lateral loading behavior of an integrated column/foundation system during the different seasons of the year.

4.5.2 LPILE Analytical Verification

To further expand on the verification process, the model was also compared against more detailed analyses that were used to create the model in the first place. This verification is provided here as the two models above only provide information in the middle and upper ranges [c_u = 150.2 kPa (21.79 psi) to 441.1 kPa (63.98 psi)] for which the model was developed. Although numerous comparisons were made (see Appendix A), this section discusses a model on the lower end of the proposed model [c_u = 48.3 kPa (7 psi)] since the experimental verification establishes validity for the middle and upper range of c_u. The remainder of this section presents the model verification for a continuous column into drilled shaft foundation of the same cross-sectional dimensions and reinforcement as the experimental verification, but with no column shaft above ground. The drilled shaft was assumed to have a five percent axial load ratio and is to be constructed in a soft cohesive soil of uniform strength with c_u = 48.3 kPa (7 psi).

Similar to the previous section, a global comparison and a more direct comparison was performed to examine the accuracy of the new model. The direct comparison, Table 4-5, examines the critical locations and values of the two different methods to add to the validation of the model. The global comparison is provided as a graph of the force-

displacement response of a detailed analysis response obtained from an analysis in LPILE (Reese et al., 2004) and the new method in Figure 4-25.

Table 4-5: Comparison of critical parameters for c_u = 48.3 kPa (7 psi) at the ultimate limit state

	Detailed Analysis		Proposed New Model		
Property	SI	English	SI	English	Error
L_{ma}	2.92 m	114.8 in	2.83 m	111.4 in	-3.08%
L_{m0}	7.29 m	286.9 in	7.15 m	281.6 in	-1.92%
L_{mb}	4.37 m	172.1 in	4.32 m	170.2 in	-1.16%
p_u	137.1 kN/m	782.6 lb/in	127.7 kN/m	729.3 lb/in	-6.86%
V_s	399.6 kN	89.8 kip	361.3 kN	81.2 kip	-9.58%
Δ_t	6.25 cm	2.46 in	6.33 cm	2.49 in	1.28%
θ_{eb}	0.0222 rad		0.023 rad		3.60%
Δ_{eb}	6.47 cm	2.55 in	6.39 cm	2.52 in	-1.24%
L_{pb}	0.70 m	27.61 in	0.69 m	27.24 in	-1.43%
θ_{pb}	0.0891 rad		0.088 rad		-1.23%
θ_p	0.179 rad		0.176 rad		-1.68%
Δ_p	0.52 m	20.59 in	0.50 m	19.58 in	-3.85%
Δ_{ea}	3.68 cm	1.45 in	3.89 cm	1.53 in	-5.52%
V_t	351.8 kN	79.1 kip	355.5 kN	79.9 kip	1.06%
Δ_u	0.65 m	25.53 in	0.66 m	26.12 in	1.54%

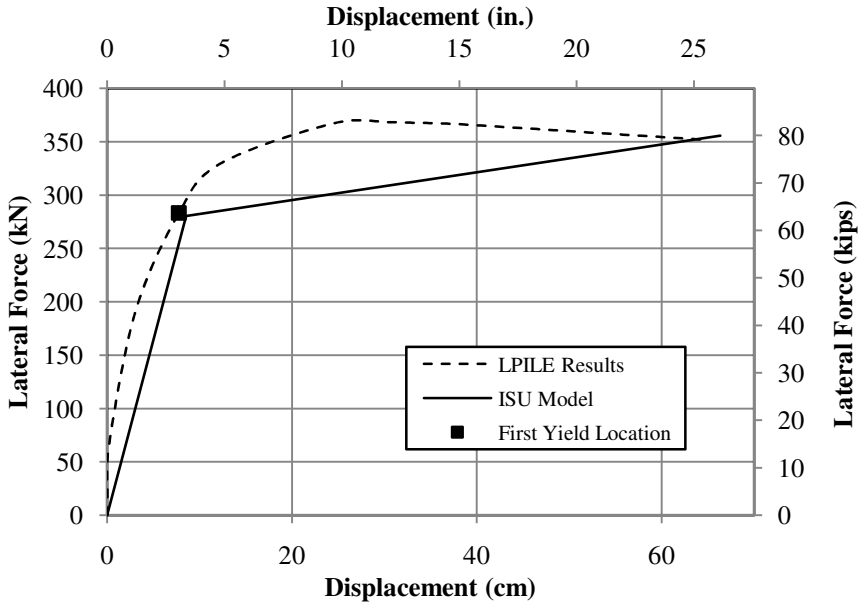

Figure 4-25: Global response comparison of new methodology with analytical model at c_u = 48.3 kPa (7 psi)

The two comparisons provided within this section further validate the accuracy of the model when determining the lateral response of a drilled shaft in clay soils. The graphical comparison shows that the yield and ultimate limit locations closely match the detailed analysis results produced using LPILE. This is seen as the yield limit state point is almost exactly on the line obtained for the detailed analysis. In addition to this, the representation shows that the ultimate limit state is captured accurately and that the effects of nonlinearity between the yield and ultimate limit states occur. For this case, the conservatism in the ultimate displacement has disappeared because this is the trial in Figure 4-8 where the minimum value in the analytical plastic hinge length, L_{mb}, was obtained. This trial is therefore the minimum value for which the model is applicable. The results of the direct comparison only further validate the model as the errors are typically within ten percent between the two methods.

The additional verification information provided in the Appendix further demonstrates the validity of the model. In each of the cases presented in this section provide a detailed comparison at the ultimate limit state and a global lateral force displacement response comparison. In the additional comparisons provided in the Appendix, the first yield limit state was typically captured within 5% of the expected force and 10% of the expected based on the detailed analyses in LPILE. At the ultimate limit state, the displacements obtained through the proposed new model are a conservative estimate and are justifiable since an integrated column/foundation system should not experience anywhere near a 100 cm (39.4 in.) displacement when subjected to a design level or greater seismic event. The top lateral load, on the other hand, was not a conservative value and typically over estimates the top lateral load at the ultimate condition. Over estimation in this manner is more appropriate in the capacity design principles so that an undesirable failure mode does not occur when the system is pushed past the point of yielding.

CHAPTER 5: SUMMARY, CONCLUSIONS AND RECOMMENDATIONS

5.1 Introduction

The research on the seismic design of drilled shaft foundations in clay soils was motivated on the basis of the challenges associated with models in practice today and the experimental testing performed by Suleiman et al. (2006) especially in high seismic regions such as Alaska where seasonal freezing is a major concern. Therefore, the objective of this research was to develop a simplified method for use in the seismic design of drilled shafts in clay that would provide a good representation of the critical locations and lateral loading response of an integrated column/foundation system. The proposed model had to capture the lateral loading response in all seasons of the year without the use of a detailed approach as this has not been handled in current approaches even though numerous models exist in practice today. The sections presented below provide a summary of the completed work, conclusions drawn from the project and recommendations developed throughout the process.

5.2 Summary

The research presented in the report started with a brief historical background on bridges and their evolvement with time. Seismic engineering practices were then examined with specific details about seismic loading, the design philosophy used in practice and concerns associated with seasonal temperature variation. Multiple foundation types were then presented along with the seismic design approaches used for each foundation. Specific emphasis was given to deep foundations, specifically drilled shafts, based on the topic of the project. The effects of soil-foundation-structure-interaction on drilled shafts were then described prior to defining the scope of research.

An extensive literature review was completed with the goal of obtaining knowledge on the lateral response of drilled shafts when subjected to design level or greater earthquakes in all seasonal conditions. Several analytical methods for determining the lateral response in design and analysis were investigated based off of current code and guideline recommendations. A seasonal freezing investigation that included analytical and experimental case studies was provided along with a broad impact study on infrastructure within the United States and Japan. During this investigation it was noted that seasonal

freezing would significantly alter the lateral load response of an integrated column/foundation system by:

- Increasing the effective elastic stiffness of the system;
- Increasing the shear demand experienced by the column and foundation shafts;
- Shifting the maximum moment location toward the ground surface;
- Reducing the lateral displacement capacity when compared to the warm weather condition; and
- Reducing the plastic hinge length.

In addition to the lateral response, it was found that material properties are effected during times of seasonal freezing with the typical trend being an increase in overall strength, thus causing a larger zone of elastic behavior. Finally, the capabilities of the sectional analysis tool to be used within the research were discussed.

An examination of the existing methods was completed, identifying the associated challenges. This process involved comparisons between detailed analyses and the common simplified methods presented within the literature review. Thus providing justification as to why a new method of determining the lateral response of integrated column/foundation systems in clay soils was needed.

A simplified method for determining the lateral response of drilled shafts in clay soils was developed. The new method was modeled as a cantilever with an effective height from the top of the bridge column to the point of maximum moment within the foundation shaft. Properties of the flexible base and spring representing soil resistance were established thus defining critical locations for an integrated column/foundation system including the maximum moment location and point of first zero moment after the maximum moment. A bilinear force-displacement curve representing the lateral load response of the system using the origin of a Cartesian coordinate system, the first yield limit state and the ultimate limit state was constructed based off of the information presented in Section 4.4. The accuracy of the method was then verified against experimental data from Suleiman et al. (2006) and detailed analyses performed in LPILE in Section 4.5.

5.3 Conclusions

Based on the completed study presented within this report, the following conclusions were drawn:

- Approximately two-thirds of about 600,000 bridges in the United States are effected by seasonal freezing alone. In addition, it was found that half of the approximately 70,000 bridges located in high seismic regions would be affected by seasonal freezing, which includes areas such as the north eastern part of California, the eastern half of Washington, Alaska and Missouri. It was also concluded that freezing and high seismicity would occur in the northern regions of Japan, especially on Hokkaido Island. Although all these bridges are effected across the world, it appears that the effects of seasonal freezing are not routinely addressed in current seismic design practice around the world.
- The detailed method used to determine the lateral load response suggested by AASHTO (2007), although accurate if correctly modeled, requires a significant amount of information about the structure and surrounding soil in order to complete the analysis.
- The method suggested for the lateral design of drilled shafts by Chai (2002) has challenges associated with its use that include the following based off of the information examined in Chapter 3:
    - Although the model was created for cohesive and cohesionless soils, it was only verified experimentally against cohesionless soils thus invalidating its use in cohesive soils;
    - The maximum moment location was found to be improperly located by 12.5% to 27.7% when compared to the detailed analyses performed in LPILE;
    - The analytical plastic hinge length was specified based off of experimental testing in cohesionless soils and is therefore not applicable to cohesive soils. This was demonstrated in Chapter 3 when it was shown that the analytical plastic hinge length was off by 27.6% and 35.9% when compared to the detailed LPILE analyses for the primary and secondary soil profiles, respectively;

- Seasonal freezing was not included in the development of the model and therefore should only be used in warm weather conditions; and
- The method also uses an idealized elastic perfectly-plastic force-displacement response between the yield and ultimate conditions which is not capturing the nonlinear effects of the material properties (soil, steel and concrete). This idealization also significantly over predicts the behavior of the integrated column/foundation system tested by Suleiman et al. (2006).

- The use of the method suggested by Priestley et al. (2007) had its own challenges and the conclusions drawn from this are as follows:
  - Although the method was developed for both cohesive and cohesionless soils, it was once again only verified against experimental data performed in cohesionless soils thus providing no validation for the cohesive soil model;
  - The model is only applicable for a limited range of soft cohesive soils and should technically only be used for the two undrained shear strengths of 20 kPa (420 psf) and 40 kPa (840 psf);
  - The method does not provide an easy means of determining the lateral force being applied to the top of the system being examined;
  - The analytical plastic hinge length used in the model is based off of the suggestions made by Chai (2002) which was previously shown to be invalid for use in cohesive soils. This challenge along with the underestimation of the controlling limit state curvature by 16% led to the underestimation of the final design displacement by 40%; and
  - The method was not created with the thought of seasonal freezing effects in mind thus limiting the model to use in warm conditions only.
- Simplified methods suggested by ATC 32 (1996) and AASHTO (2009) were also found to have the following challenges associated with their use:
  - The equivalent fixed based cantilever method is only applicable within the elastic range of loading and will not capture the inelastic action where the most significant displacement will occur in the system;

  - When compared to a detailed analysis in LPILE, the effective fixity location where the maximum moment would occur was found to be over predicted by approximately 100%. This is a major concern as this point is where the most damage to the system will occur when subjected to a design level or greater earthquake;
  - The shear is assumed to be constant along the length of the shaft, which is incorrect once the soil begins to resist the lateral movement. This is a concern as an increase in shear typically occurs in the shaft below the ground surface; and
  - No consideration was given to the effects of seasonal freezing in the development of the model thus limiting it use to warm weather conditions.
- A new method was developed for the lateral loading response of drilled shafts that can capture both the elastic and inelastic range during all seasons of the year. The new model can be run using a structural analysis program or through the use of hand calculations as desired. In addition, the model is applicable in soils that range from soft to very stiff.
- The new method is able to effectively provide a bilinear force-displacement curve for the lateral load response of an integrated column/foundation system. The new method does this through the location of the yield and ultimate limit states, as defined within the report, using minimal input parameters about the shaft and surrounding soil;
- Verification using the experimental data by Suleiman et al. (2006) demonstrated that the model is able to effectively capture the critical locations within the system (e.g., the maximum moment location), the global-force displacement response and localized effects in the system (e.g., translation and rotation at the maximum moment location). The following conclusion were drawn from the verification:
  - the ultimate lateral force in both warm and freezing conditions was within 10% of a detailed analysis;
  - the ultimate displacement for the SS1 was found to be 23% less than the experimental data by Sritharan et al. (2007) which is a conservative estimate due to the assumption purposely made for the analytical plastic hinge length;

  - The maximum moment and zero moment location were located accurately with less than 8% error when compared to the experimental findings from the test in warm conditions. When compared to the test in cold conditions, these locations were located accurately with less than 6% error;
  - The proposed model predicts the secant stiffness to the first yield location within 5% of the experimental value;
  - The second slope in the warm test comparison under predicts the lateral shear force for an equivalent displacement between yield and ultimate by an average of 10%; and
  - The effects of seasonal freezing were effectively handled by varying material properties for the soil, steel and concrete as seen in the SS2 global comparison.
- The analytical verification of the proposed new model provided the following conclusions:
  - The secant stiffness to the first yield location is within 10% of the detailed analysis performed in LPILE;
  - The yield and ultimate shear forces at the top of the column were predicted within an error of approximately 1%;
  - The yield displacement was found within approximately 10% and the ultimate displacement was within 2.3% of the LPILE analysis; and
  - The second slope under predicts the lateral shear force by an average of 13%.

5.4 Recommendations

Throughout the duration of the project, a number of challenges were identified within codes and guidelines when determining the lateral response of bridge columns that continue into the ground as drilled shafts in cohesive soils. These challenges led the author to develop a new simplified method that would determine a bilinear force-displacement response for the aforementioned system using minimal input parameters thus reducing the need for a detailed analysis using soil springs and numerical calculation methods. This new method was verified against available experimental data and analytical modeling techniques in LPILE (Reese et al., 2004). During the development of the method, the following recommendations were established:

- the use of a tri-linear curve in determining the lateral response could be investigated to more accurately capture the shear demands experienced by the system;
- further full-scale experimental testing should be performed in cohesive soils to verify the effectiveness of the model;
- more analyses need to be run with differing structural parameters to better define the range over which the new method is applicable;
- an examination into cohesionless soils should be performed in the future to determine whether or not the same model may be used with this soil type thus creating a more coherent method for all soil types; and
- the use of different materials, such as ultra high performance concrete, should be investigated to further expand on the capabilities of the model to capture the lateral loading response.

REFERENCES

American Association of State and Highway Transportation Officials (AASHTO). (1998). *LRFD bridge design specifications, 2nd edition.* Washington D.C.: AASHTO.

AASHTO. (2007). *LRFD bridge design specifications with 2008 interim revisions, customary U.S. units, 4th edition.* Washington D.C.: AASHTO.

AASHTO. (2009). *Guide specifications for LRFD seismic bridge design.* Washington D.C.: AASHTO.

Applied Technology Council (ATC). (1996). *Improved seismic design criteria for California bridges: provisional recommendations.* Redwood City, California: Applied Technology Council.

Ashour, M., Norris, G. and Pilling, P. (1998). "Lateral loading of a pile in layered soil using the strain wedge model." *Journal of geotechnical and geoenvironmental engineering* 124(4): 303-315.

Bowles, J. E. (1988). *Foundation analysis and design, 4th edition.* United States of America: McGraw-Hill Book Company.

Broms, B. B. (1964). "Lateral resistance of piles in cohesive soils." *Journal of soil mechanics foundation division, American Society of Civil Engineers* 90(SM2), 27-63.

Bruneau, M., Uang, C-M. and Whittaker, A. (1997). *Ductile design of steel structures.* New York: Mc-Graw Hill.

Budek, A. M., Priestley, M. J. N. and Benzoni, G. (2000). "Inelastic seismic response of bridge drilled-shaft rc pile/columns." *Journal of structural engineering* 126(4): 510-517.

Bureau of Transportation Statistics. (Accessed Online: 2007). "Conditions of U.S. Highway Bridges By State." Washington D.C.: United States Department of Transportation. http://www.bts.gov/current_topics/2007_08_02_bridge_data/html/bridges_by_state.html

California Department of Transportation (Caltrans). (1990). *Bridge design aids: pile shaft design*: 12-30 to 12-49. (Accessed online: 2009 through http://www.dot.ca.gov).

Chai, Y. H. (2002). "Flexural strength and ductility of extended pile-shafts I: Analytical model." *Journal of structural engineering* 128(5): 586-594.

Chai, Y. H. and Hutchinson, T. C. (2002). "Flexural strength and ductility of extended pile-shafts II: Experimental study." *Journal of structural engineering* 128(5): 595-602.

Crowther, G. S. (1990). "Analysis of laterally loaded piles embedded in layered frozen soil." *Journal of geotechnical engineering* 116(7): 1137-1152.

Das, B. M. (2004). *Principles of Foundation Engineering, 5th Edition.* United States of America: Thomson, Brooks/Cole.

Davisson, M. T. and Robinson, K. E. (1965). "Bending and buckling of partially embedded piles." *Proceedings of the sixth international conference S. M. and F. E.* Montreal, Canada: University of Toronto Press. pp. 243-246.

DeGaetano, A. T., and Wilks, D. S., (2001), "Development of Frost Depth Maps for the United States." *Research report.* Upper Marlboro, Maryland: National Association for Home Builders (NAHB) Research Center, Inc.

Filiatrault, A. and Holleran, M. (2001). "Stress-strain behavior of reinforcing steel and concrete under seismic strain rates and low temperatures." *Materials and structures* 34: 235-239.

Filiatrault, A. and Holleran, M. (2001). "Characteristics of reinforced concrete bridge components under seismic strain rates and low temperatures." *Proceedings of the 18th US-Japan bridge engineering workshop, St. Louis.* FHWA: 49-63.

Iowa Department of Transportation (Accessed Online: September 2009). http://www.i235.com/ped_bridge_2.htm

Japanese Meteorological Agency. (Accessed Online: August 2008). http://www.jma.go.jp/jma/indexe.html

Lee, G. C., Shih, T. S. and Chang, K. C. (1988a). "Mechanical properties of concrete at low temperature." *Journal of cold regions engineering* 2(1): 13-24.

Lee, G. C., Shih, T. S. and Chang, K. C. (1988b). "Mechanical properties of high-strength concrete at low temperature." *Journal of cold regions engineering* 2(4): 169-178.

Levings, J. C. (2009: In progress). "Development of a versatile section analysis tool for use in seismic design." *Master's Thesis.* Ames, Iowa: Iowa State University.

Levings, J. C. and Sritharan, S. (2009: In Progress). "Stress-strain characteristics of ASTM A706 mild steel reinforcement at low temperatures." *To be submitted to a journal.*

Merriam-Webster. (Accessed Online: October 22, 2008). Bridge definition. http://www.merriam-webster.com/dictionary.

Parametric Technology Corporation (PTC). (2007). *Mathcad, version 14.0.0.163.* Needham: PTC.

Poulos, H. G. and Davis, E. H. (1980). *Pile foundation analysis and design.* New York: Wiley.

Priestley, M. J. N., Seible, F. and Calvi, G. M. (1996). *Seismic design and retrofit of bridges.* New York: John Wiley & Sons, Inc.

Priestley, M. J. N., Calvi, G. M. and Kowalsky, M. J. (2007). *Displacement-based seismic design of structures.* Pavia, Italy: IUSS Press

Reese, L. C. and Welch, R. C. (1975). "Lateral loading of deep foundations in stiff clay." *Journal of geotechnical engineering division* 101(GT7): 633-649.

Reese, L. C., Wang, S. T., Isenhower, W. M. and Arrellaga, J. A. (2000). *LPILE plus 4.0, technical manual.* Austin: Ensoft, Inc.

Reese, L. C., Wang, S. T., Isenhower, W. M., Arrellaga, J. A. and Hendrix, J. (2004). *LPILE plus 5.0, user's manual.* Austin: Ensoft, Inc.

Reese, L. C., Wang, S. T.. Isenhower, W. M. and Arrellaga, J. A. (2004). *LPILE plus 5.0, technical manual.* Austin: Ensoft, Inc.

Robertson, P. K. and Campanella, R. G. (1983). "Interpretation of cone penetration tests. Part II: Clay." *Canadian geotechnical journal* 20(4): 734-745.

Sayles, F. H. and Haines, D. (1974). "Creep of frozen silt and clay." *Technical report 252, Cold regions research and engineering laboratory.*

Sehnal, Z. A., Kronen, H. and Marshall, A. L. (1983). "Factors influencing the low temperature strength of concrete." *Proceedings 2nd international conference on cryogenic concrete, Amsterdam.* London: Concrete Society of UK. pp. 1-11.

Sritharan, S., Suleiman, M. T. and White, D. J. (2007). "Effects of seasonal freezing on bridge column-foundation-soil interaction and their implications." *Earthquake spectra* 23(1): 199-222.

Sritharan, S. and Shelman, A. (2008). "An assessment of broad impact of seasonally frozen soil on seismic response of bridges in the U.S. and Japan." *Proceedings of the 24th US-Japan bridge engineering workshop, Minneapolis.* FHWA: 429-440.

Suarez, V. and Kowalsky, M. J. (2007). "Displacement-based seismic design of drilled shaft bents with soil-structure interaction." *Journal of earthquake engineering* 11: 1010-1030.

Suleiman, M. T., Sritharan, S. and White, D. J. (2006). "Cyclic lateral load response of bridge column-foundation-soil systems in freezing conditions." *Journal of structural engineering* 132(11): 1745-1754.

Weaver, J. S. and Morgenstern, N. R. (1981). "Pile design in permafrost." *Canadian geotechnical journal* 18: 357-370.

Wotherspoon, L. M., Sritharan, S. and Pender, M. J. (2009: In Progress). "Modelling the response of cyclically loaded bridge columns embedded in warm and seasonally frozen soils." *Engineering Structures Journal*.

United States Geological Survey (USGS). (Accessed Online: 2009) http://www.usgs.gov.

United States Geological Survey (USGS). (Accessed Online: July 6, 2009) About earthquakes: earthquake facts. *Earthquake hazards program web site.* http://earthquake.usgs.gov/learning/facts.php.

United States Geological Service. (2002). (Accessed Online: August 2008). "0.2 second spectral acceleration with a 10 percent probability of exceedance in 50 years seismic hazard map." *USGS*. http://earthquake.usgs.gov/research/hazmaps/products_data/2002/maps/.

APPENDIX: COMPARISON OF PROPOSED NEW MODEL WITH DETAILED ANALYSES IN LPILE

- Additional Analytical Verification #1

Table A-1: Input parameters for additional analytical verification #1

Soil Properties		
c_u	48.3 kPa	7 psi
γ_m	21.2 kN/m^3	0.078 lb/in^3
ε_{50}	0.007	
Structural Properties		
D	0.61 m	24 in.
L_{col}	2.69 m	106 in.
L_f	10.4 m	410 in.
ALR	5 %	
M-ϕ Response	See Section 4.3.2	

Table A-2: Comparison of critical parameters at the ultimate limit state for additional analytical verification #1

	Detailed Analysis		Proposed New Model		
Property	SI	English	SI	English	Error
L_{ma}	4.11 m	161.7 in.	4.13 m	162.6 in.	0.49%
L_{m0}	8.71 m	342.9 in.	8.75 m	344.6 in.	0.49%
L_{mb}	4.60 m	181.2 in.	4.63 m	182.1 in.	0.65%
p_u	110.2 kN/m	629.1 lb/in	108.3 kN/m	618.4 lb/in	-1.71%
V_s	155.7	35.0 kip	155.7 kN	35.0 kip	0%
Δ_t	8.28 cm	3.26 in.	9.96 cm	3.92 in.	20.29%
θ_{eb}	0.0244 rad		0.024 rad		-1.64%
Δ_{eb}	10.01 cm	3.94 in.	9.96 cm	3.92 in.	-0.50%
L_{pb}	0.83 m	32.87 in.	0.74 m	29.13 in.	-10.84%
θ_{pb}	0.106 rad		0.094 rad		-11.32%
θ_p	0.199 rad		0.188 rad		-5.53%
Δ_p	0.83 m	32.59 in.	0.78 m	30.57 in.	-6.02%
Δ_{ea}	6.68 cm	2.63 in.	4.09 cm	1.61 in.	-38.77%
V_t	113.4 kN	25.5 kip	116.1 kN	26.1 kip	2.35%
Δ_u	1.03 m	40.37 in.	0.99 m	39.14 in.	-3.05%

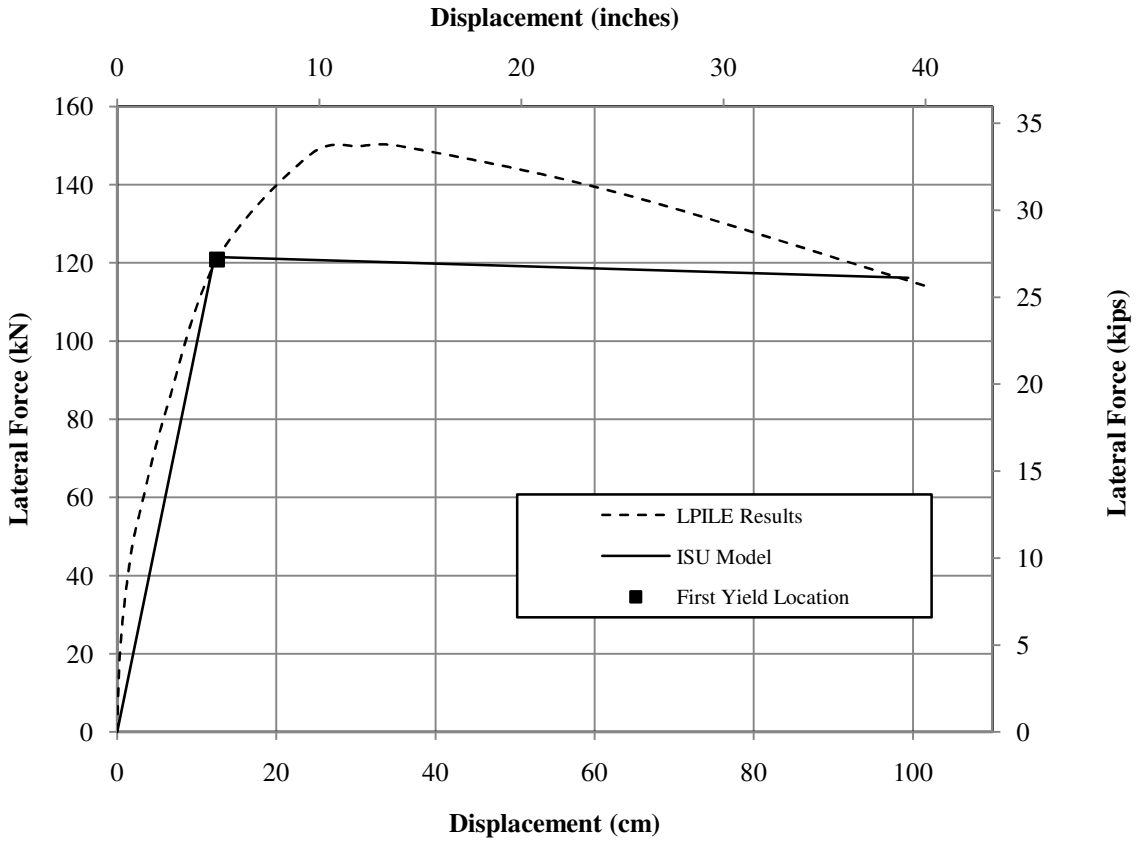

Figure A-1: Global response comparison of new methodology with additional analytical verification #1

- Additional Analytical Verification #2

Table A-3: Input parameters for additional analytical verification #2

Soil Properties		
c_u	48.3 kPa	7 psi
γ_m	21.2 kN/m^3	0.078 lb/in^3
ε_{50}	0.007	
Structural Properties		
D	0.61 m	24 in.
L_{col}	6.10 m	240 in.
L_f	10.4 m	410 in.
ALR	5 %	
M-ϕ Response	See Section 4.3.2	

Table A-4: Comparison of critical parameters at the ultimate limit state for additional analytical verification #2

	Detailed Analysis		Proposed New Model		
Property	SI	English	SI	English	Error
L_{ma}	6.71 m	264.3 in.	6.79 m	267.3 in.	1.19%
L_{m0}	11.48 m	452.1 in.	11.29 m	444.6 in.	-1.66%
L_{mb}	4.77 m	187.8 in.	4.50 m	177.3 in.	-5.66%
p_u	94.2 kN/m	537.9 lb/in	97.95 kN/m	559.3 lb/in	3.98%
V_s	58.3 kN	13.1 kip	68.1 kN	15.3 kip	16.81%
Δ_t	9.14 cm	3.60 in.	8.56 cm	3.37 in.	-6.35%
θ_{eb}	0.0256 rad		0.024 rad		-6.25%
Δ_{eb}	17.20 cm	6.77 in.	15.95 cm	6.28 in.	-7.27%
L_{pb}	0.87 m	34.37 in.	0.72 m	28.37 in.	-17.24%
θ_{pb}	0.111 rad		0.092 rad		-17.12%
θ_p	0.221 rad		0.183 rad		-17.19%
Δ_p	1.48 m	58.3 in.	1.24 m	48.95 in.	-16.22%
Δ_{ea}	16.76 cm	6.60 in.	4.01 cm	1.58 in.	-76.1%
V_t	6.81 kN	1.53 kip	26.4 kN	5.94 kip	288%
Δ_u	1.86 m	73.08 in.	1.53 m	60.18 in.	-17.65%

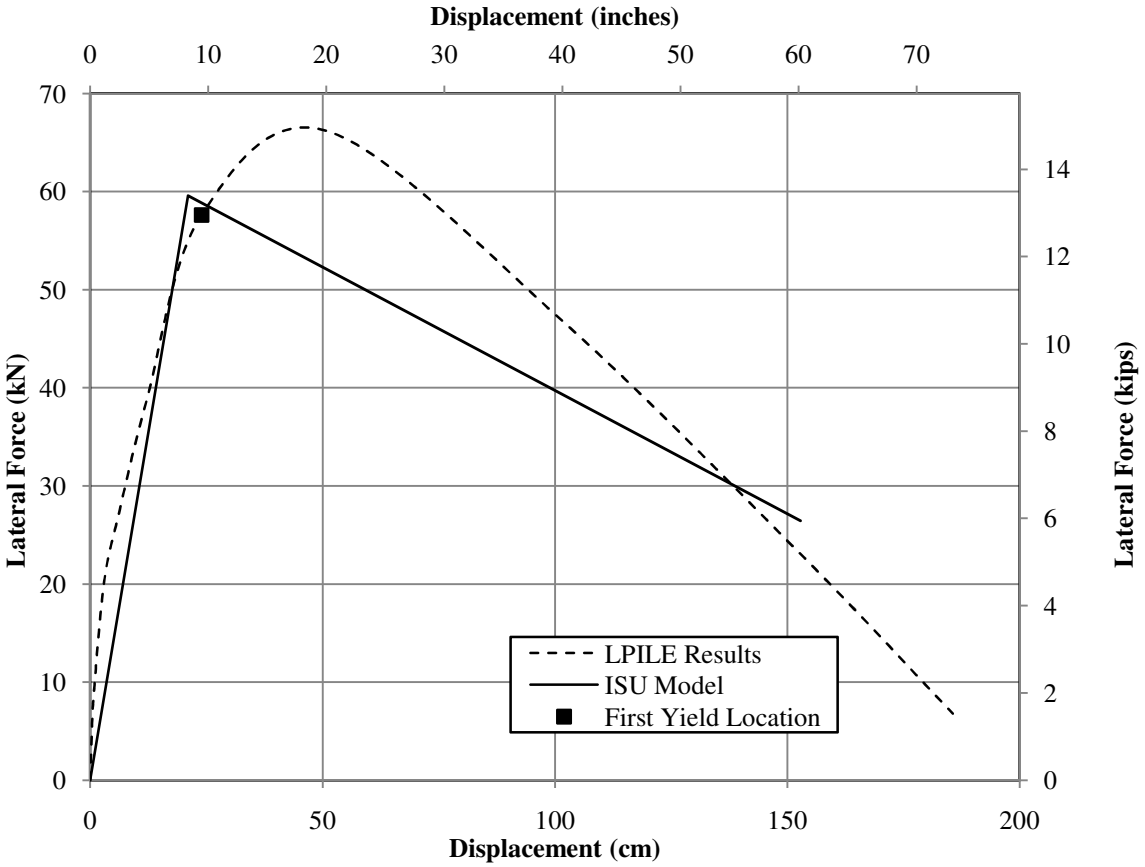

Figure A-2: Global response comparison of new methodology with additional analytical verification #2

- Additional Analytical Verification #3

Table A-5: Input parameters for additional analytical verification #3

Soil Properties		
c_u	168.6 kPa	24.455 psi
γ_m	21.2 kN/m^3	0.078 lb/in^3
ε_{50}	0.005	
Structural Properties		
D	0.61 m	24 in.
L_{col}	0 m	0 in.
L_f	10.4 m	410 in.
ALR	5 %	
M-ϕ Response	See Section 4.3.2	

Table A-6: Comparison of critical parameters at the ultimate limit state for additional analytical verification #3

	Detailed Analysis		Proposed New Model		
Property	SI	English	SI	English	Error
L_{ma}	1.87 m	73.8 in.	1.85 m	72.93 in.	-1.07%
L_{m0}	4.80 m	189.0 in.	4.73 m	186.4 in.	-1.46%
L_{mb}	2.93 m	115.2 in.	2.88 m	113.4 in.	-1.71%
p_u	374.7 kN/m	2139.5 lb/in	398.6 kN/m	2276.2 lb/in	6.38%
V_s	702.4 kN	157.9 kip	738.4 kN	166.0 kip	5.13%
Δ_t	3.35 cm	1.32 in.	3.38 cm	1.33 in.	0.90%
θ_{eb}	0.0156 rad		0.015 rad		-3.85%
Δ_{eb}	2.92 cm	1.15 in.	2.82 cm	1.11 in.	-3.48%
L_{pb}	0.53 m	20.72 in.	0.46 m	18.15 in.	-12.40%
θ_{pb}	0.067 rad		0.059 rad		-11.94%
θ_p	0.13 rad		0.117 rad		-10.00%
Δ_p	0.24 m	9.53 in.	0.22 m	8.54 in.	-8.33%
Δ_{ea}	1.55 cm	0.61 in.	2.18 cm	0.86 in.	40.98%
V_t	676.1 kN	152.0 kip	708.2 kN	159.2 kip	4.75%
Δ_u	0.30 m	11.79 in.	0.30 m	11.84 in.	0.42%

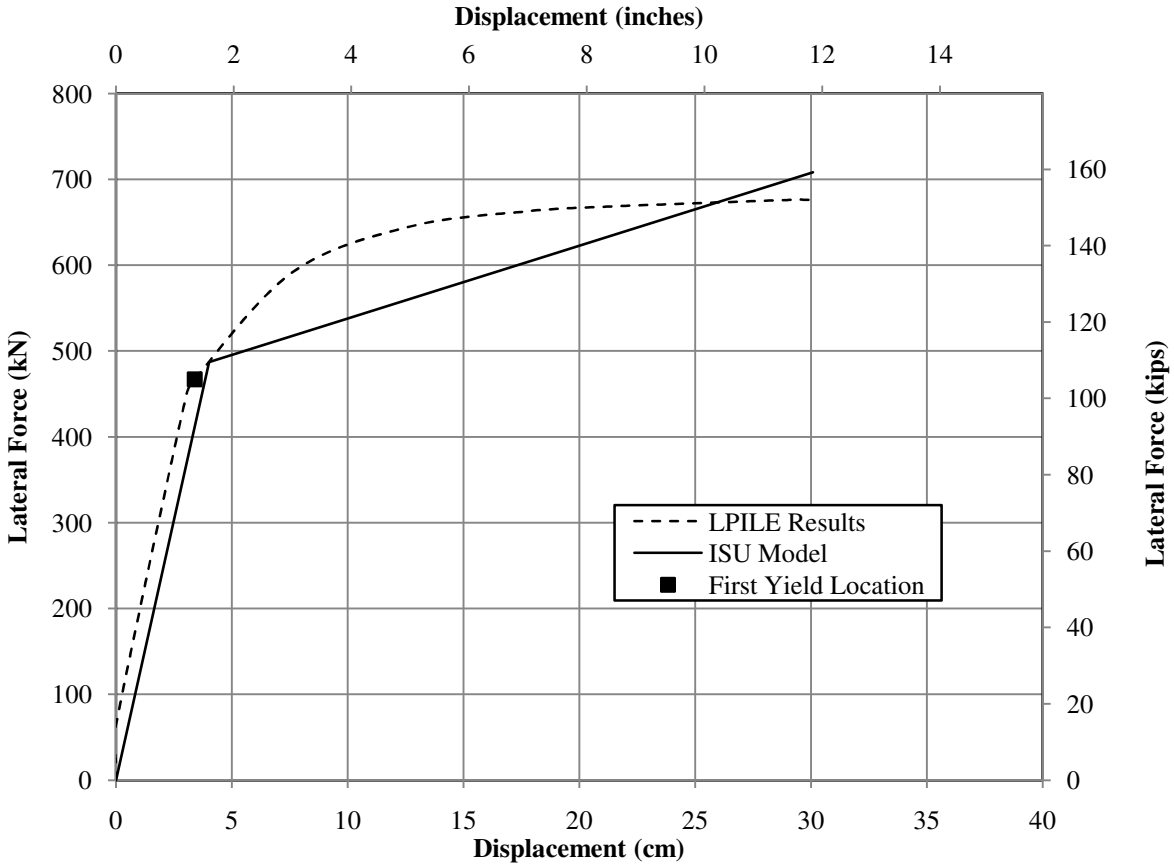

Figure A-3: Global response comparison of new methodology with additional analytical verification #3

- Additional Analytical Verification #4

Table A-7: Input parameters for additional analytical verification #4

Soil Properties		
c_u	168.6 kPa	24.455 psi
γ_m	21.2 kN/m^3	0.078 lb/in^3
ε_{50}	0.005	
Structural Properties		
D	0.61 m	24 in.
L_{col}	2.69 m	106 in.
L_f	10.4 m	410 in.
ALR	5 %	
M-ϕ Response	See Section 4.3.2	

Table A-8: Comparison of critical parameters at the ultimate limit state for additional analytical verification #4

	Detailed Analysis		Proposed New Model		
Property	SI	English	SI	English	Error
L_{ma}	3.32 m	130.7 in.	3.36 m	132.3 in.	1.20%
L_{m0}	6.50 m	256.0 in.	6.50 m	256.1 in.	0.04%
L_{mb}	3.18 m	125.3 in.	3.14 m	123.8 in.	-1.26%
p_u	301.6 kN/m	1722.4 lb/in	341.0 kN/m	1946.9 lb/in	13.06%
V_s	189.5 kN	42.6 kip	228.2 kN	51.3 kip	20.42%
Δ_t	4.34 cm	1.71 in.	4.04 cm	1.59 in.	-6.91%
θ_{eb}	0.0174 rad		0.017 rad		-2.30%
Δ_{eb}	5.77 cm	2.27 in.	5.59 cm	2.20 in.	-3.12%
L_{pb}	0.61 m	24.15 in.	0.50 m	19.81 in.	-18.03%
θ_{pb}	0.078 rad		0.064 rad		-17.95%
θ_p	0.14 rad		0.128 rad		-8.57%
Δ_p	0.48 m	18.8 in.	0.43 m	16.92 in.	-10.42%
Δ_{ea}	4.19 cm	1.65 in.	3.30 cm	1.30 in.	-21.24%
V_t	174.8 kN	39.3 kip	179.7 kN	40.4 kip	2.80%
Δ_u	0.59 m	23.36 in.	0.56 m	22.01 in.	-5.08%

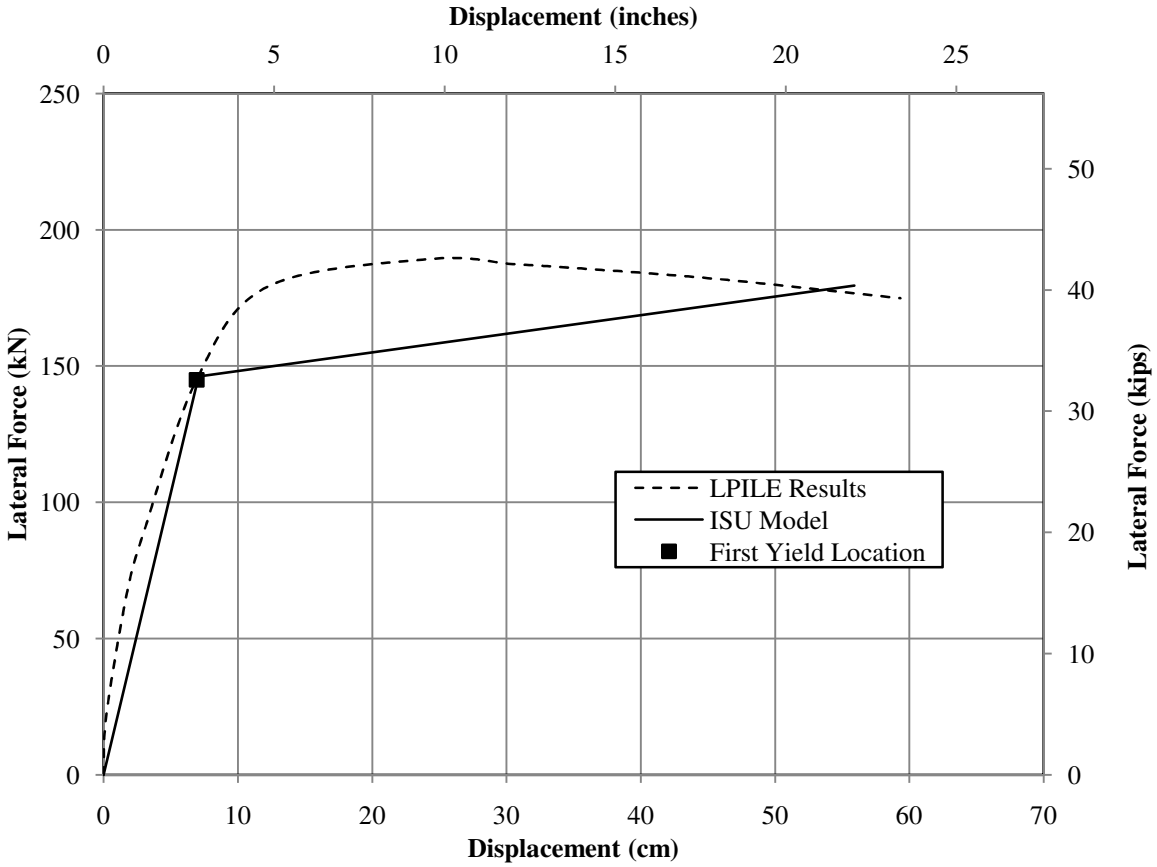

Figure A-4: Global response comparison of new methodology with additional analytical verification #4

- Additional Analytical Verification #5

Table A-9: Input parameters for additional analytical verification #5

Soil Properties		
c_u	168.6 kPa	24.455 psi
γ_m	21.2 kN/m^3	0.078 lb/in^3
ε_{50}	0.005	
Structural Properties		
D	0.61 m	24 in.
L_{col}	6.10 m	240 in.
L_f	10.4 m	410 in.
ALR	5 %	
M-ϕ Response	See Section 4.3.2	

Table A-10: Comparison of critical parameters at the ultimate limit state for additional analytical verification #5

	Detailed Analysis		Proposed New Model		
Property	SI	English	SI	English	Error
L_{ma}	6.38 m	251.3 in.	6.37 m	250.8 in.	-0.16%
L_{m0}	9.61 m	378.4 in.	9.72 m	382.7 in.	1.14%
L_{mb}	3.23 m	127.1 in.	3.35 m	131.9 in.	3.72%
p_u	263.8 kN/m	1506.6 lb/in	321.7 kN	1837.0 lb/in	21.95%
V_s	75.6 kN	17.0 kip	88.1 kN	19.8 kip	16.53%
Δ_t	4.19 cm	1.65 in.	4.57 cm	1.80 in.	9.07%
θ_{eb}	0.0174 rad		0.018 rad		3.45%
Δ_{eb}	11.10 cm	4.37 in.	11.23 cm	4.42 in.	1.17%
L_{pb}	0.59 m	23.33 in.	0.54 m	21.1 in.	-8.47%
θ_{pb}	0.075 rad		0.068 rad		-9.33%
θ_p	0.17 rad		0.136 rad		-20.00%
Δ_p	1.06 m	41.6 in.	0.87 m	34.16 in.	-17.92%
Δ_{ea}	15.01 cm	5.91 in.	6.43 cm	2.53 in.	-57.12%
V_t	35.7 kN	8.03 kip	51.6 kN	11.6 kip	44.54%
Δ_u	1.33 m	52.5 in.	1.09 m	42.9 in.	-18.05%

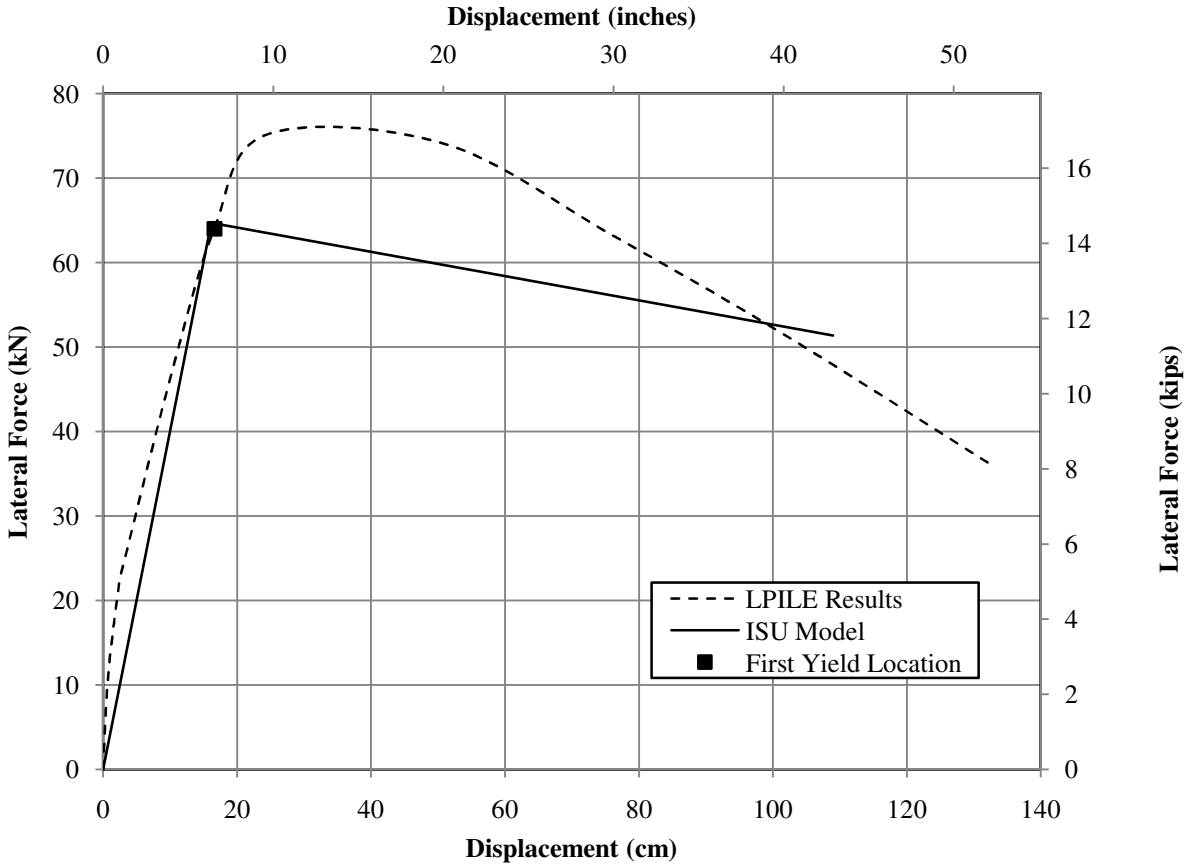

Figure A-5: Global response comparison of new methodology with additional analytical verification #5

- Additional Analytical Verification #6

Table A-11: Input parameters for additional analytical verification #6

Soil Properties		
c_u	379.2 kPa	55 psi
γ_m	21.2 kN/m^3	0.078 lb/in^3
ε_{50}	0.004	
Structural Properties		
D	0.61 m	24 in.
L_{col}	0 m	0 in.
L_f	10.4 m	410 in.
ALR	5 %	
M-ϕ Response	See Section 4.3.2	

Table A-12: Comparison of critical parameters at the ultimate limit state for additional analytical verification #6

	Detailed Analysis		Proposed New Model		
Property	SI	English	SI	English	Error
L_{ma}	1.39 m	54.67 in.	1.22 m	48.03 in.	-12.15%
L_{m0}	3.60 m	141.8 in.	3.62 m	142.6 in.	0.56%
L_{mb}	2.21 m	87.14 in.	2.40 m	94.59 in.	8.55%
p_u	748.8 kN/m	4276 lb/in	827.2 kN/m	4723.5 lb/in	10.47%
V_s	1040.0	233.8 kip	1009.3 kN	226.9 kip	-2.95%
Δ_t	1.85 cm	0.73 in.	2.16 cm	0.85 in.	16.44%
θ_{eb}	0.0117 rad		0.013 rad		11.11%
Δ_{eb}	1.63 cm	0.64 in.	1.57 cm	0.62 in.	-3.68%
L_{pb}	0.38 m	15.13 in.	0.38 m	15.14 in.	0.07%
θ_{pb}	0.0488 rad		0.049 rad		0.41%
θ_p	0.10 rad		0.0977 rad		-2.30%
Δ_p	0.14 m	5.32 in.	0.12 m	4.69 in.	-11.84%
Δ_{ea}	0.86 cm	0.34 in.	0.97 cm	0.38 in.	11.76%
V_t	1014.2 kN	228.0 kip	1060.0 kN	238.3 kip	4.52%
Δ_u	0.17 m	6.57 in.	0.17 m	6.52 in.	-0.76%

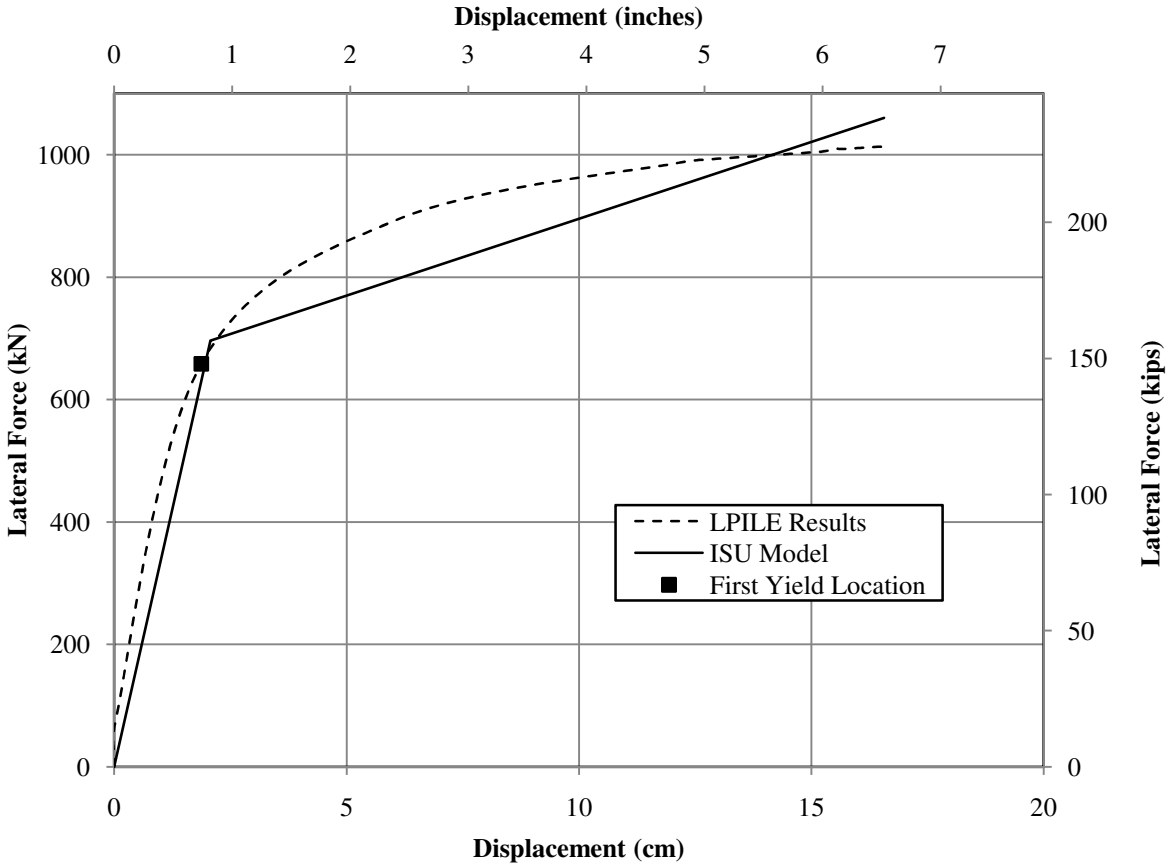

Figure A-6: Global response comparison of new methodology with additional analytical verification #6

- Additional Analytical Verification #7

Table A-13: Input parameters for additional analytical verification #7

Soil Properties		
c_u	379.2 kPa	55 psi
γ_m	21.2 kN/m^3	0.078 lb/in^3
ε_{50}	0.004	
Structural Properties		
D	0.61 m	24 in.
L_{col}	2.69 m	106 in.
L_f	10.4 m	410 in.
ALR	5 %	
M-ϕ Response	See Section 4.3.2	

Table A-14: Comparison of critical parameters at the ultimate limit state for additional analytical verification #7

	Detailed Analysis		Proposed New Model		
Property	SI	English	SI	English	Error
L_{ma}	3.06 m	120.4 in.	3.01 m	118.4 in.	-1.66%
L_{m0}	5.45 m	214.6 in.	5.37 m	211.3 in.	-1.54%
L_{mb}	2.39 m	94.20 in.	2.36 m	92.98 in.	-1.30%
p_u	572.3 kN/m	3268.0 lb/in	727.9 kN/m	4156.4 lb/in	27.18%
V_s	209.5 kN	47.1 kip	228.6 kN	51.4 kip	9.12%
Δ_t	2.29 cm	0.90 in	2.06 cm	0.81 in.	-10.00%
θ_{eb}	0.0129 rad		0.013 rad		0.78%
Δ_{eb}	3.94 cm	1.55 in.	3.78 cm	1.49 in.	-3.87%
L_{pb}	0.44 m	17.37 in.	0.38 m	14.88 in.	-14.34%
θ_{pb}	0.0561 rad		0.048 rad		-14.44%
θ_p	0.11 rad		0.096 rad		-12.73%
Δ_p	0.33 m	13.1 in.	0.29 m	11.37 in.	-13.21%
Δ_{ea}	3.51 cm	1.38 in.	2.74 cm	1.08 in.	-21.74%
V_t	203.7 kN	45.8 kip	209.1 kN	47.0 kip	2.62%
Δ_u	0.42 m	16.39 in.	0.37 m	14.75 in.	-10.01%

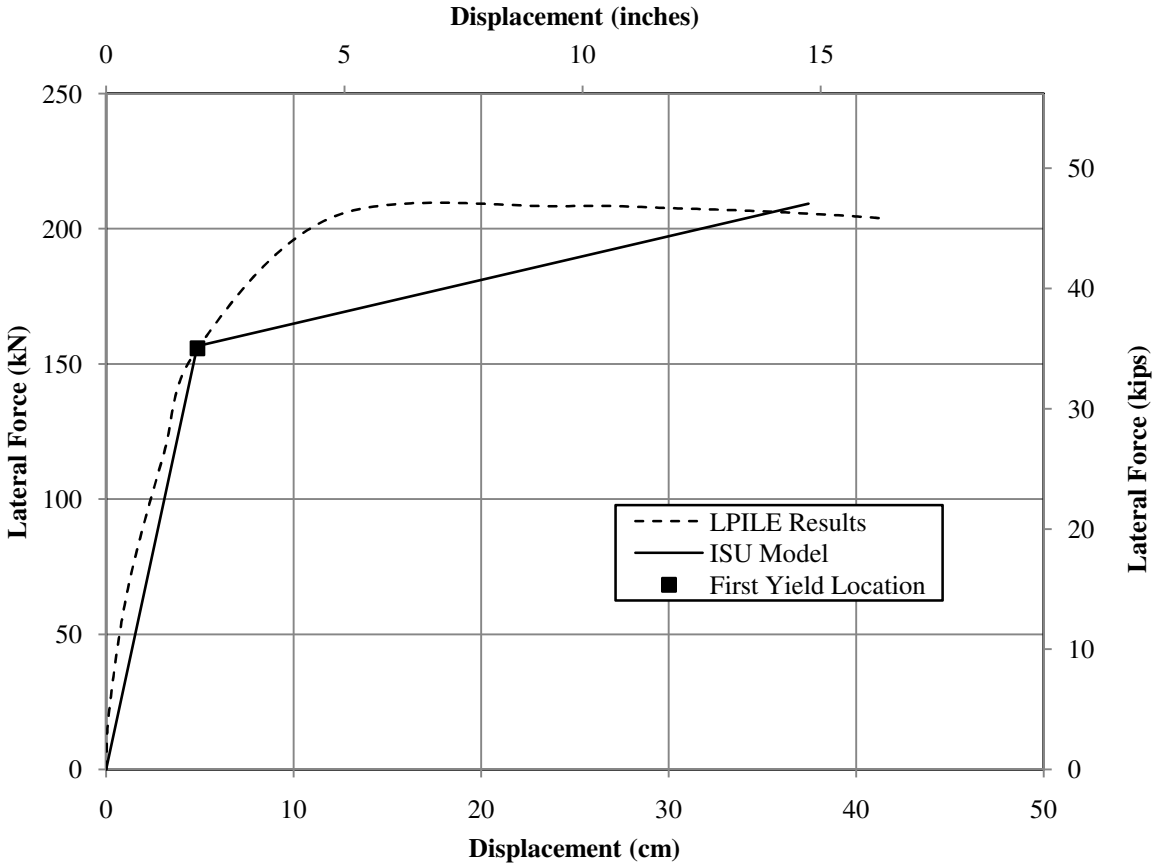

Figure A-7: Global response comparison of new methodology with additional analytical verification #7

- Additional Analytical Verification #8

Table A-15: Input parameters for additional analytical verification #8

Soil Properties		
c_u	379.2 kPa	55 psi
γ_m	21.2 kN/m^3	0.078 lb/in^3
ε_{50}	0.004	
Structural Properties		
D	0.61 m	24 in.
L_{col}	6.10 m	240 in.
L_f	10.4 m	410 in.
ALR	5 %	
M-ϕ Response	See Section 4.3.2	

Table A-16: Comparison of critical parameters at the ultimate limit state for additional analytical verification #8

	Detailed Analysis		Proposed New Model		
Property	SI	English	SI	English	Error
L_{ma}	6.27 m	247.0 in.	6.26 m	246.6 in.	-0.16%
L_{m0}	8.68 m	341.9 in.	8.82 m	347.2 in.	1.55%
L_{mb}	2.41 m	94.87 in.	2.36 m	100.6 in.	6.04%
p_u	516.4 kN/m	2948.9 lb/in	711.9 kN/m	4065.2 lb/in	37.85%
V_s	91.6 kN	20.6 kip	119.7 kN	26.9 kip	30.58%
Δ_t	2.21 cm	0.87 in.	2.54 cm	1.00 in.	14.94%
θ_{eb}	0.0129		0.014 rad		8.53%
Δ_{eb}	8.10 cm	3.19 in.	8.51 cm	3.35 in.	5.02%
L_{pb}	0.43 m	16.94 in.	0.41 m	16.09 in.	-5.02%
θ_{pb}	0.0547 rad		0.052 rad		-4.94%
θ_p	0.14 rad		0.104 rad		-25.71%
Δ_p	0.86 m	33.9 in.	0.65 m	25.62 in.	-24.42%
Δ_{ea}	14.33 cm	5.64 in.	7.90 cm	3.11 in.	-44.86%
V_t	49.8 kN	11.2 kip	66.3 kN	14.9 kip	33.04%
Δ_u	1.09 m	43.08 in.	0.84 m	33.08 in.	-23.21%

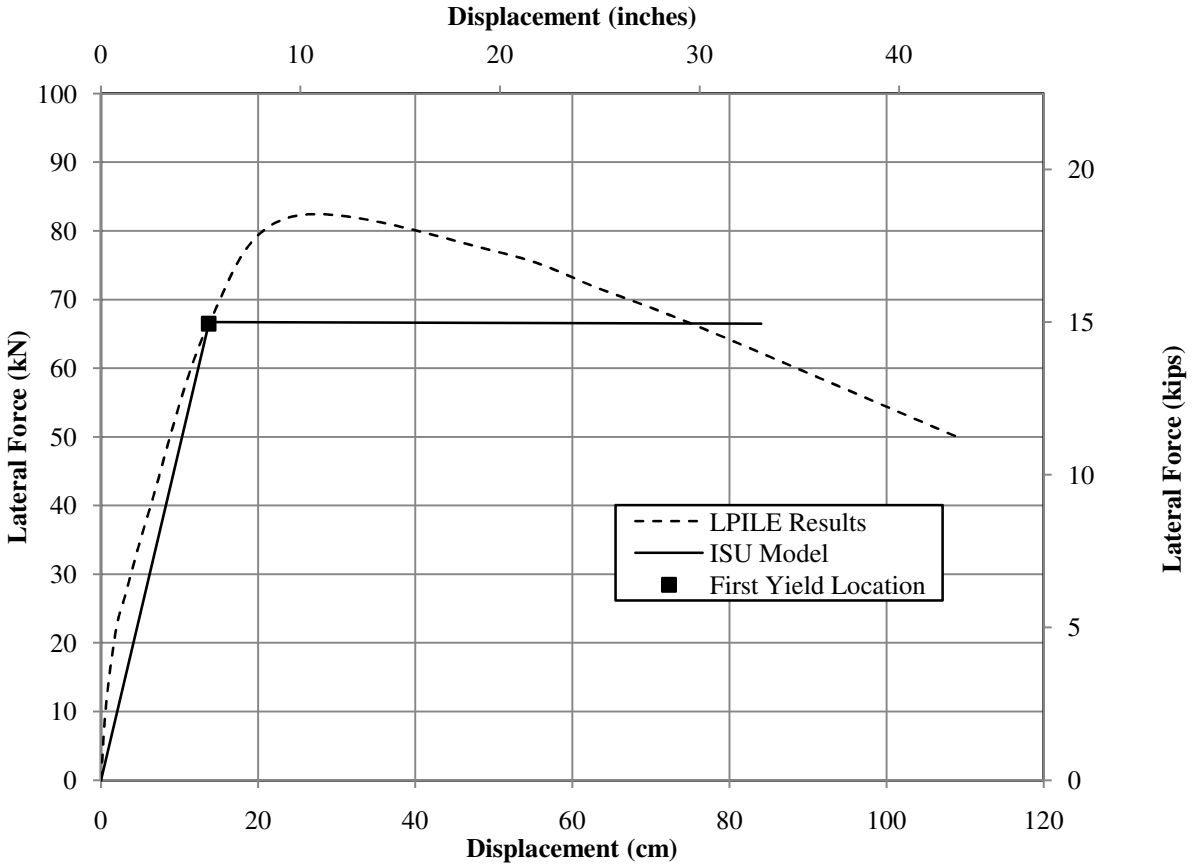

Figure A-8: Global response comparison of new methodology with additional analytical verification #8